12-2007

Nanomaterial Composites for the Detection of Nerve Gas Analogs

Yogesh Datar
Western Michigan University

NANOMATERIAL COMPOSITES FOR THE DETECTION OF NERVE GAS ANALOGS

by

Yogesh Datar

A Thesis
Submitted to the
Faculty of The Graduate College
in partial fulfillment of the
requirements for the
Degree of Master of Science
Department of Chemistry

Western Michigan University
Kalamazoo, Michigan
December 2007

ACKNOWLEDGMENTS

First of all, I would like to express my deep and sincere gratitude to my research advisor Dr.Subra Muralidharan. His most valuable guidance and support are of great value to me and are the basis of my research.

I would like to express my sincere thanks to my research committee members: Drs. Ekkhard Sinn, Yirong Mo, and Sherine Obare for spending their precious time to review my research work. Also, I would like to thank instrument specialist Dr.Raymond Sung, who was very helpful in teaching analytical techniques. I warmly thank Mike Coleman, at Altair Nanotech for helping me with the x-ray diffraction analysis. Also, I would like to thank late Mr. John Stout for helping me with microscopy technique. I owe my sincere thanks to my lab colleagues and my group members. I also wish to thank people who helped me and made my stay comfortable at western michigan university.

I owe my most sincere thanks to my family; because of their extraordinary support I was able to enjoy my journey towards my master's degree. This work would have been impossible to achieve without their support.

I greatly acknowledge the funding from Department of Energy, Office of Basic Energy Sciences.

Yogesh Datar

NANOMATERIAL COMPOSITES FOR THE DETECTION OF NERVE GAS ANALOGS

Yogesh Datar, M.S.

Western Michigan University, 2007

The basis of the research work described here is the use of nanocomposite materials built by bottom-up approach for the selective detection of nerve gas analogs. Nanocomposites materials constructed by using nanoparticle-monomer-receptor (NMR) concept have been utilized to detect nerve gas analogs DCP and DMMP. Synthetic approach used in the construction of nanosensors involved use of robust platforms such as silica nanoparticles and fluorescent quantum dots. Highly conjugated receptor molecules were synthesized by using stilbeneoid compounds. A complete opto-nanosensor was developed by anchoring highly conjugated receptor molecules onto the silica nanoparticles as well as onto the quantum dots. The opto-nanosensors developed were analyzed for their efficacies to detect nerve gas analogs. They exhibited different Uv-Vis, excitation, and emission behavior than their individual building blocks. Nanosensors showed change in their emission behavior after interacting with nerve gas analogs. The interaction was quantified by measuring association constants between nerve gas analogs and nanosensor. Nanosensors based on quantum dots showed relatively better change in their emissive behavior after interacting with nerve gas analogs. The nanosensors based on NMR concept constructed by the "*bottom-up*" approach could achieve practical application.

TABLE OF CONTENTS

Table of Contents- Continued

CHAPTER

Table of Contents- Continued

CHAPTER

Table of Contents- Continued

CHAPTER

Table of Contents-Continued

CHAPTER

Table of Contents- Continued

CHAPTER

Table of Contents-Continued

LIST OF TABLES

LIST OF FIGURES

List of Figures- Continued

LIST OF SCHEMES

CHAPTER I

INTRODUCTION

1.1 History of Chemical Warfare Agents

Since the 14th century, the use of chemical and biological weapons is recognized as a threat to humanity. Numerous incidents have been documented since then. The first known recorded use of biological agents was during the 14th century siege of Kaffa which is the modern day Fedossia, Ukraine. A relatively recent example is the use of smallpox as a biological weapon against Native Americans in the 18th century.[1] Organophosphorus compounds and their structural simulants also have the potential to be very effective chemical warfare weapons and they were used in World War I, II, as well as during the Cold War. In the 1980s the use of the nerve gas sarin and mustard gas in the Gulf War is well known to the world. Although a convention prohibiting the production, stockpiling and the use of chemical weapons was implemented, the Japanese extremist group, AUM Shinrikyo, used sarin gas in Matsumoto in 1994 and in the Tokyo subway in 1995 killing and injuring innocent people. The stockpiling of chemical warfare agents (CWA) is a threat to society. There are cases where people suffered from leakage of these stored CWAs. For instance, in Samukawa and Kanagawa, Japan, injuries have occurred due to the direct leakage of stockpiled CWAs from containers. Among the reported cases, people in Kamisu and Ibaragis, Japan, also suffered health issues from drinking water, which was contaminated by CWA leakage.[2] Nevertheless, several countries are known to have manufactured and stockpiled CWAs and related weapons. Currently, there is a great

possibility that chemical and biological warfare agents might be used as a means of terrorism.[1, 3-6]

1.2 Introduction and Classification of Nerve Gas Agents

Nerve gas agents are structural mimics of organophosphate compounds which are generally used as insecticides and pesticides. The development of nerve gas agents was a by-product of insecticide production during research and development.[3] The general chemical structure of these organophosphorus compounds can be described as a compound with tetrasubstituted phosphorus (V) center, an oxygen or sulfur atom double bonded to the phosphorus, a leaving group and two substituents which differ widely depending on the subclass.[1]

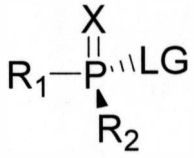

Figure 1.1General formula of nerve gas agents[1]

(where LG= Leaving group, X=CN, F, S, O and R_1, R_2 = alkyl groups)

At the molecular level, nerve agents are characterized as compounds that contain at least one carbon-phosphorus bond.[1] These highly toxic organophosphorus compounds are subdivided into two main types; V and G. This classification is based on additional functionalities and unique properties of each individual member. During the early 1930s, when a German chemist observed that organophosphorus compounds could be poisonous, the first production of G-agents was developed during World War II. As a result of this discovery, Cyclosarin (GF), Tabun (GA), Sarin (GB), and Soman (GD), which contain fluorine substituents, were developed. Figure1.2 shows the chemical structure of Tabun, Soman, and Sarin. After World War II, further research in this field

resulted in the discovery of new types of nerve agents. V-agents (VG, VM, VX, and VE) which are up to ten-times more poisonous than G-type nerve gas agents. VX and the Russian VX (R-VX) are examples of V agents containing a thioester linkage. Compared to G-type nerve gas agents, which are poorly persistent, V-type nerve gas agents are highly persistent and this property allows chemists to distinguish between G-type and V-type nerve gas agents [3]

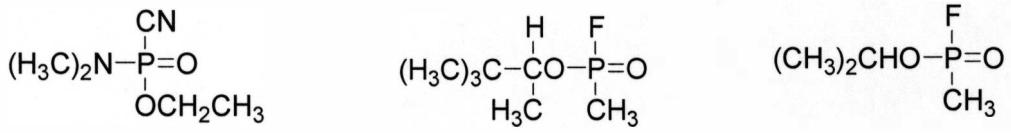

TABUN SOMAN SARIN

Figure1.2 G-series nerve gas agents

Though nerve gas agents are referred to as gases; they all are high boiling liquids. They are far more toxic than the agents used in World War I mustard gas, chlorine, phosgene and even more toxic than cyanide. [1, 7]

1.3 Mechanism of Nerve Gas Reaction on Human Beings

The extreme toxicity of organophosphorus compounds can be attributed to the inhibition of the activity of enzyme acetylcholinesterase (AChE).[8] This enzyme plays a key role in the body by maintaining concentrations of the neurotransmitter acetylcholine within the synaptic cleft of the nervous system. When AChE is functioning properly, this serine esterase hydrolyzes acetylcholine yielding acetate, choline and regenerating the active enzyme. This degradation process results in a lowered level of acetylcholine and ultimately the termination of nerve impulses. Organophosphorus compounds will produce serine-phosphoester adduct by undergoing nucleophilic attack to block serine residue of AChE. Thus, the excess production of acetylcholine due to adduct formation causes

cholinergic overstimulation, resulting in death caused by respiratory failure. The nerve gas mechanism on human beings can be seen below in figures 1.3 and 1.4.

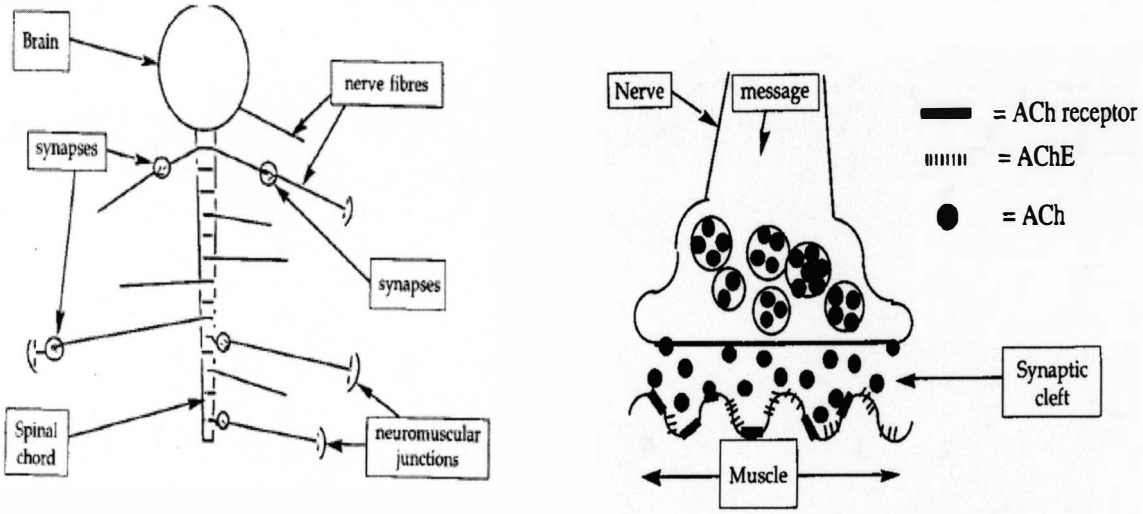

Figure 1.3 Central Nerves System (left side), Message transmission by ACh receptor (right side) [7]

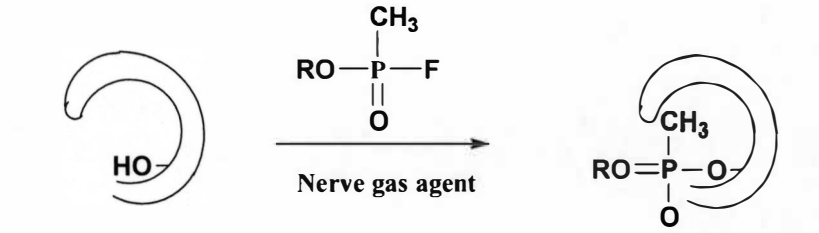

Figure 1.4 Interaction of nerve gas agent on AChe [7]

Table 1.1 Toxicity of the most important nerve agents on humans

Nerve Agent	LCt_{50}	LD_{50}	Boiling point
	Inhalation (mg min/m^3)	Skin (mg/individual)	^{o}C
Tabun	200	4000	240
Sarin	100	1700	147
Soman	100	300	167
V-agents	50	10	Over 300

Pretreatment and antidote - Pretreatment consists of a NAP (Nerve Agent Protection) tablet based on the prophylactic type. It can only be used before a nerve gas attack. Another treatment uses a mixture of two compounds, atropine (an anticholegenic) and oxime, to stop the action of the nerve gas agent. This method can be used during or after the nerve gas agent attack. [6]

The most important chemical reactions of nerve agents take place directly at the labile P-X (Figure 1.1) bond which can be easily broken by nucleophilic attack. In aqueous solution, decomposition of nerve gas agents is accelerated by the addition of base. The product of decomposition is a non-toxic phosphoric acid. Similarly, nerve gas agents react with water, however, the reaction depends on the pH of the water. Sarin is hydrolyzed to non-toxic products very easily, which is not true in the case of VX. VX is only hydrolyzed in strongly basic solutions. [1]

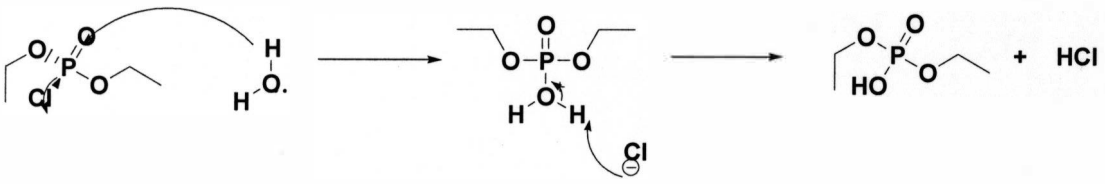

Figure 1.5 Hydrolysis of nerve gas analog Diethylchlorophosphonate (DCP)

1.4 Criteria for a Chemical to be a Chemical Warfare Agent (CWA)

A CWA must be highly toxic, however, it should not be difficult to use. Long term storage and packing of CWAs must be achievable without degradation or damaging the packing materials. A typical CWA must not loose its activity by reacting with air or water in the atmosphere. CWAs are classified in these several groups; nerve agents, asphyxiant/blood agents, vesicant agents, choking/pulmonary agents, lachrymatory agents and cytotoxic proteins. According to the Chemical Weapons Convention of 1993 substances are considered chemical weapons if they cause injury, death, or paralyzed performance to a human being or animal by chemical effect.[3] Several countries have participated in unlawful activities as per the international convention. This, combined with the emergence of terrorist organizations capable of producing viable chemical or biological warfare agents, has fueled the need for developing selective, sensitive, reliable and affordable detection methods. [1]

1.5 Detection of Nerve Gas Agents

Different detection methods for CWAs have been developed which include: interferometry, gas chromatography-mass spectrometry, surface acoustic wave (SAW) devices, enzymatic assays, and electrochemistry. But, the present detection methods have limitations on them due to weaker response, non-specificity, limited selectivity, poor sensitivity, complicated operations, space consumption, recognition in real-time, and false signaling. [3, 5]

In most of the cases where CWAs have been used, on-site detection and monitoring of CWAs are required. The on-site CWA detection process is classified into the following two subclasses, 1) mobile portable detectors for individuals and 2) fixed set up assembly at a specific site. Although, the sensing technology is advancing, there is no universal device that meets all of the CWA detection requirements. [2]

In order to overcome these limitations the design of colorimetric or fluorimetric chemosensors or optosensors is an alternative to the classical methods. However, one of the most simple and easy means of chemical detection is the exhibition of an optical event. One specific optical event is the change in emissive behavior in the presence of a target moiety. In addition, optical detection is a low-cost alternative and can be performed with readily available instrumentation. In some cases, optosensors can allow detection by the naked eye for rapid but crude determinations. Documented examples strongly suggest that the application of chromo-fluoregenic molecular concepts for the visual detection of nerve agents will be an area of growing research.

First chromo-fluorogenic nerve agent detection was reported by Schonemann in 1944, where Schonemann oxidized certain amines to give various colored products in the presence of organophosphate compounds. Also, the direct relation between emission intensity and concentration of nerve gas agents allows one to use this method for detection and estimation of small amounts of nerve gas agents. [3, 4, 7-9]

Distinguishing various CWAs from chemically similar organophosphate compounds is one of the limiting factors in developing a universal detector. Methylphosphonic acid (MPA), a degradation product of CWAs, can be used as an excellent marker for the detection of nerve gas agents.[1, 4, 5, 8] The principle behind a chemosensor is the reaction

between a receptor moiety and a phosphoryl or an acyl group from the nerve agents. This reaction yields fluorescent esters which then exhibit a change in optical behavior. *"Switch-On"* (enhancement in emission intensity) sensors are more reliable than *"Switch-Off"* (quenching of emission intensity) sensors because their signal arises from a low background. As high background intensity and photobleaching does not affect *"Switch-On"* sensors, false positive replies are rarely observed.[6] Another method to generate an optical event is the mixing and matching of tailored ligands and specifically selected metal ions. The sensor complex formed between the tailored ligands and the metal complexes can exhibit different selectivity and optical response depending on the nerve gas agents.[9]

Optical signal amplification of the formation or breaking of the covalent bond can be gained via several means. First, the indicator molecule reacts with the analyte via a specific functional group directly attached to the chromophore and thus brings a change in electron delocalization within the chromophore by altering the electron acceptor/donor strength of this functional group. This is named as internal charge transfer. Second, the interaction with the analyte causes a photo induced electron transfer, an indirect effect on chromophore, from the receptor molecule to the fluorophore conjugated with a spacer.[10]

In brief, the measurement of optical response from a chromophore sensitive to a given analyte is a well-established approach which is widely used for building reliable optical sensors. This is mainly because of the low cost, high response rate, high sensitivity and selectivity typical of such systems.[11]

1.6 Requirements for a Successful Sensor

An ideal nanosensor should have properties such as; 1) high specificity to the analyte molecule, 2) the ability to adjust the distance between nanoparticle and fluorophore as a response to the target molecule concentration, and the most crucial parameter is 3) the response time of the sensor. Developments in sensing technology are forcing us to believe that one should be able to develop a simple method for the detection of organophosphate nerve gas agents in the near future. One method of detection would be the use of a receptor, a fluorescent molecule, and a surface modified nanoparticle which will result in the change in fluorescence based on highly narrowed detection of the nerve gas agents. The binding affinity between receptor molecules and analytes is probably the most important parameter outside of its fluorescence that will contribute to sensor performance. [8]

Consequently, development of sensors based on the change in optical properties of chemosensors is undoubtedly the most promising technology in the early detection of chemical weapons. [11, 12]

1.7 Central Hypothesis

Highly conjugated aromatic compounds having a nitrogen atom free to interact with the target molecules acts as a receptor in a complete nanosensor assembly. This interaction of receptors with a target moiety is followed by the change in an emissive behavior of receptors due to the formation of an adduct. The receptor molecules attached to more conjugated stilbene like compounds would enhance signal intensity. Anchoring the conjugated receptor-stilbene system to either luminescent nanoparticles or to robust silica nanoparticles would amplify the signal transduction. Hence, sensors based on the nanoparticle-monomer-receptor (NMR) concept would provide selective as well as quantified detection of nerve gas analogs.

In the same context, the research described in this thesis enables us to design optochemosensors based on *"bottom-up"* technology by using self-assembling advanced nanomaterials. This *"bottom-up"* approach gives us the freedom of choosing building blocks of nanosensor depending on target analytes as well as allows us to detect nerve gas analogs present in micro-molar concentration. The nerve gas analog nanosensors described in this thesis are based on a very novel *"bottom-up"* concept called NMR Sensors. The NMR approach utilizes building blocks of nanosensors. In this project the building blocks of nanosensors are silica nanoparticles or ZnS:Mn/ZnS quantum dots, a stilbene monomer, and two receptors. Figure 1.6 explains the concept more clearly.

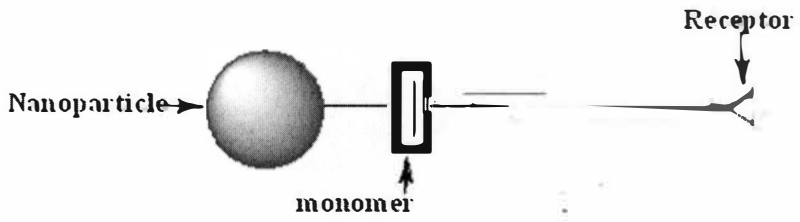

Figure 1.6 NMR Sensor for detection of nerve gas analogs
(Nanoparticles = silica nanoparticles, ZnS:Mn/ZnS quantum dot, stilbene monomer, receptors)

The synthesis, characterization, and development of these building blocks and of the nanosensors by using these building blocks will be explained in later chapters and is the primary focus of the research described in this thesis.

1.8 Objectives of the Present Study

1) To construct Nanosensors I, II, and III and characterize them based on their spectral properties as well as fluorescence decay.
2) Analyze the efficiency of Nanosensors I, II, and III towards selective detection of nerve gas analogs DCP, DMMP and HCl.
3) Determine the association strength between Nanosensor-I, II, and III, its components and target molecules DCP, DMMP, and HCl by calculating association constants. The association constant values will enable us to gain better knowledge of the interactions as well as the performance of Nanosensors I, II and III.

1.9 Nerve Gas Analogs Used for Research Purpose

1) Diethylchlorophosphonate (DCP) shown in Figure 1.7 is a well-known mimic of the actual G series nerve gas agents.
2) Dimethylmethylphosphonate (DMMP) shown in Figure 1.7 is also a commonly used nerve gas analog.

3) Hydrochloric acid (HCl) shown in Figure 1.7 is a hydrolysis product of DCP and is a corrosive chemical.

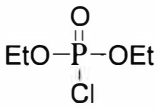

DCP

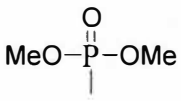

DMMP

HCl

Figure 1.7 Nerve gas analogs

1.10 Constructed Nanosensors

Nanosensor-I, II, and III constructed for the selective detection of model compounds (DCP, DMMP, and HCl) employed in this research are shown in Figure 1.8

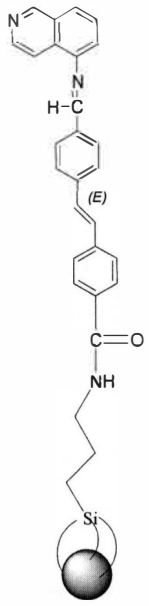

Nanosensor-I

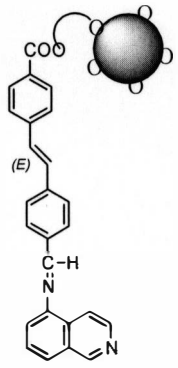

Nanosensor-II

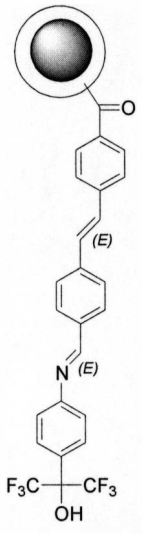

Nanosensor-III

Figure 1.8 Schematic representation of Nanosensors-I, II, and III

Chapters 2-4 describe in detail the synthesis, the characterization, the development and the spectral properties of Nanosensors-I, II, and III.

1.11 Instrumentation

All synthesized compounds and their intermediates were characterized by ^{1}H NMR, ^{13}C NMR, FT-IR, LC/MS, UV-Vis spectroscopy, emission spectroscopy, and fluorescence lifetime decay. Silica nanoparticles and ZnS:Mn/ZnS QD nanocrystals were examined by transmission electron microscopy (TEM). UV-Vis spectra are reported as absorbance (A) vs. λ (nm). Emission spectra are reported as intensity vs. λ (nm). Emission lifetime studies were recorded as intensity vs. time (ns). The ^{13}C and ^{1}H NMR spectra are reported in δ (ppm) values with tetramethylsilane (TMS) as an internal standard.

The research described in this thesis was performed by using below mentioned instruments.

1) Emission and Lifetime studies: All luminescence as well as lifetime studies reported in this thesis were performed on a Edinburgh time resolved and steady state fluorescence spectrophotometer. For lifetime fluorescent studies the obtained data was fitted by using F-900 Data acquisition and analysis software.

The light sources used for luminescent as well as lifetime measurements are as noted below;

1. Xe lamp 900: continuous excitation source for steady state studies.

2. nF 900: the nanosecond Hydrogen flashlamp excitation source for lifetime studies.

3. Pulsed diode lasers: picosecond diode lasers for lifetime studies.

PMT (cooled environment) was used as detector.

2) Nuclear Magnetic Resonance (NMR): NMR studies mentioned in this thesis were performed by using an Eclipse 400 FT-NMR Spectrometer provided by a JEOL JNM-

ECP 400 FT NMR System. The NMR data was treated with Delta NMR software. The solvents for NMR were d_3-methanol, d_6-DMSO, *d*-chloroform.

3) Liquid chromatography-Mass spectrometry (LC-MS): LC-MS studies mentioned in this research work were done on a Shimadzu LC/MS-2010EV High-Performance Liquid Chromatograph/Mass Spectrometer. The instrument was used with the following specifications; Stationary Phase: 5 μm, C_{18} silica gel, Mobile Phase: MeOH/H_2O (gradient), Flow rate: 0.6 mL/min, Ionization: APCI (low flow rate Atmospheric Pressure Chemical Ionization), ESI (Electro Spray Ionization).

Detector: UV detector. LC-MS data was obtained by using LC-MS solution software.

4) UV-Vis absorption measurements: The UV-Vis absorption spectra reported here were taken either on Perkin Elmer UV/Vis Lambda20 Spectrophotometer or on Shimadzu UV-2101 PC UV-Vis scanning spectrophotometer. Winlab was the software for Perkin-Elmer data collection and UV-Probe software was used for Shimadzu.

5) FT-IR measurements: FT-IR spectra reported in this thesis were taken on Broker Equinox 55 FT-IR Spectrometer. The data obtained was viewed by OPUS software.

6) X-ray diffraction analysis: X-ray diffraction analysis of ZnS:Mn/ZnS was done at Altair Nanotech, Reno, Nevada on a Rigaku Ultima. This instrument has cross beam optics and a graphite monochromator. Also it has auto-variable slits which can be moved depending on the sample.

7) Transmission Electron Microscopy (TEM): TEM technique was used to analyze naked silica nanoparticles as well as surface modified silica nanoparticles. The instrument used was a JEOL JEM-1230 Transmission electron microscope. The accelerating voltage was 80KV. Samples prepared for TEM were dispersion of silica nanoparticles in water taken

on copper grids (400mesh) coated with carbon. The samples on the grid were air dried before analyzing under the microscope.

1.12 Reagents

The following reagents were used to synthesize and characterize compounds. Ethyl alcohol USP (absolute-200 proof) was purchased from Aaper Alcohol and Chemical Co. and used as received. 3-Aminopropyltriethoxysilane (APTS) 99% and Tetraehtylorthosilicate (TEOS) 99.999% were purchased from Sigma-Aldrich, Inc. Ammonium hydroxide A.C.S reagent, Assay (NH_3) w/w min.28%-max. 30%, normality-14.8 was obtained from Fisher Scientific. 5-Aminoisoquinoline 99% was purchased from Sigma-Aldrich Inc. 2-(4-Aminophenyl)-1,1,1,3,3,3-hexafluoropropanol 96% was purchased from Alfa-Aesar. Toluene anhydrous 99.8%, dimethyl sulfoxide, Chromosolv Plus >99.7%, and acetic acid 99.7% were purchased from Sigma-Aldrich Inc. Mili-Q water filtered from U.S.Filter Purelab plus UV/UF was used. Reagents required to synthesize ZnS:Mn/ZnS (core/shell) ($1/16^{th}$) QDs, zinc acetate dihydrate, sodium sulfide, manganese dioxide, and methanol were purchased from Sigma-Aldrich Inc. Sodium sulfide was kept in a vacuum desiccator in order to keep it moisture free. Nerve gas analogs diethylchlorophosphonate and dimethylmethylphosphonate were used as received. Hydrochloric acid (HCl) was received from Fischer Scientific Inc. Acetonitrile used for spectroscopic studies was obtained from both Sigma-Aldrich Inc. and EM science. The solvents dimethylsulfoxide-d_6 and chloroform-*d* used for NMR studies were obtained from Sigma-Aldrich Inc.

CHAPTER II

BUILDING BLOCKS OF NANOSENSORS

2.1 Introduction to Silica Nanoparticles

In the last two decades the development of studies on chemical sensors has been a focus of attention. Sensors based on chips or "Lab-on-Chip" is the center of research interest.[13] Hence, to build a portable nanosensor, monodispersed, monolayer forming nanoparticles (NPs) are being used.[14, 15] Among the most investigated NPs, silica nanoparticles (Si-NPs) occupy the prominent position in research, because of their relatively easy synthesis and their broad range of applications.[16] It is well know that at the nanometer level, the size of the material is of utmost importance because the quality of these applications is highly dependent on the size and size distribution of nanoparticles.[17] Si-NPs exhibit excellent properties such as transparency to light, photophysical inertness and ease with which Si-NPs can be functionalized by reacting with alkoxysialne derivatives. These properties make them the best choice for use in fluorescence chemosensors. Also, Si-NP based chemosensors can be stored as a dry powder.[11, 18] Si-NPs offer a large hydrodynamic radius and large surface area which causes non-specific binding with any other functional groups such as an amine group, an acid group, or a receptor moiety.[15]

The size of the particles can be controlled by selecting a particular type of silicon alkoxide and alcohol for synthesis. Generally, the formation of silica nanoparticles occurs in two steps. First, the formation of silanol groups due to hydrolysis and second, the formation of siloxane bridges by a condensation polymerization reaction. The condensation reaction is governed by the reaction conditions. Depending on these

reaction conditions, the condensation might result in the formation of a three dimensional network or single layer monodispersed particles. However, hydrolysis is a very slow reaction, though it can be accelerated by addition of acids or bases which are used as catalysts. The most commonly used catalyst in the formation of Si-NPs is ammonium hydroxide. Ammonium hydroxide increases the rate of hydrolysis, and the rate of condensation which results in increased water concentration. In such a condition, if every other reaction parameter is optimized, the reaction leads to the formation of smaller particles.[17]

2.2 Mechanism of Formation of Si-NPs

Among the mechanisms suggested for the formation of Si-NPs, the mechanism suggested by Bogush and Zukoski is that the nucleation of particles occurs continuously throughout the reaction and not by the traditional nucleation and growth mechanism. Bogush and Zukoski proposed a nucleation and aggregation mechanism whereby small particles nucleate and then aggregate until they reach a colloidally stable size. At this stage, due to the diffusion of larger particles into the solution, aggregation between nucleating smaller particles and larger particles occur. Hence, colloidally stable particles can grow during this process. Later in the reaction, constantly forming small particles must aggregate onto the growing particles before they can reach a colloidally stable size. These particles formed in the earlier stage and having low density, then collapse upon reaching a certain size and become colloidally stable towards aggregation.[19]

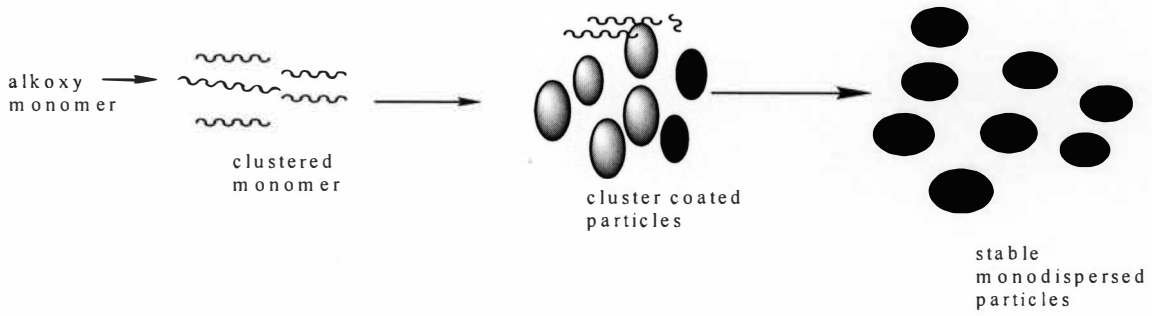

Figure 2.1 Formation of silica nanoparticles

2.3 Various Methods to Synthesize Si-NPs

There are two general routes for the preparation of Si-NPs, the Stober method and the reverse microemulsion method. Although the Stober method[20] only cost a few hours and the reaction conditions can be easily controlled, the uniformity of the particles is limited.[21] Reverse microemulsion method- Among the available techniques used to synthesize Si-NPs, water-in-oil microemulsion is one of the most widely used methods. In the reverse microemulsion method, water nanodroplets are formed in an organic medium which causes the formation of reverse micelles. These micelles are then used as nanoreactors for the formation of NPs. The particle size and the size of reverse micelles can be controlled by maintaining the water/oil ratio. Particles synthesized by reverse microemulsion method show great promise in size control, uniformity and in the further development of sensors.[14, 21] The water/oil reverse microemulsion system makes use of Triton X-100 (surfactant, an amphiphilic molecule), cyclohexane (oil), n-hexanol which acts as a co-surfactant and water. These reactants together form a thermodynamically stable system. The water droplets present in the bulk oil phase serve as nanoreactors for the synthesis of nanoparticles.[22]

2.4 Experimental

Synthesis of silica nanoparticles– Nanosized monodisperse colloidal silica particles can be prepared by a simple procedure from tetraalkoxysilanes in alcoholic solution. Formation of silica nanoparticles is due to the base catalyzed hydrolysis and condensation of monomers. The schematic representation of formation of Si-NPs is in scheme 2.1:

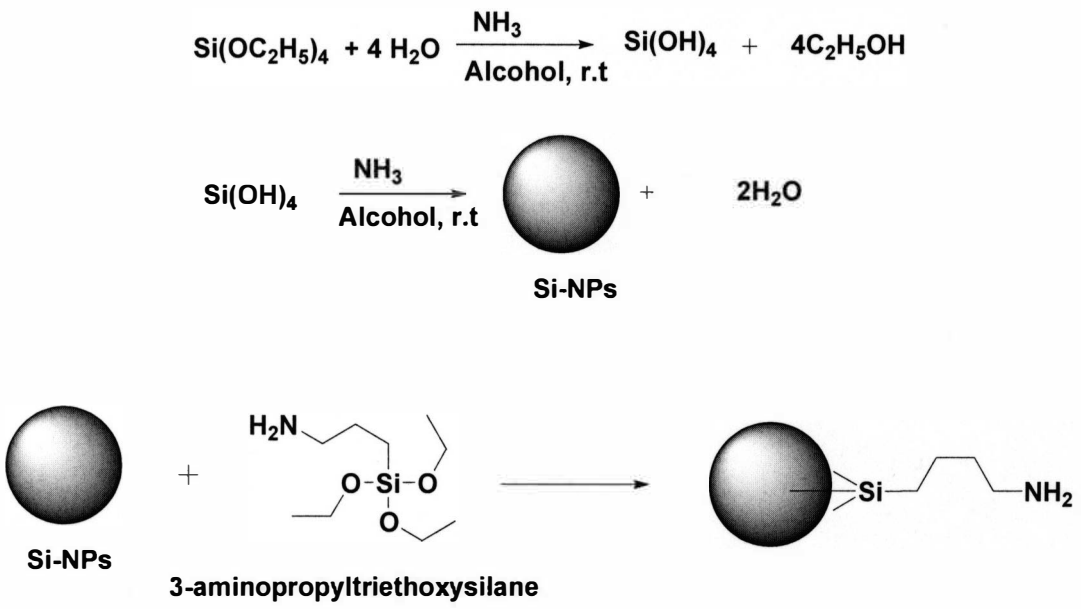

Scheme 2.1 Synthesis of silica nanoparticle[19]

Synthesis of silica nanoparticles by the Stober method-

In a clean round bottom flask, 100 mL of ethanol was taken and to this 3 mL of tetraethylorthosilicate (TEOS) was added. This was quickly followed by the addition of 2.5 mL of aqueous ammonia (conc.) and 2.4 mL of D.I water. This reaction solution was stirred vigorously for three hours at 35^0C. After three hours, 2 mL of TEOS was added and the reaction was stirred for next three hours. At the end of the reaction, the turbid solution of silica nanoparticles was subjected to rotary evaporation to get rid of any excess ammonia. Rotary evaporation was repeated several times with periodic additions

of fresh ethanol. Silica nanoparticles were then characterized by Transmission Electron Microscopy (TEM) and Fourier transform-Infrared (FT-IR) spectroscopy.

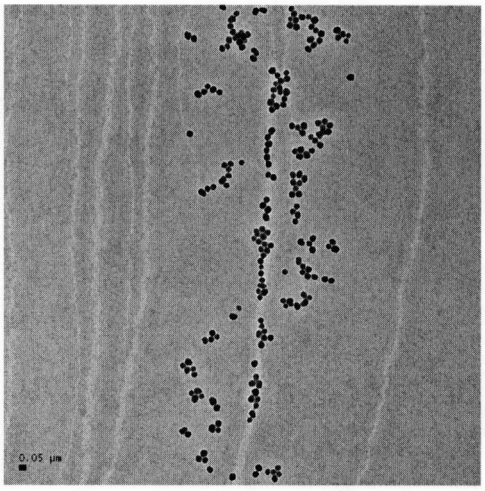

Figure 2.2 TEM image of silica nanoparticles by the Stober method

Synthesis of silica nanoparticles by Reverse microemulsion method – In a clean round bottom flask 7.5 mL cyclohexane was added and kept for stirring. To this cyclohexane 1.6 mL of hexanol, 1.77gm of Triton X-100, 400 µL milli-Q water, and 100 µL aqueous ammonia were added and stirred for thirty minuets. At the end of thirty minuets, 100 µL TEOS was added and the reaction was stirred vigorously for another ten hours. After ten hours, 50-70 mL of 200 proof ethanol was added to the reaction to precipitate silica nanoparticles. Thus precipitated Si-NPs were subjected to rotary evaporation to get rid of the excess ammonia as well as ethanol. Additional washings of ethanol could remove excess ammonia completely.[15, 23]

2.5 Silanization of Si-NPs

Silanization of Si-NPs prepared by the reverse microemulsion method was done in a one-step method and a two-step method. In the one-step method, after the addition of TEOS, 50 µL of APTS was added to the reaction mixture and the reaction continued for ten

hours. In this method, Si-NPs obtained were washed several times with propanol and warm ethanol to get rid of unbound APTS and collected by centrifugation.[16] In the two-step method, Si-NPs were prepared without the addition of APTS. The Si-NPs were obtained in the form of dry powder after centrifugation and drying; they were redispersed in 25 mL of 200 proof ethanol and 50μL APTS was added to this dispersion. The reaction was stirred for ten hours to obtain maximum surface coverage.[21] The naked Si-NPs and modified Si-NPs were further characterized by TEM and FT-IR spectroscopy.

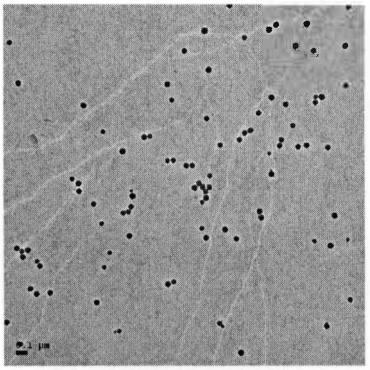

1) Unmodified Si-NPs

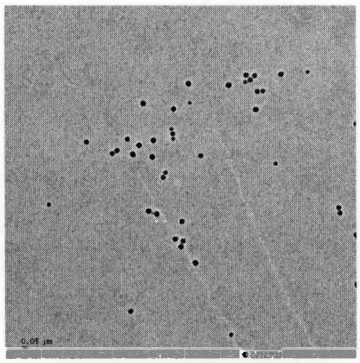

2) Unmodified Si-NPs

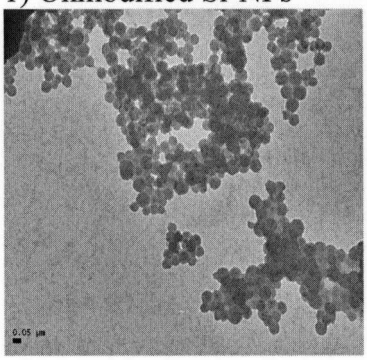

3) Silanized Si-NPs

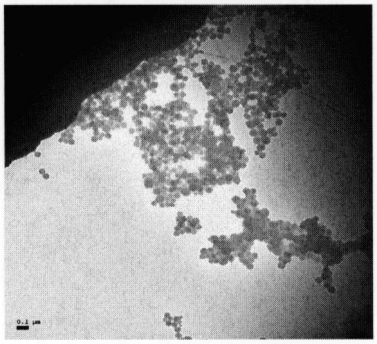

4) Silanized Si-NPs

Figure 2.3 Represents unmodified silica nanoparticles prepared by Stober as well as reverse microemulsion method (1, 2) and represents silanized silica nanoparticles (3, 4)

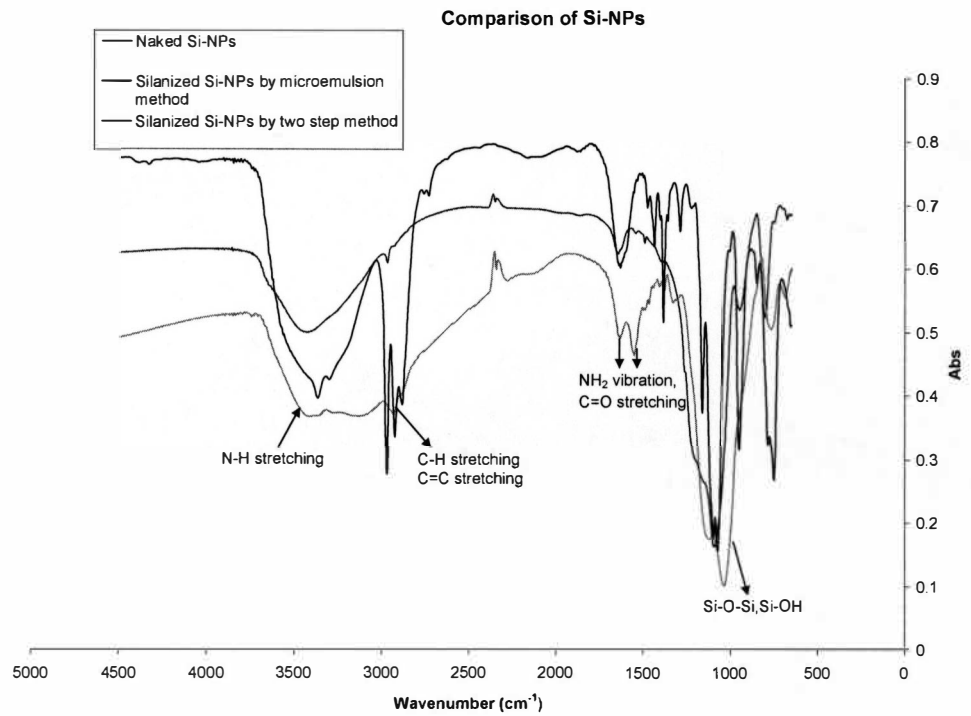

Figure 2.4 FT-IR spectra of naked Si-NPs, silanized Si-NPs by reverse microemulsion, silanization of Si-NPs by two step method

2.6 Results and Discussion

As mentioned earlier, the efficient use of Si-NPs depends on their size, shape, and monodispersity. Based on the method of adding Aminopropyltriethoxysilane (APTS), the reaction is classified as a one-step or two-step method of silanization. In the one-step method, APTS was added one hour after the addition of TEOS while the formation of Si-NPs is about to complete. The one-step method was used to modify Si-NPs obtained by the reverse microemulsion method. In the two-step method, a dry powder of Si-NPs was obtained by the Stober method, and then modification was performed in ethanol as mentioned in the procedure above. As indicated in the TEM images in figure 2.3, Si-NPs are obtained by the Stober method as well as by the reverse microemulsion method. Both of the methods showed formation of monodisperse, round shaped, highly dense Si-NPs.

The Si-NPs obtained by the Stober method are about 35-40nm in diameter, and the Si-NPs obtained by the reverse microemulsion method are approximately 50nm in diameter. Si-NPs modified by the two-step method showed poor silanization results as compared to Si-NPs modified by the one-step method shown in figure 2.3. Aggregated Si-NPs affirm the modification is done on the surface of Si-NPs. Si-NPs posses a negative potential due to Si-OH groups present on the surface which causes their zeta (ξ) potential value to be high. Due to the high zeta (ξ) potential Si-NPs would not to aggregate and will show uniform dispersity. However, modification with amine group decreases the negative potential of Si-NPs due to the protonaiton reaction of amine groups. This results in the decrease in the value of the zeta (ξ) potential causing aggregation of Si-NPs. Thus, indicated by TEM images of silanized Si-NPs in Figure 2.3, 3), 4), it can be confirmed that the aggregation of Si-NPs is due to the addition of amines onto the surface.[21] Various amounts of APTS (30 μL, 50 μL, 100 μL) were tried for silanization purposes. However, there was not much difference in the coverage achieved. The excess APTS and its polycondensates can be removed by washing with warm ethanol and propanol.[24]

FT-IR spectroscopy was used to further analyze the modification of Si-NPs. The interpreted FT-IR results are that: the Si-O-Si, and Si-OH stretching is attributed to the set of peaks in the range of 850cm^{-1} to 1100 cm^{-1}. The band from 2875 cm^{-1} to 3000 cm^{-1} is assigned to the stretching and bending frequencies of alkanes. C=O, and C=C stretching mode is near 1640 cm^{-1}. The peak at 3375 cm^{-1} is attributed to N-H stretching as indicated in figure 2.4. The band at 798 cm^{-1} is due to the bending mode of NH_2, and O-H stretching might be around 3350 cm^{-1}.[25, 26]

The reason behind using ethanol (EtOH) as a solvent for modification of the Si-NPs is the protic nature of ethanol and therefore it has the ability to form hydrogen-bonds with the Si-O surface. Due to the highly favored interaction between the ethanol and Si-NP surface, a solvent layer is formed around the nanoparticles. This layer prevents non-specific adsorption on the Si-NP's surface. Also, the condensate products of APTS are known to have better solubility in ethanol. Silane concentration might not affect the amount of silane groups per nanoparticle.[27] APTS is used as a coupling agent because of the reactivity of the amino groups toward other functional groups. Also, there is a large amount of knowledge available in the literature on coupling reactions. In Si-NP modification, a base catalyzed reaction proceeds through formation of pentacoordinate transition states which results from a bimolecular nucleophilic attack on the silicon atom. In this case OH^- acts as a nucleophile and attacks the silicon atom. Thus an increase in the concentration of this catalyst results in an increase in the reaction rate. Therefore, the hydrolysis rate increases if the concentration of NH_3 and water is increased.[23] APTS is known to autocatalyze its own hydrolysis and condensation due to the basic character of its amino group.[27]

2.7 Introduction to Quantum Dots

Due to their unique photophysical properties, inorganic semiconductor nanocrystals (NCs) also known as quantum dots (QDs) have gained very much attention as a new member of the fluorophore family. Quantum dots (QDs) having a luminescent nature, especially those made from the II-VI type semiconductors are of great interest. Their optoelectronic properties are a function of the physical confinement of excitons, in which excited electrons that are bound to the holes are left behind in the valence band. Quantum

confinement results when nanocrystals (NCs) and excitons have almost similar dimensions.[28] At such a small dimension, the spatial confinement of charge carriers cause noticeable changes in the energy levels available to electrons and holes in the NCs. This enables the absorption and emission properties of the crystals to be altered by tuning their particle size. It is well known that as the size of QDs decrease, the effective band gap increases. This is the origin of the unique size dependent optical properties of QDs. NCs have advantages over conventional organic dyes which tend to posses low resistance to photobleaching, narrow absorption profiles, emission spectra that tail to the red, and greater luminescent lifetime.[25, 28-30] QDs show broad continuous absorption band. This property of QDs allows one to excite them in a wide range of wavelengths. Depending on the distance between the acceptor and donor, NCs can transfer energy to one or more acceptors.[31-35]

Fundamental characterization of the QD's surface and its relation with the photophysical properties has revealed that the emissive behavior of QDs is strongly dependent on the surface structure.[36] Thus, the interaction between an analyte and QD surface can be analyzed by monitoring the change in emissive behavior of the QDs after reacting with a specific analyte. This emission change would be due to the change in charge on the QD's surface after interacting with an analyte. The change in emissive behavior of QDs after interacting with a specific analyte is the basis of optosensors.

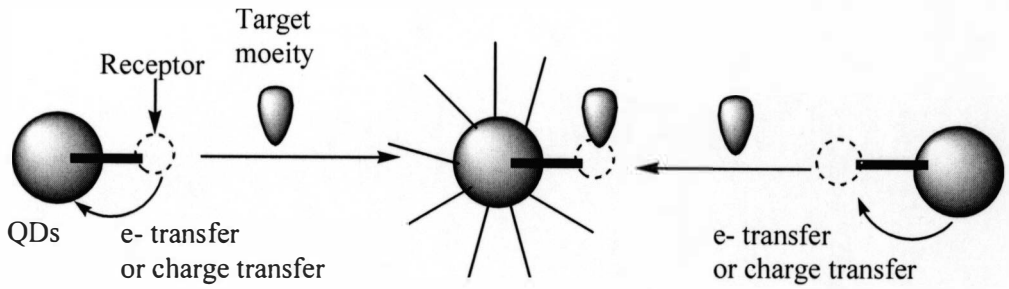

Figure 2.5 Represents the interaction of QD-receptor conjugated system with target molecule showing change in emission

Among the various types of QDs studied, core-shell type composite quantum dots show excellent photophysical properties to be of industrial, as well as lab-scale use.[37] Passivation of non-radiative recombination sites can improve the emissive properties of QDs. The change in the radius of NCs might change its quantum confinement which leads to the change in emission, as well as excitation wavelength of NCs. This can be calculated by the Brus eqation.

For example, a commonly used luminescent semiconductor, zinc sulfide (ZnS), having a band gap energy of approximately 3.6eV, when doped with another inorganic material such as Mn^{2+}, can be used as an optical probe for sensing purposes.[38] In this particular case, Mn^{2+} ions that are recombination centers for excitons show strong luminescent character. NCs of this type, when coated with inorganic material of high luminescence, would result in increased quantum yield and improved photostability. Due to their size dependent behavior, QDs of any size can be synthesized to get a desired wavelength's fluorescence. QDs having an absorption wavelength shorter than their emission wavelength show continuous absorption spectrum. Due to this property, an assembly of QDs conjugated with luminescent receptors can be excited by using one excitation source. Also, it distinguishes emission from the spectrum of a conjugated receptor

molecule. QDs can be excited at any wavelength shorter than their fluorescence as well as at any wavelength far way from the excitation of the acceptor molecule.[37-41]

2.8 Generation of Luminescence from QDs

When quantum dots are photo-excited, electron-hole pairs are generated and upon their recombination, fluorescent light is emitted. This generation of fluorescentt light can be explained as follows. In an ideal semiconductor crystal the ground state is occupied by a set of electrons which are called valence bands. These valence bands are separated apart from a set of unoccupied electronic energy levels called conduction bands. Conduction and valence bands are separated enough so that the crystal structure can be energetically stable. In the case of electronic excitation of these crystal structures a hole is created in the valence band due to the transition of an electron from its occupied energy level to the desired energy level in the conduction band. This process of the creation of an electron-hole pair generates a bound state known as exciton. The generation of exciton is the origin of luminescence.[30]

Even though QDs offer some of the most excellent properties which are a must for applications in optical detection systems, their use was limited by insolubility in aqueous solution and thus QDs needed to be coated or modified. These modified QDs show relatively better solubility in aqueous media. Overcoated or functionalized QDs became popular building blocks for chemosensors. An extremely promising idea of using QDs for optical sensing purposes is a reality at present and with continuous efforts by the scientific community, will definitely improve the idea and its applications in various fields.[28, 36]

2.9 Synthesis of ZnS:Mn/ZnS QDs

Synthesis of Manganese doped zinc sulfide:zinc sulfide core: shell (ZnS: Mn/ZnS) quantum dots (ZnS:Mn/ZnS (core/shell) ($1/16^{th}$) QDs).-

The ZnS:Mn/ZnS (core/shell) ($1/16^{th}$) QDs were synthesized by the following procedure modified from literature[42] and also was optimized in our lab. Zinc Dodecyl Sulfate ($Zn(DS)_2$) is a precursor salt required for synthesis of QDs.

Preparation of $Zn(DS)_2$- Zinc acetate hydrate $Zn(CH_3COOH)$ (4.39 g, 20 mmol) was dissolved in 100 mL of methanol and was added to the solution of Sodium dodecyl sulfate (SDS) (11.52 g, 40 mmol) in 200 mL of ethanol at $70^{o}C$. The resultant solution was heated for approximately 30 minutes until the total volume was reduced to ca.100 mL, then the reaction solution was cooled to room temperature. The solution was then vacuum filtered to obtain white crystalline solids which then were washed twice with 200 proof ethanol. This crystalline solid was then dried overnight in a vacuum desiccator over anhydrous $CaCl_2$. $Zn(DS)_2$ precursor salt prepared by the above discussed method was then used to synthesize QDs.

Synthesis of ZnS:Mn/ZnS (core/shell) ($1/16^{th}$)QDs- A doping solution of manganese sulfate ($MnSO_4$) was made by adding 0.015g of $MnSO_4$ into 1000 mL of milli-Q water. In a separate beaker, 100 mL of milli-Q water was added to which 0.039 g of sodium sulfide (Na_2S) was added and this solution was stirred for 15 minutes. After 15 minutes, 0.5 mL of $MnSO_4$ solution was added to the above solution which is followed by the addition of 0.2975 g of $Zn(DS)_2$ precursor salt. This solution was then allowed to stir for 30 minutes. After 30 minutes, 4 mL of this QDs solution was taken into a vial and checked for its UV-Vis absorbance and emission properties.

2.10 Results and Discussion

It is well known that the semiconductor NC's behavior is dependent on band gap energy, crystal lattice, and particle size. The excellent luminescent properties of QDs are due to the quantum confinement effect. Therefore it is reasonable to characterize them based on their optical properties.

2.11 Spectral Characteristics of ZnS:Mn/ZnS (core/shell) (1/16th) QDs

The above prepared ZnS:Mn/ZnS QDs were characterized for UV-Vis, excitation, and emission properties.

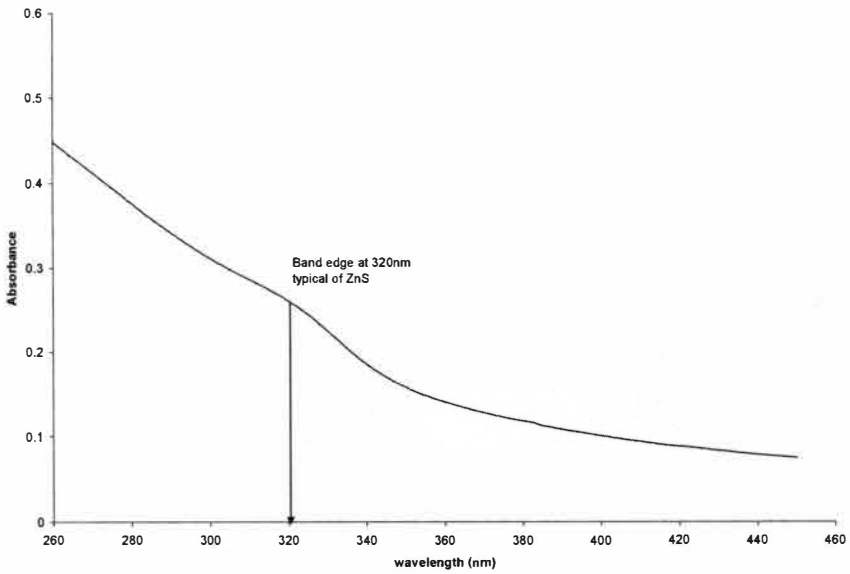

Figure 2.6 UV-Vis absorption spectrum of ZnS:Mn/ZnS QDs in CH_3CN

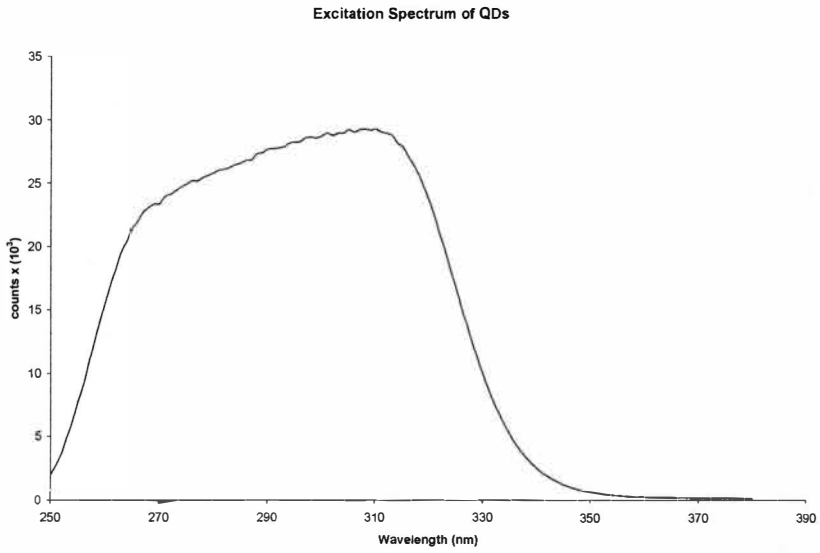

Figure 2.7 Excitation spectrum of ZnS:Mn/ZnS QD in CH_3CN

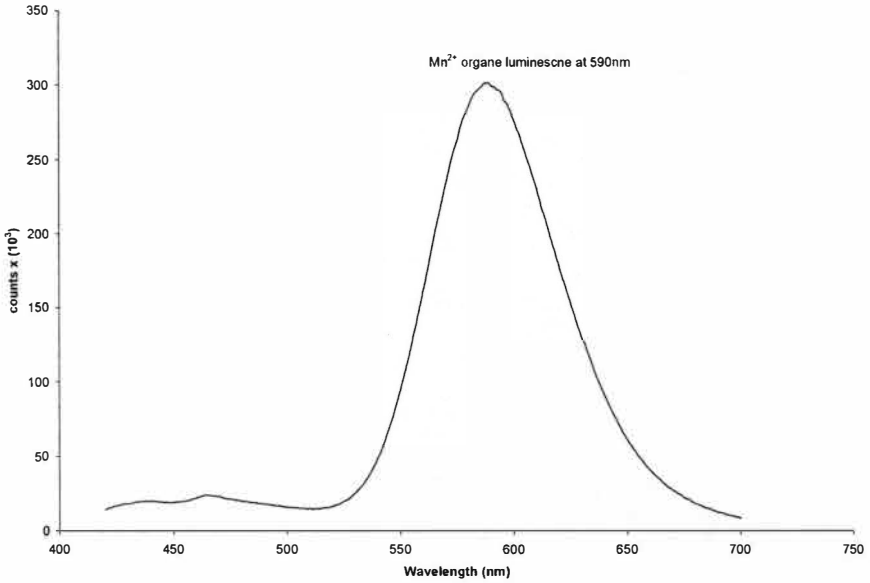

Figure 2.8 Emission spectrum of ZnS:Mn/ZnS QDs in CH_3CN

Figures 2.6, 2.7, and 2.8 show absorption, excitation, and emission spectra of ZnS:Mn/ZnS QDs respectively. In order to calculate the size of nanocrystals, a first order approximation given by the Brus equation can be used by knowing the band gap energy for ZnS:Mn QDs. For nanocrystals of Zns:Mn the relation is as follow.

$$r(E) = 0.32\text{-}0.29 * \sqrt{E\text{-}3.49}/2(3.50\text{-}E)$$

Based on this equation, assuming the band gap energy of ZnS:Mn nanocrystal 3.6eV, the size of QDs synthesized is calculated to be 3.2nm in radius.[40]

In figure 2.8 the emission spectrum showed a sharp, symmetric peak at 590nm, which is due to an orange luminescence originating from Mn^{2+} ion on Zn^{2+} sites. The mechanism explaining the orange luminescence from Mn^{2+} is given below.

In this particular type of ZnS:Mn/ZnS QDs, the d-electronic states of dopant Mn^{2+} ion provides luminescent centers while interacting with s-p electronic states of host ZnS which is generally the target of excitation source. This leads to faster energy transfer to d-electronic states of Mn^{2+} from the s-p electronic states of ZnS. When the ZnS lattice is doped with Mn^{2+}, it occupies Zn sites in the nanocrystal causing the radiative recombination between $^4T_1$-$^6A_1$ states. This radiative transition is of a much higher magnitude luminescent compared with bulk ZnS. To excite this tetrahedrally coordinated Mn^{2+} on ZnS the lattice, band-to-band excitation is used. This electronic interaction is the basis of energy transfer in QDs yielding high luminescent orange emission.[38, 40, 43, 44]

2.12 Interaction of ZnS:Mn/ZnS (core/shell)(1/16th) QDs with DCP, DMMP, and HCl

Before using QDs as a component of a nanosensor, their interaction with nerve gas analogs was monitored as a control experiment. During these experiments, dispersion of QDs in acetonitrile was achieved by sonicating for 30 minutes and UV-Vis absorbance was maintained below 0.25Abs to avoid the saturation effect. This solution was then reacted with various concentrations of DCP, DMMP, and HCl.

2.12.1 Interaction of ZnS:Mn/ZnS (core/shell)(1/16th) QDs with DCP

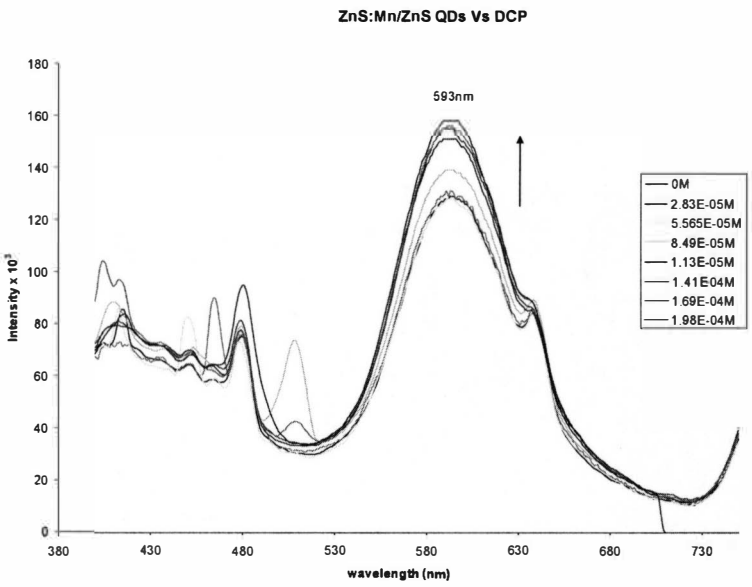

Figure 2.9 Shows interaction of QDs with different concentrations [2.83E-05M-1.98E-04M] of DCP

2.12.2 Interaction of ZnS:Mn/ZnS (core/shel)(1/16th) QDs with DMMP

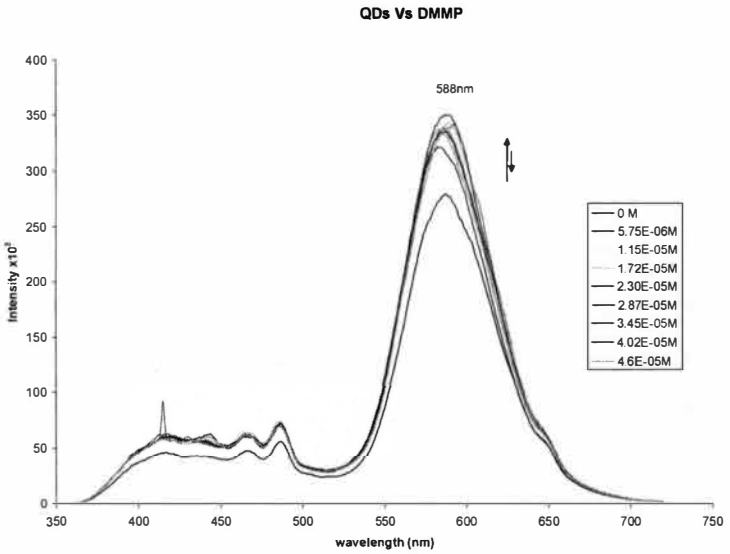

Figure 2.10 Shows change in emission intensity of QDs with varying concentrations [5.75E-06M to 4.6E-05M] of DMMP

2.12.3 Interaction of ZnS:Mn/ZnS (core/shell) (1/16th) QDs with HCl

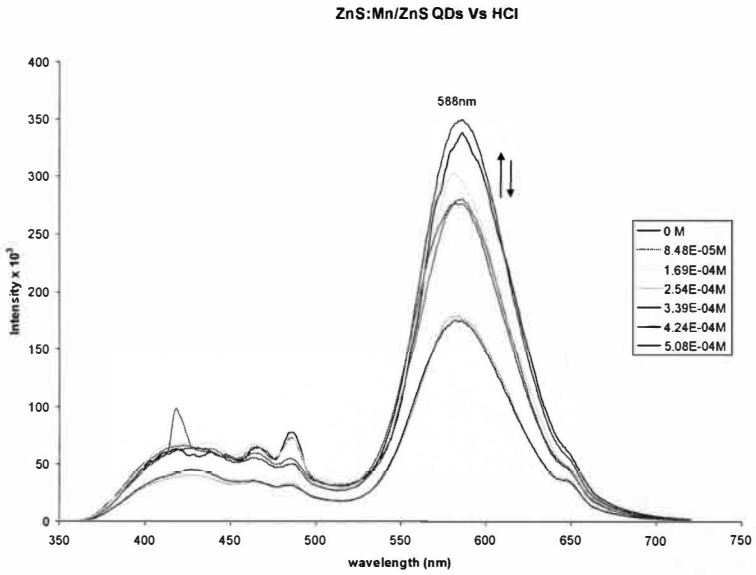

Figure 2.11 Shows change in emission intensity of QDs with different concentrations [8.48E-05M-5.08E-4M] of HCl

Figures 2.9, 2.10, and 2.11 represent change in emission intensity of ZnS:Mn/ZnS (core/shell) (1/16th) QDs after interacting with DCP, DMMP, and HCl. In the case of DCP reacting with QDs, figure 2.9 shows enhancement in emissive behavior at the emission wavelength of 590nm. A small peak at 410nm is due to undoped ZnS. This *"Switch-On"* type behavior shown by ZnS:Mn/ZnS (core/shell) (1/16th) QDs might be due to the change in energy of exciton resulting from surface passivation by DCP molecules. In the case of DMMP and HCl (figures 2.10, and 2.11) QDs showed irregular emissive behavior. This phenomenon needs to be addressed in detail with lifetime studies.

2.13 X-ray Diffraction Analysis of ZnS:Mn/ZnS (core/shell) (1/16th)

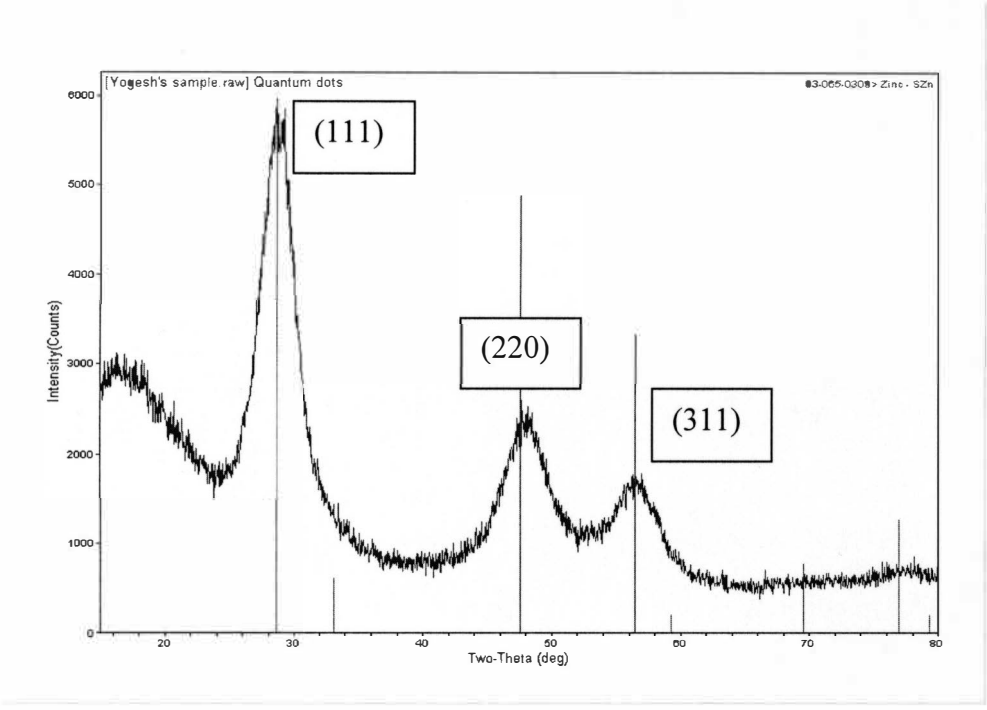

Figure 2.12 Shows XRD patterns of ZnS:Mn/ZnS QDs powder

Powder X-Ray diffraction was carried out on ZnS:Mn/ZnS QDs prepared as discussed in the Section 2.9. Figure 2.12 shows the wide angle X-ray diffractogram of powdered samples of ZnS:Mn/ZnS QDs. In the X-ray diffractogram showed above, it is easy to point out (111), (220), (311) planes of QDs meaning that the quantum dots are zinc blended phase cubic structures. The broader lines could be due to the finite size of QDs which indicates their nanocrystalline nature, except in the region of 2θ=16-20^{o}, which might be due to the amorphous phase present in the Na_2S.[45]

2.14 Introduction to Stilbene Compound

Initially developed for the synthesis of conjugated polymers, oligophenylene vinylene (OPVs) are gaining more attention recently for their use in chemosensing. In the last 20 years, research interest on developing OPVs has grown rapidly due to their excellent

optical-electronic properties which offer applications in technologies such as light emitting diodes (LEDs), solar cells, sensory systems and many more. OPVs have excellent charge transport properties, longer lifetimes, efficient light emitting properties, and better stability.[46, 47] The emissive properties of OPVs can be changed by altering the band gap which is highly dependent on the conjugation length of the oligomer.[48] For example, three conjugated ring OPVs have larger band gap than the five conjugated, and they emit at longer wavelengths.[49] Stilbene chromophores are members of the OPV family which are used in polymers as a brightener. The interaction between the excited state of stilbene and the ground state of the same is the reason behind the excellent optical properties of stilbene. Scientists have worked to improve the emissive properties of OPVs by altering the charge density as well as the electron density. Improved energy transfer along the backbone of stilbene allows the photoexcitation to emit a light of a particular wavelength. Higher quantum efficiency can be achieved by the efficient electron transfer from an excited state of an OPV to a lower unoccupied molecular orbital of an acceptor.[50, 51] Modified stilbene compounds are the best choice for applications in near UV-Vis light region. Due to their unique properties they can be considered as a component in the fabrication of novel chromo based sensors.[52] In fact, OPVs have been termed as electronic wires having a donor group at one end and acceptor group on the other, thus increasing their charge carrier mobility. They also show crystal structure dependent behavior.[53, 54] These highly emissive and stable optical platforms are considered as the building blocks of *"bottom-up"* technology.

2.15 Synthesis of Stilbene Compound (1S)

Among the many routes to synthesize alkenes, a Wittig synthesis is the most famous one. In a typical Wittig synthesis, a double bond is made by two conjugated carbon units and so highly complex and large molecules can be synthesized in an easy manner. Also, the position of the double bond is fixed in Wittig synthesis which not the case with other synthetic methods where the location of a double bond is an issue. This route also offers the possibility of attaching the desired functional groups to the central carbon chain.[55, 56]

In a different stepwise route followed by Yu *et al*, two different carbon units are coupled with an alkene conjugation. According to this method, the Heck reaction and the Horner-Wadsworth-Emmons reaction can be used to synthesize stilbene. Synthesis of a stilbene is done by utilizing only one monomer with a phosphonate ester group in one end and a acetal-protected aldehyde in the other. The conjugation of the two separate units can be achieved by the Horner-Wadsworth-Emmons reaction after which deprotection of an aldehyde is performed.[53] Stilbenes have a tendency to aggregate through π- π* interactions and this property makes them ideal candidates for the design of self-assembling sensor devices.

Synthesis - In a 100 mL round bottom flask, α-Bromo-*p*-toluic acid (100 mg) (0.465 mol) was dissolved in 50 mL of anhydrous toluene and then $P(OEt)_3$ (0.089 mL) (85 mg) (0.512 mol) (1.1 eq) was added to the solution. The resulting reaction mixture was refluxed for 14 hours. After 14 hours, this reaction mixture was cooled down to room temperature to form white crystals of the desired compound (1I). Compound (1I) (100 mg) (0.36 mol) was then dissolved in freshly distilled THF, with vigorous stirring in a round bottom flask. After 30 minutes, terepthaldehyde *mono*-(diethyl acetal) (76 mg)

(0.36 mol) (73 µL) was added and this reaction mixture was refluxed for 30 minutes. In this reaction mixture, potassium *tert*-butoxide (49 mg) (0.43 mol) was added and the reaction was allowed to be refluxed for 14 more hours to obtain compound (2I). Compound (2I) is then subjected to acidification with HCl (6 N, 10mL approx.) until the pH of the solution reached 2. After this point the reaction mixture was stirred for two hours. The solvent (THF) was removed by rotary evaporation and the obtained solid was washed several times with water, ethanol and with ether. This mixture was then filtered to obtain a new yellow colored solid and was named (1S). The overall yield of this reaction was found out to be 53 %. Schematic representation of synthesis of (1S) compound is shown below:

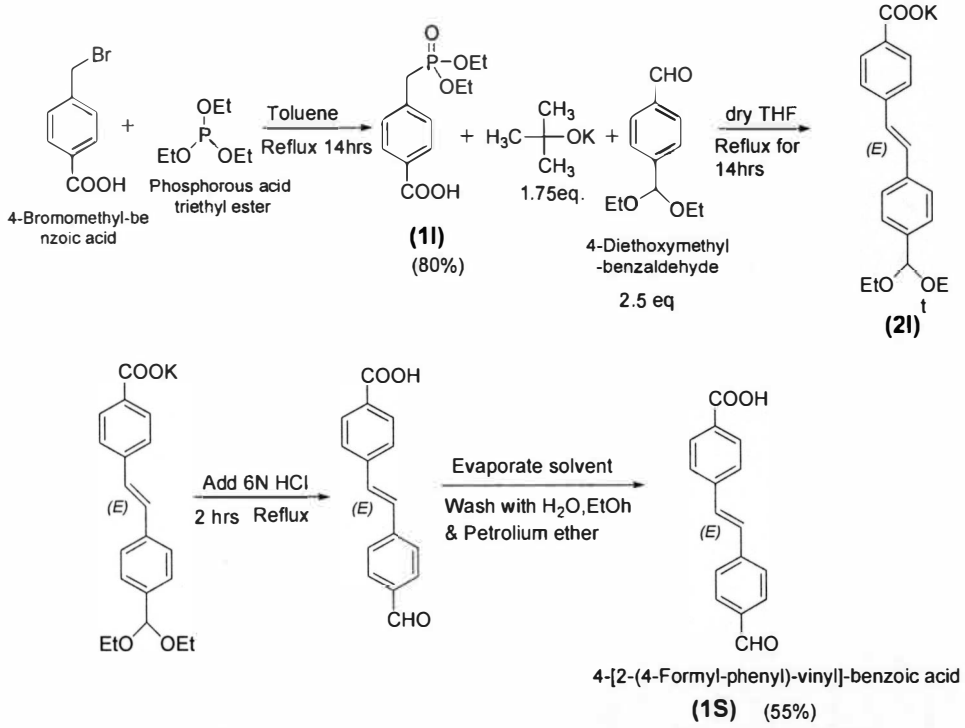

Scheme 2.2 Synthetic scheme of preparation of compound (1S)

2.16 Results and Discussion

The most critical step in the synthesis of the compound (1S) shown in scheme 2.1 is the formation of the intermediate (2I). The intermediate compound (2I) formation is based on the Arbuzov reaction. It was observed that this synthetic route is highly sensitive to air and moisture. THF used in this reaction was freshly distilled. The reagent in this reaction p-*tert*-BuOK should be dry enough so that it should not bring moisture to the reaction. At the end of the reaction, THF should be removed via rotary evaporated and the final product should be washed with plenty of water, ethanol and ether. The washed product is then dried in a vacuum oven before characterizing it.

The stilbene compound (1S) prepared was characterized by ^{1}H NMR and its optical properties.

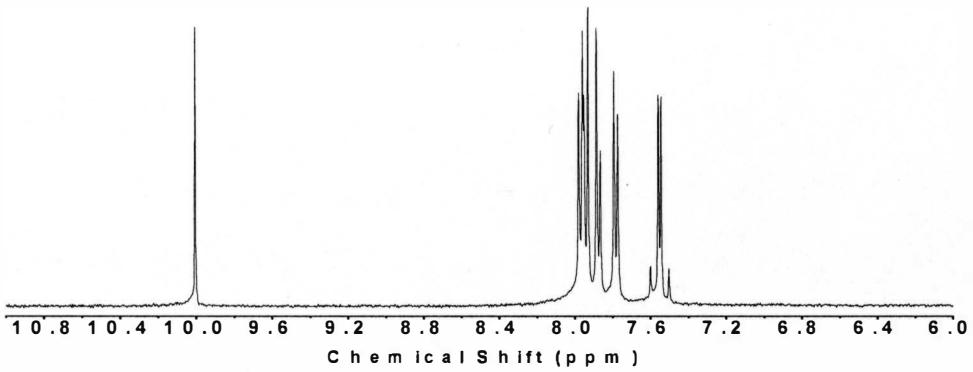

Figure 2.13 ^{1}H NMR of stilbene compound (1S) taken in DMSO-d_6

^{1}H NMR (DMSO-d_6, 400MHz) δ: 7.50-7.60 (q. 2H), 7.7-8.0 (4d, 8H), 10.0(s,1H)

2.17 Spectral Characterization of Compound (1S)

The photophysical properties of stilbene like compounds are extremely promising for optoelectronic devices since OPVs possess highly conjugated π-π * interactions which are a good source of generating optical events in the optoelectronic devices. In the process of generating optical events based on the change in emission intensity of stilbene like compounds, formation of excimers, solvent media, and aggregation of molecules are very crucial factors. Therefore, characterizing OPVs by their optical properties is useful for developing optical probes or optical sensors. Spectral studies were performed with a solution containing acetonitrile (CH_3CN) and compound (1S) with a of concentration 4 X 10^{-6} M. The below mentioned are UV-Vis, excitation, and emission spectra of compound (1S).

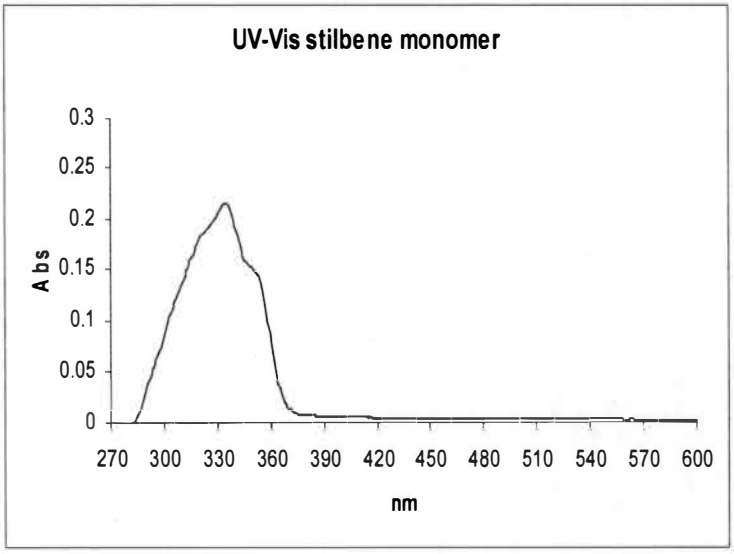

Figure 2.14 UV-Vis spectrum of stilbene (1S) in CH_3CN

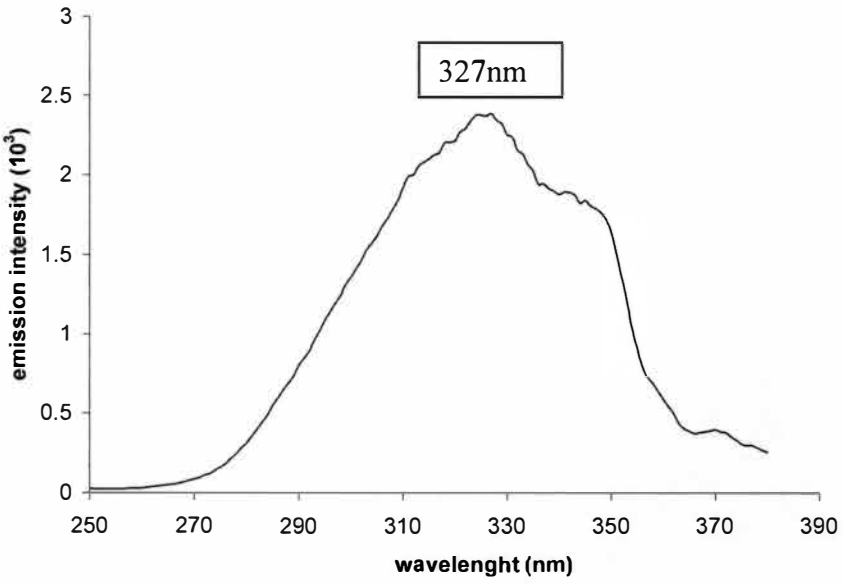

Figure 2.15 Excitation spectrum of compound (1S) in CH_3CN, λ_{max}= 439nm

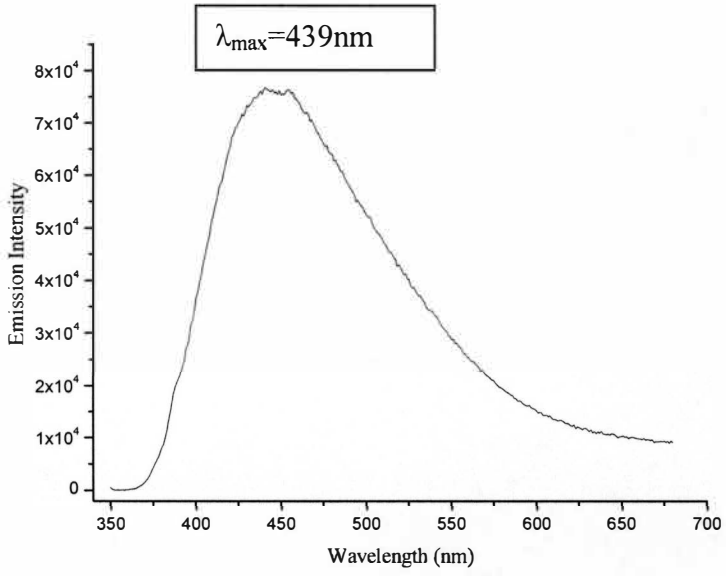

Figure 2.16 Emission spectrum of compound (1S) in CH_3CN, excited at 339nm

The emission spectrum of compound (1S) in the figure 2.16 shows a peak at 439nm which is due to the π-π* interaction between highly conjugated stilbene. After exciting an electron in the conjugation system of compound (1S) the electron occupies an excited

state and while returning back to the ground state this excited electron emits light in a radiative way through intersystem crossing. Energy migration occurring along the backbone of compound (1S) facilitates the process of photoluminescence.[50]

CHAPTER III

RECEPTORS

3.1 Introduction to Receptors

Development of highly fluorescent, and target selective receptors is rapidly growing to satisfy the need of sensing technology. In the last couple of years a whole plethora of various receptors specific to target molecule was developed. The principle behind designing a receptor specific to a target molecule is interaction between a functional group attached to a receptor and a target moiety, where this interaction generates various detectable changes into the sensory system. Depending on the formation of a leaving group which occurs because of the interaction between a receptor and a target molecule, the efficiency of a sensor can be determined. This approach of having a reactive functional group at the end of the receptor molecule offers the possibility of tuning optical behavior and time response of the sensor.[3] The association of a receptor molecule with an organophosphate agent causes change in the fluorescence response and either the signal enhancement or signal quenching can be monitored. The association of a receptor molecule and an analyte increases quantum yield. These processes of observable differences in emissive nature of receptor after interacting with analyte molecule is due to either the alteration in electron density distribution or electron transfer between them. The energy transfer, electron transfer, and alteration of electron density causes signal transduction which is then observed on electronic display device. The conjugation length of receptor molecule can be engineered to modulate the emissive response of receptor.[31] These changes can be monitored in a number of ways based on sensory system. Most of the receptor molecules used in the detection of nerve gas agents is based on a principle of

forming a hydrogen bond with the target molecule by acting either as a donor or as an acceptor. The positively charged receptor groups can easily interact with negatively charged phosphonate group of nerve gas agents. In fact, numerous receptors have been developed on the basis of interaction of nerve gas agent with acetylcholine enzyme.[57]

3.2 Synthesis of Receptors

Schiff's bases are among the most widely used receptors. The imine group is well studied because it's found in most of the natural products. In a typical Schiff's base reaction, an amine reacted with an aldehyde in a suitable solvent in the presence of an acidic catalyst yields imine group or Schiff's base. In the reaction of Schiff's base synthesis, formation of water and pushing the reaction towards product are important steps and an acidic catalyst helps in achieving these steps.[42]

In the present study described here, two receptors, namely Receptor-I and Receptor-II were synthesized by using a standard method used to synthesize Schiff's base. In a synthetic scheme mentioned below; ethanol was used as a reaction solvent since most of the Schiff's base reactions reported in the literature suggests use of protic solvents such as ethanol.[58] However, the same reaction of synthesis of Receptor-I and II was performed in acetonitrile in order to confirm the documented results, unfortunately the reaction did not progress and did not yield desired compound.

3.3 Synthesis of Receptor-I

In a 100 mL clean round bottom flask, compound 1S (50 mg) (0.1984 mol) was dissolved in 30mL heated ethanol. After almost complete dissolution of compound 1S, (35 mg) (0.2427 mol) of 5-aminoisoquinoline was added to the reaction mixture and 15 mL ethanol was added to the same, followed by addition of three drops of acetic acid (99.7 %) which acts as a catalyst in Schiff's base formation. The reaction scheme of synthesis of Receptor-I is as shown in scheme 3.1

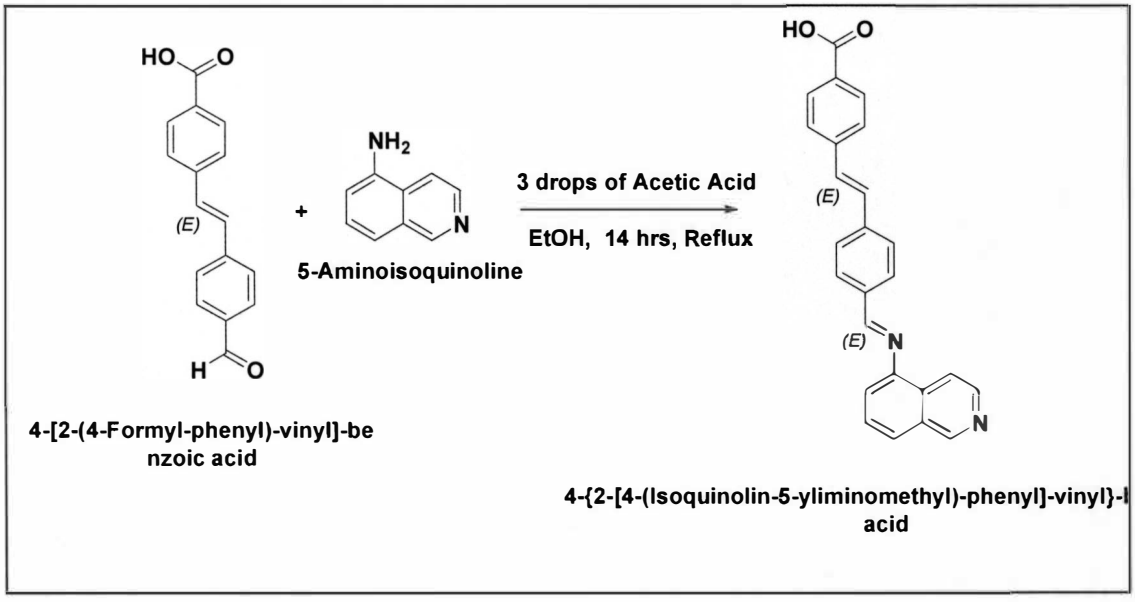

Scheme 3.1 Synthesis of Receptor-I

(Receptor-I = 4-(2-[4-(Isoquinolin-5-yliminomethyl)-phenyl]-vinyl)-benzoic acid)

3.4 Results and Discussion

The above formed Receptor-I was characterized by using analytical techniques ^{1}H NMR and Liquid chromatography/mass spectrometry (LC/MS).

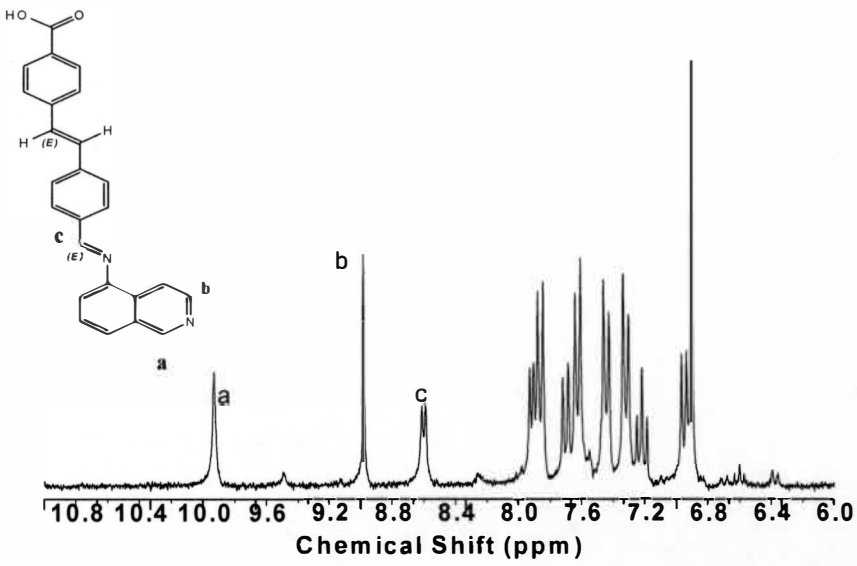

Figure 3.1 ^{1}H NMR of Receptor-1 in DMSO-d_6

^{1}H NMR peak assignment: (1s-1H-9.35ppm), (1s-1H-8,7ppm), (1s-1H-8.5ppm), (1q-4H-8.15ppm), (2d-4H-7.96ppm-8.01ppm), (3d-6H-7.54ppm-7.87ppm).

The formation of Receptor-I was confirmed by observing a peak at 8.7ppm which is typically an imine bond formation characteristic. Also, absence of an aldehyde peak at 10.00ppm further confirms that no stilbene compound (1S) is left unreacted.

In order to confirm the formation of Receptor-I, liquid chromatography mass spectrometry (LC-MS) was used. Below shown is the LCMS spectrum of Receptor-I

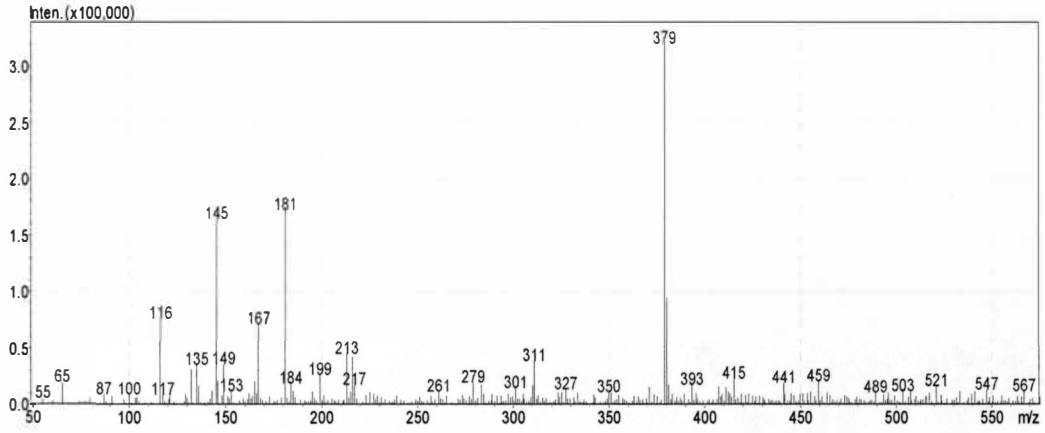

Figure 3.2 LC-MS spectrum of Receptor-I in methanol

In the above shown LCMS spectrum by negative ion mode of Receptor-I, molecular ion peak at (m/z =379) confirms the formation of Receptor-I (molecular weight=380).

3.5 Spectral Characterization of Receptor-I

As mentioned earlier, luminescent molecules such as organic dyes, OPVs show excellent emissive properties depending upon the oligomer length as well as the extended π-conjugation. In order to use Receptor-I in the sensor assembly its spectral characteristics need to be analyzed. Spectral properties of Receptor-I are shown below:

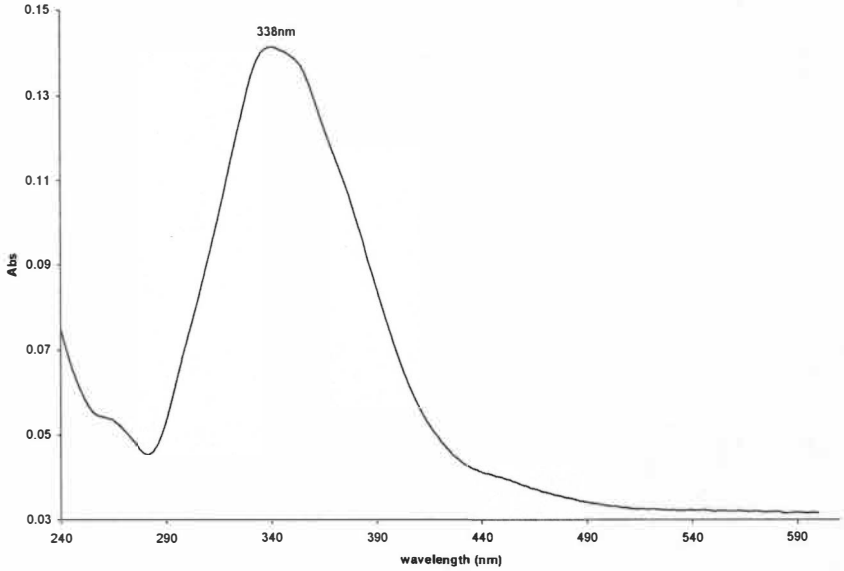

Figure 3.3 UV-Vis absorption spectrum of Receptor-I in CH_3CN, emission λ_{max}=434nm

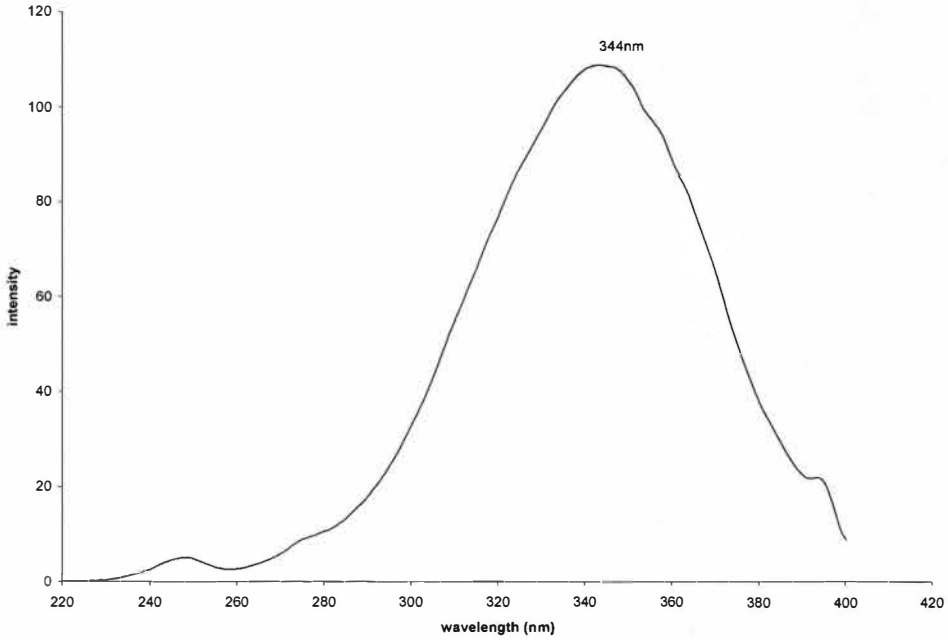

Figure 3.4 Excitation spectrum of Receptor-I in CH_3CN, λ_{max}=434nm

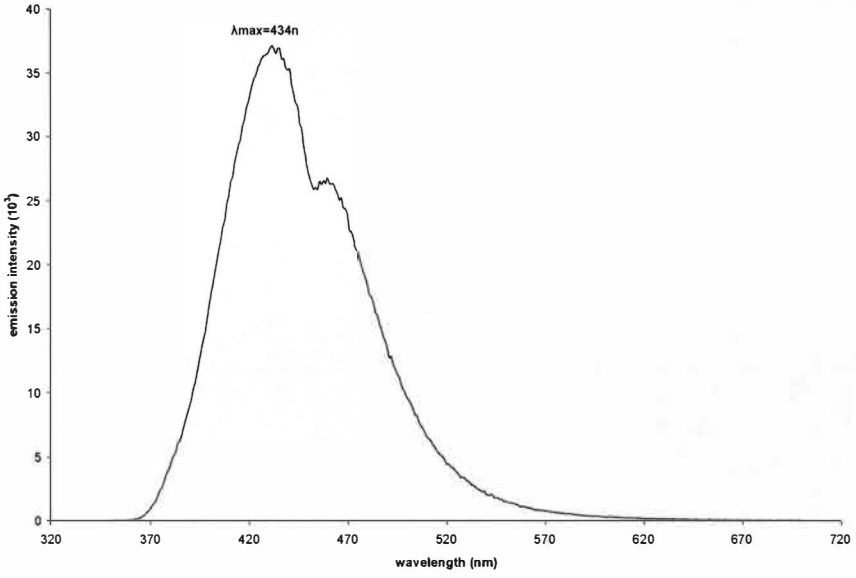

Figure 3.5 Emission spectrum of Receptor-I in CH_3CN, excited at 339nm

Figures 3.3, 3.4, and 3.5 show UV-Vis absorption, excitation and emission spectra of Receptor- I respectively. The UV-Vis absorption spectrum shown here is almost similar to that of stilbene compound (1S) with small change in the shape. This modification in

UV-Vis spectrum might be due to increase in the conjugation of the molecule. The excitation spectrum of Receptor-I shows a peak at 344nm which is nearly same as the excitation spectrum of the compound (1S). The emission spectrum of Receptor-I shows emission maxima at around 434nm which is shifted towards red color when compared to emission spectrum of compound (1S). This quenching may be attributed to intersystem crossing between triplet state or to the relaxation of the excited state. When aromatic compounds of a highly conjugated system are linked with amino groups, quenching does occur due to above mentioned reason.[59] This redshift can also be attributed to shorter band gap energy due to the increased conjugation.[49]

3.6. Interaction of Receptor-I with Nerve Gas Analogs as a Control Experiment

In order to check the efficiency of Receptor-I as one of the building blocks of nanosensor towards detection of nerve gas analogs; various concentrations of nerve gas analogs (DCP, DMMP, and HCl) were reacted with known concentration of solution of Receptor-I [9.27E-06M] in acetonitrile. The interaction between nerve gas analogs and Receptor-I was monitored by change in its emission behavior.

3.6.1 Interaction of Receptor-I with DCP

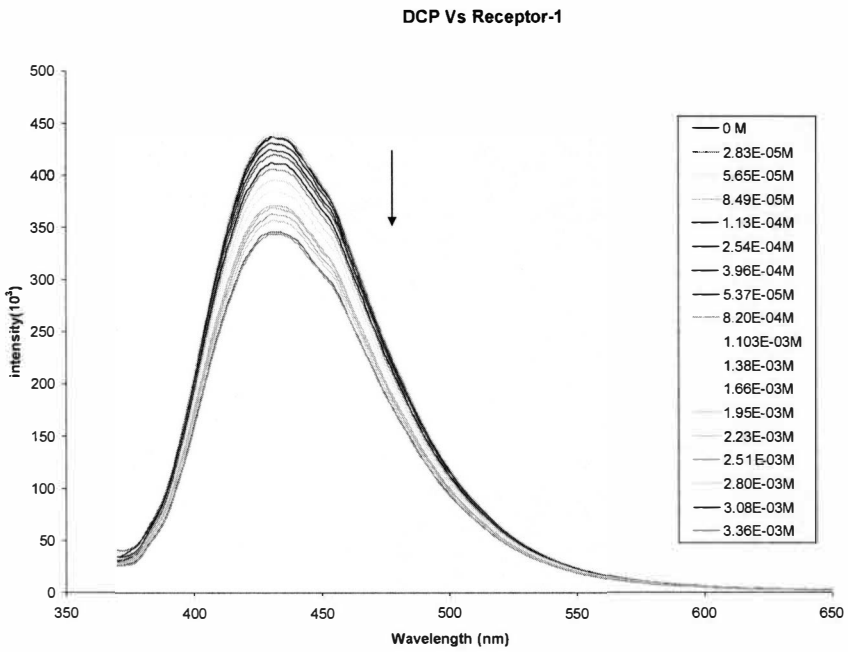

Figure 3.6 Change in emission intensity of Receptor-I [9.27E-06M] with various concentrations [2.83E-05M to 3.36E-03M] of DCP

3.6.2 Interaction of Receptor-I with DMMP

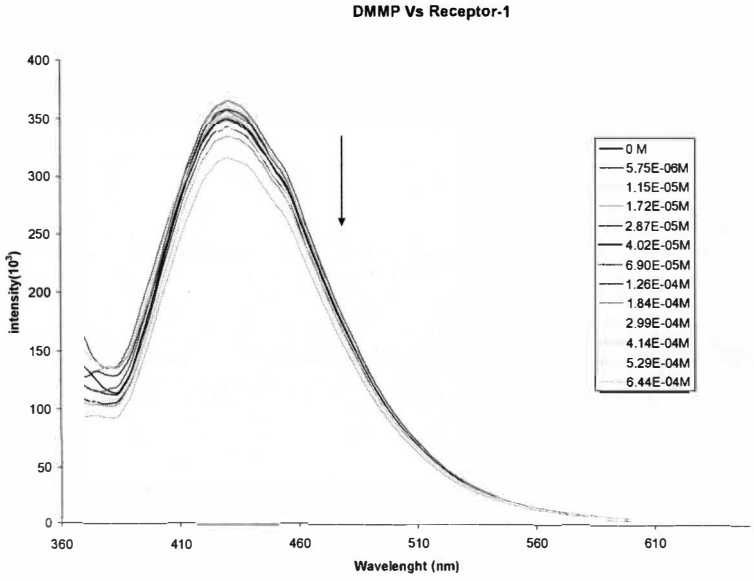

Figure 3.7 Change in emission intensity of Receptor-I [9.27E-06M] after adding various concentrations of 5.75E-05M to 6.44E-4M] of DMMP

3.6.3 Interaction of Receptor-I with HCl

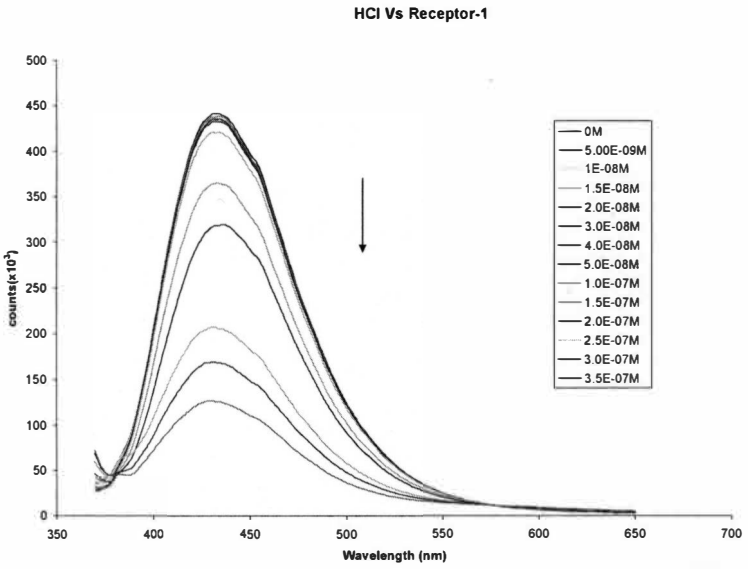

Figure 3.8 Change in emission intensity of Receptor-I [9.27E-06M] after interacting with various concentrations of [5.00E-09M-3.5E-07] HCl

Figures 3.6, 3.7, and 3.8 shown above represent change in emission intensity of Receptor-I after interacting with various concentrations of DCP, DMMP, and HCl respectively. Figure 3.6 shows quenching of emission intensity after the interaction between Receptor-I and DCP occurs. This quenching may be attributed to adduct formation between amine group of Receptor-I and DCP. Here the lone pair on nitrogen plays an important role by changing the electron density near an adduct. Though there is quenching in emission intensity, the emission maxima did not change. Also the shape of spectrum did not show any change in it. In case of DMMP interaction with Receptor-I, the change in emission intensity was smaller compared to the interaction of DCP with Receptor-I. This is not surprising because DMMP is not expected to form a leaving group as easily as DCP and hence might not be able to form adduct quickly enough. Surprisingly, HCl showed better interaction with Receptor-I as compared to both DCP, DMMP. This might be due to

decrease in the pH after addition of HCl to Receptor-I solution. By lowering the pH, HCl quenches fluorescence of adduct.[6] None of the nerve gas agents changed emission maxima nor the shape of emission peak after interacting with Receptor-I

3.7 Association Equilibrium Constant Calculations

In order to quantify the interaction of Receptor-I with various nerve gas analogs such as DCP, DMMP, and HCl, the association equilibrium constants were calculated by using a C/I model. C/I model works on a principle that change in emission intensity of Receptor-I after measured additions of nerve gas agents is directly related to the concentration of nerve gas agents. Unlike other models, the C/I model can be used to find out the association constant between the nerve gas analog and Receptor-I regardless of the enhancement or the quenching in emission intensity. Also, the earliest methods of detecting nerve gas agents were based on the same principle. In the case of emission quenching; the association constant can be calculated by using following equation: $I/[R] = \alpha + K[T]$ where I=intensity, [R]= conc. of Receptor, K= association constant, [T]= conc. of nerve gas analog, α= intercept of from the linear plot of I/[R] Vs [T].

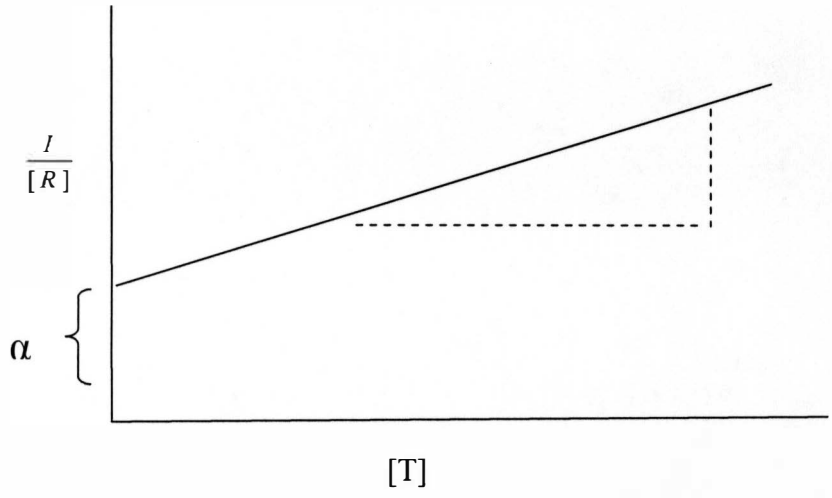

Figure 3.9 Shows linear plot of change in emission intensity divided by concentration of receptor I/[R] Vs different concentrations of nerve gas analog [T]

By plotting the above shown graph, the association constant can be calculated by multiplying the slope and intercept.

In case of emission enhancement, to calculate the association constant, a plot of conc. of receptor [R] divided by change in emission intensity I Vs conc. of nerve gas analog [T].

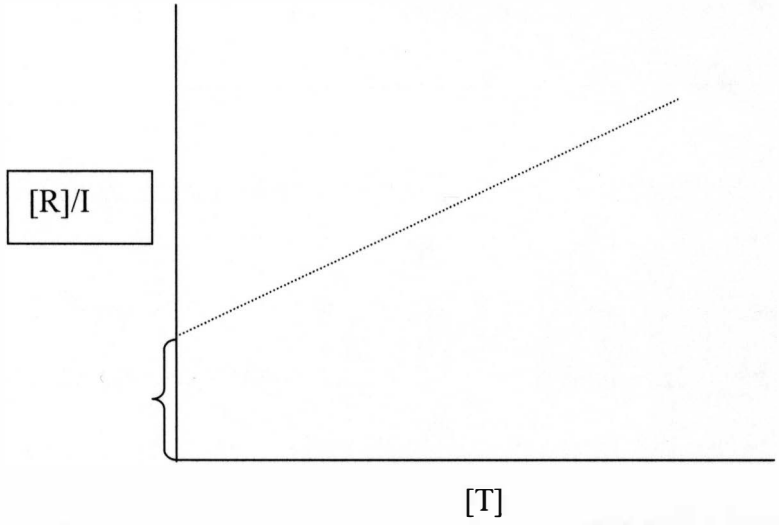

Figure 3.10 Represents a linear plot of receptor conc. [R] divided by change in emission intensity I Vs conc. of nerve gas analog [T]

In order to calculate the association constant between the receptor and nerve gas analog when there is enhancement in the emission intensity; slope from the above graph divided

by intercept will result in association constant. Association constant suggests the strength of the interaction between receptor and nerve gas analogs, i.e. larger the association constant, stronger the interaction. Association constants for interaction between Receptor-I and nerve gas analogs DCP, DMMP, and HCl are calculated by using the C/I model and are shown below:

3.7.1 Association Constant of Receptor –I with DCP

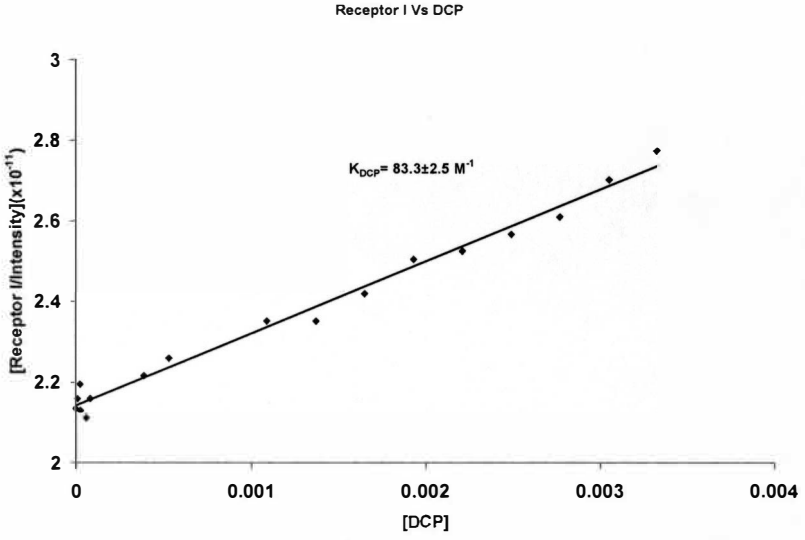

Figure 3.11 Association constant plot of Receptor-I Vs DCP

3.7.2 Association Constant Plot of Receptor-I with DMMP

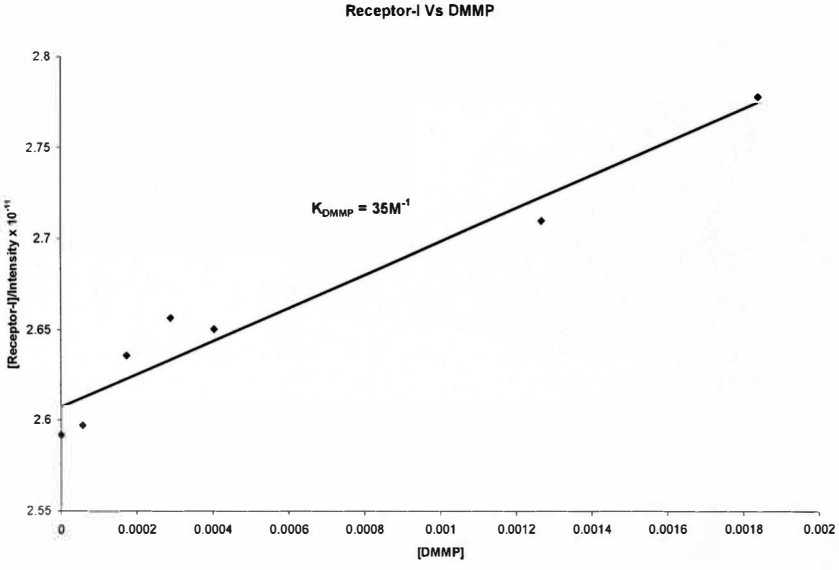

Figure 3.12 Association constant plot of Receptor-I Vs DMMP

3.7.3 Association Constant of Receptor-I with HCl

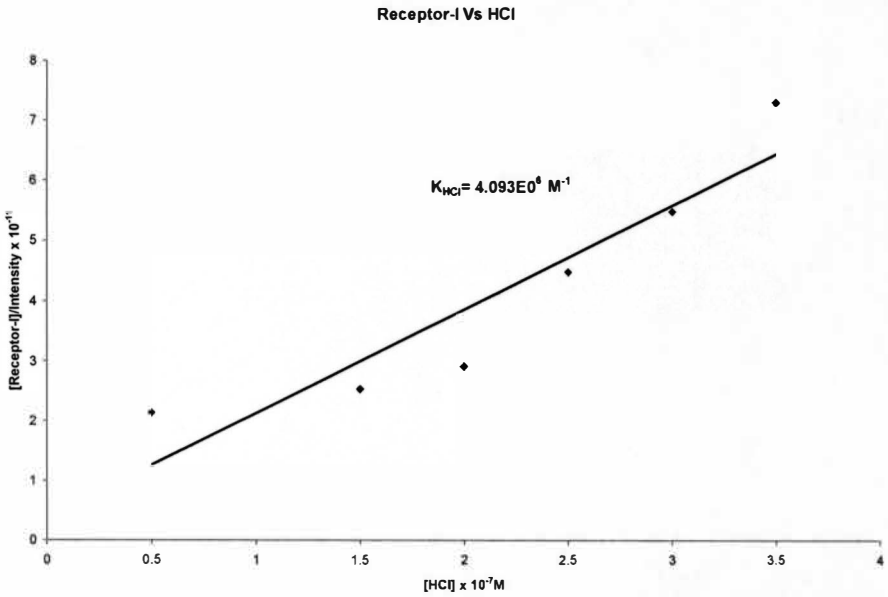

Figure 3.13 Association constant plot of Receptor-I Vs HCl

Summary of association constants of Receptor-I Vs nerve gas analogs:

Table 3.1 Association constants of Receptor-I after interacting with nerve gas analogs

	K_{DCP} M^{-1}	K_{DMMP} M^{-1}	K_{HCl} M^{-1}
Receptor I	83.3±2.5	35	$4.0390x10^{6}$

The association constant values mentioned above indicates interaction of nerve gas analog with Receptor-I. These association constant values are based on C/I model and the values of slope and intercept are calculated by using regression analysis of data points either/or equation of line method. However, these values still indicate strength of interaction between Receptor-I and nerve gas analogs. From the summary of association constants shown above (table 1.2) DCP and DMMP did not show higher association constants as compared to HCl. The weak association of DCP with Receptor-I could be due to the decrease in pH caused by formation of HCl during the interaction. However, in the case of HCl, the association constant is very high compared to DCP and DMMP. This

might be attributed to electronegativity of chlorine which makes phosphonyl a very strong electrophyle and thus can form a strong leaving group.[60] The process of formation of leaving group shows quenching in the emission intensity of Receptor-I. It was observed that higher concentrations of HCl were suddenly quenching the emission intensity to a very low value. This feature could not be addressed based on the studies performed.

Overall, Receptor-I showed considerable interaction with HCl as compared to DCP and DMMP where the interaction was relatively weak. However, in each case the quenching of emission intensity of Receptor-I was observed.

3.8 Emission Lifetime Study of Receptor-I

The ability of a chromophore such as Receptor-I to form an excimer by changing its electron distribution among the excited and ground state can be understood by analyzing the lifetime of excimer formed. Fluorescence decay or lifetime of an excimer formed would be able to provide more information about the interaction between Receptor-I and nerve gas analogs. In the same regard, emission lifetime studies were performed on Receptor-I. In order to perform lifetime studies on Receptor-I a solution of Receptor-I in CH_3CN was used. The excimer formation was achieved by exciting electron from an external source either hydrogen or laser lamp. In case of Receptor-I hydrogen lamp was used as excitation source. The emission lifetime study of Receptor-I is shown below:

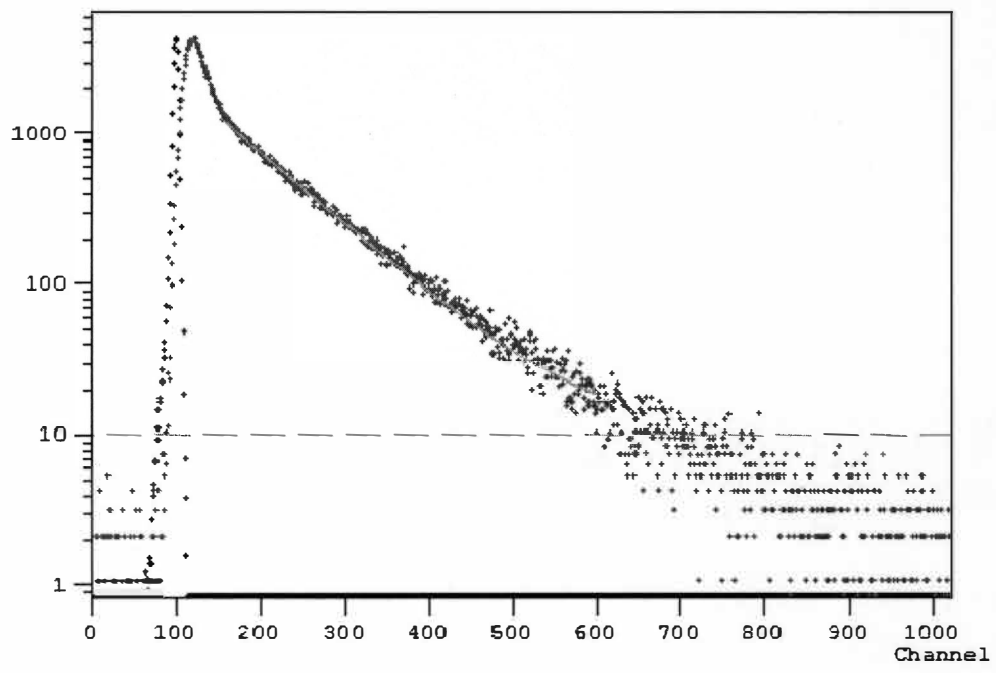

Figure 3.14 Emission lifetime decay of Receptor-I excited at 339nm, λ_{max}= 434nm

Lifetime decay of Receptor-I (Figure 3.14) shows two lifetimes of Receptor-I, however shorter lifetime (below 0.5ns) is because of exponential fitting of curve and this lifetime falls into the time of rise of excimer and thus need not be considered but for application purpose; but it should be considered for mathematical fitting of the curve to obtain the actual lifetime of excimer. The fluorescence lifetime data obtained by instrument was then exponentially fitted with the help of the software (F-900) to obtain the actual values of lifetime. The normalized fluorescence data was obtained by using Discrete Component Analysis (Tail-fitting) method and results obtained are as follows:

Table 3.2 Normalized fluorescence decay of Receptor-I

χ^2 1.188

Exp Num	B	F	τ (ns)
1	1256.	100.0	8.850

The above shown result of emission lifetime decay of Receptor-I showed that it has a lifetime of 8.85ns. This lifetime is attributed to π-π^* interaction between ground state and

the excited state of excimer. The excited electron undergo radiative decay by emitting fluorescence giving rise to an excimer which has a lifetime of 8.85ns in case of Receptor-I. Organic receptors based on stilbene compounds having higher conjugation are expected to have lifetime in the range of 5-10ns.[55]

The analysis of Receptor-I for its performance as an optical probe, shows that Receptor-I can be used in further research as a building block of nanosensor.

3.9 Receptor-II

In order to synthesize different receptors and check their efficiency as a sensing probe in a nanosensor; Receptor-II was prepared. Receptor-II and Receptor-I falls in the same category of organic compounds i.e. Schiff's base type organic compounds. Though Receptor-II was synthesized by reacting stilbene compound (1S) with the 4-aminophenylhexafluoropropanl it has a free group (OH) different than the free group (:N) of Receptor-I. Therefore Receptor-II is expected to behave in a different manner as compared to Receptor-I.

3.10 Synthesis of Receptor-II

In a 100 mL clean round bottom flask, compound 1S (50 mg) (0.1984 mol) was dissolved in 30mL heated ethanol. After almost complete dissolution of compound 1S, (35 mg) (0.2427 mol) of 4-aminophenylhexafluoropropanol was added to the reaction mixture and 15 mL ethanol was added to the same, followed by addition of 3 drops of acetic acid (99.7 %) which acts as a catalyst in Schiff's base formation. The reaction scheme of synthesis of receptor-II is shown as below:

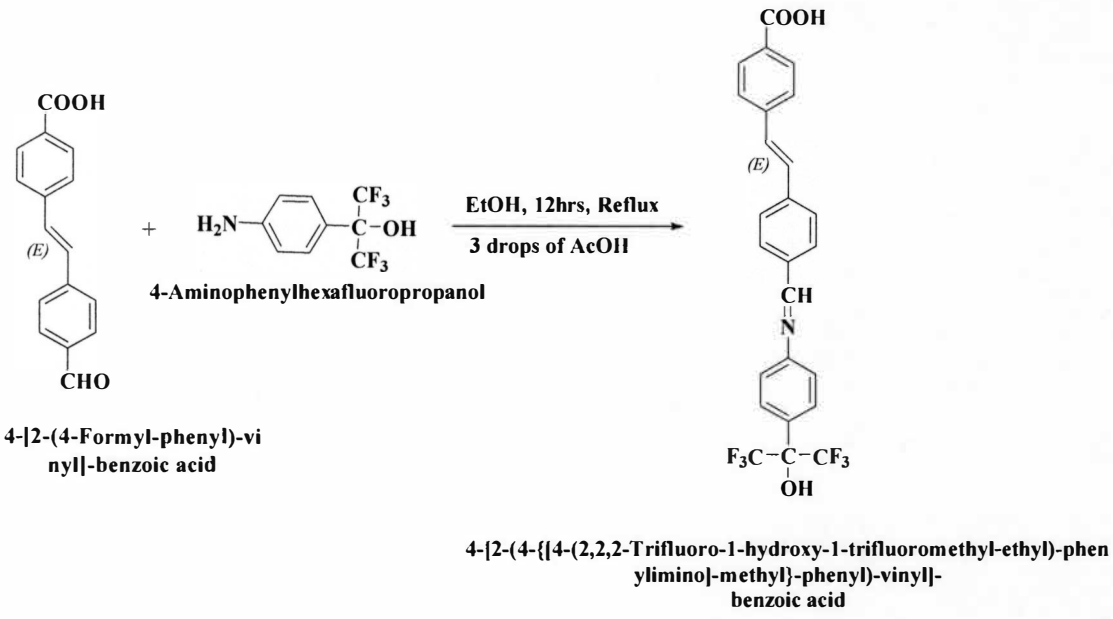

Scheme 3.2 Synthesis of Receptor-II

(Receptor-II = 4-[2-(4-([4-(2,2,2-Trifluoro-1-hydroxy-1-trifluoromethyl-ethyl)-phenylimino]-methyl)-phenyl)-vinyl]-benzoic acid)

3.11 Results and Discussion

The above prepared Receptor-II was characterized by using ^{1}HNMR and Liquid chromatography mass spectrometry (LCMS). In the below shown ^{1}H NMR, absence of aldehyde peak (10.00ppm) of stilbene compound confirms the completion of reaction. Also, a new peak at 8.7ppm is due to formation of imine bond between aldehyde of stilbene compound (1S) and 4-aminophenylhexafluoropropanol.

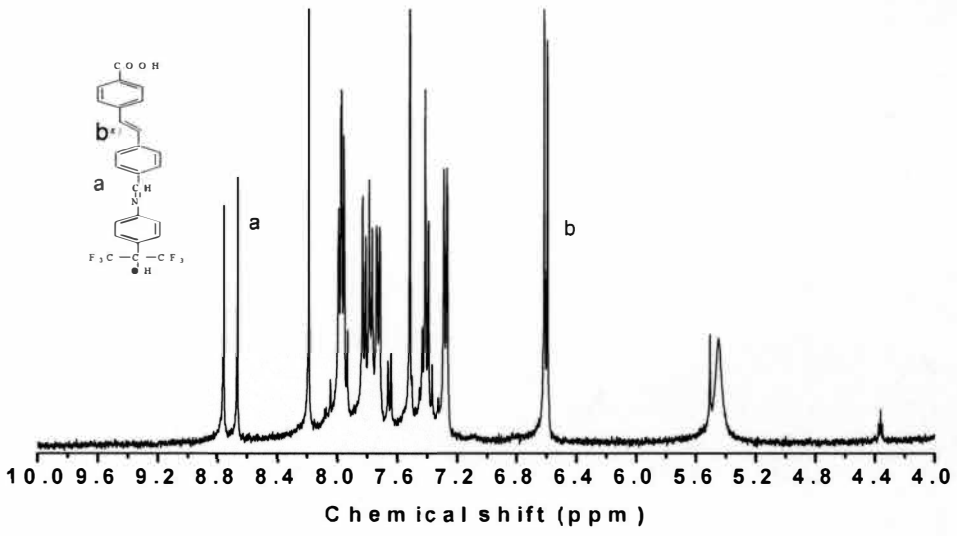

Figure 3.15 ^{1}H NMR of Receptor-II in DMSO-d_6

^{1}H NMR peak assignment: (1d-1H-8.7ppm), (1d-2H-6.6ppm), (md-12H-7.2ppm-8.1ppm), (1s-1H-5.5ppm).

Further confirmation of result obtained by ^{1}H NMR is achieved by doing LCMS analysis of Receptor-II. Below shown is the LCMS result of Receptor-II dissolved in MeOH

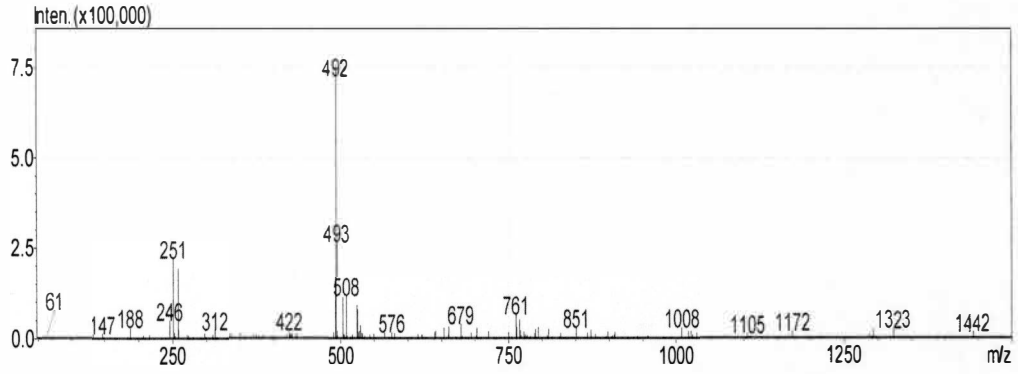

Figure 3.16 LCMS of Receptor-II

The above shown LCMS spectrum of Receptor-II indicates molecular ion peak at m/z = 492 when the instrument was under negative ion mode. This molecular ion peak at 492 confirms the formation of Receptor-II having molecular weight 493.

3.12 Spectral Characterization of Receptor-II

In order to use Receptor-II as an optical probe in nanosensor to detect nerve gas analogs, its spectral properties such as UV-Vis absorption, excitation, and emission were analyzed. Spectral studies were performed in solution of Receptor-II in acetonitrile (CH_3CN) having final concentration of Receptor-II [1.01E-05M]. Also interaction of Receptor-II with nerve gas analogs was studied as is mentioned below:

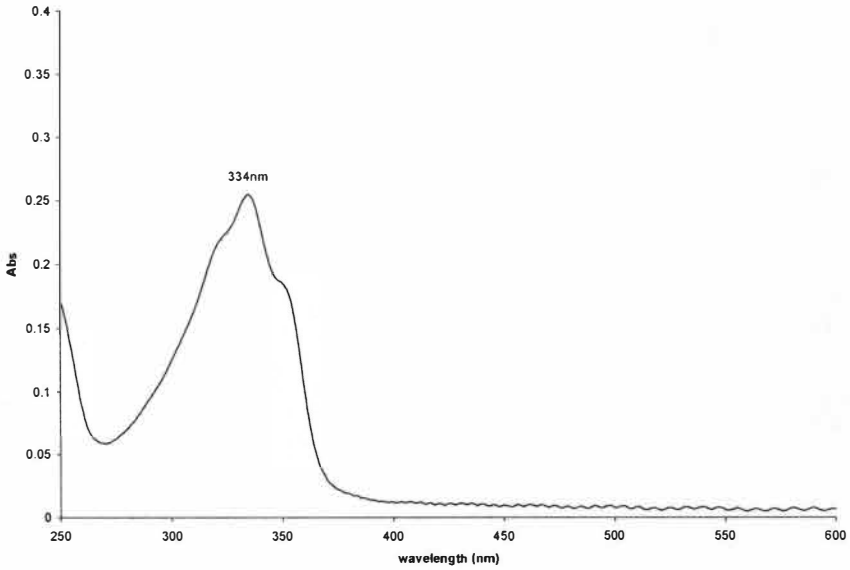

Figure 3.17 UV-Vis absorption scan of Receptor-II in CH_3CN

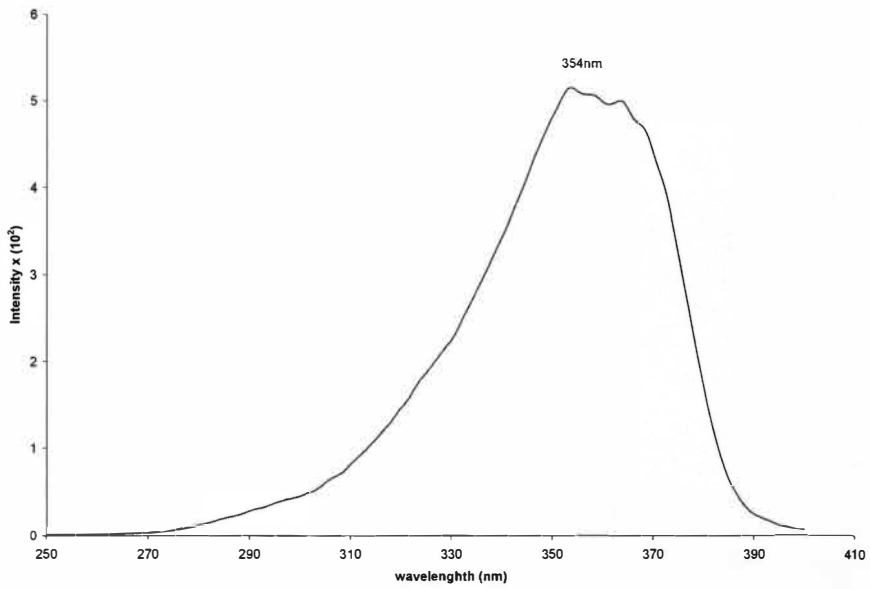

Figure 3.18 Excitation spectrum of Receptor-II in CH_3CN, emission maxima=409nm

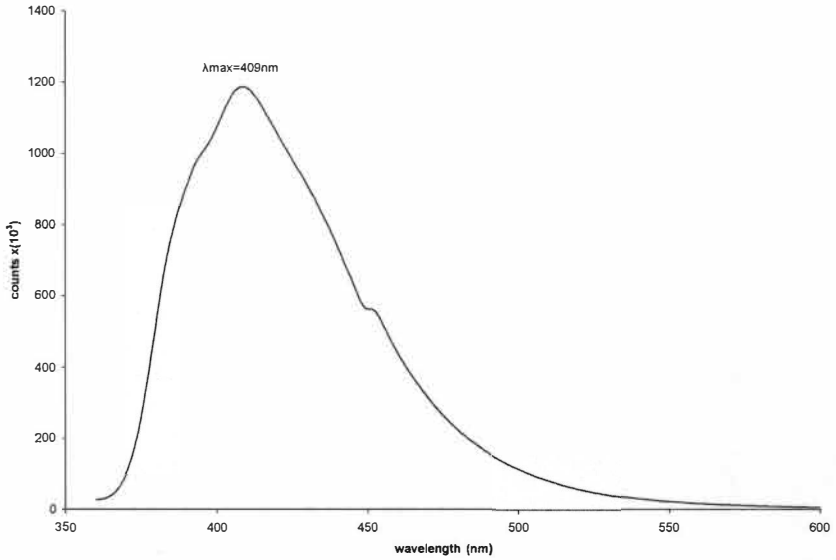

Figure 3.19 Emission spectrum of Receptor-II in CH_3CN, excitation maxima at 354nm

Figures 3.17, 3.18, and 3.19 represent UV-Vis absorption, excitation and emission spectra of Receptor-II respectively. The UV-Vis and excitation spectra of Receptor-II have similar structure as compared to stilbene compound (1S). However, there is a blue shift in the excitation spectrum (excitation maxima at 354nm) of Receptor-II as compared to excitation spectrum (excitation maxima at 326nm) of stilbene compound (1S). This

blue shift may be attributed to the improved conjugation as well as highly electronegative fluorine atoms in 4-aminophenyalhexafluoropropanol. The highly electronegative fluorine atoms may alter the electron distribution throughout the molecule resulting in shifting of the excitation maxima. Comparing the emission spectrum of Receptor-II with emission spectrum of stilbene compound (1S) and with Receptor-I, it was observed that emission maxima (λ_{max} = 409nm) of Receptor-II undergoing redshift as compared to emission maxima (λ_{max}= 443nm) of stilbene compound (1S) and emission maxima of Receptor-I (λ_{max} = 434nm). This quenching might be due to the increased conjugation length which widens the band gap energy. Thus it is confirmed that Receptor-II showed different behavior than stilbene compound (1S) and Receptor-I. It can be used as an optical probe in development of nanosensor.

3.13 Interaction of Receptor-II with DCP, DMMP, and HCl

In order to check the efficiency of Receptor-II as an optical probe in detecting nerve gas analogs (DCP, DMMP, and HCl) a known concentration of Receptor-II [1.01E-05M] was reacted with varying concentrations of nerve gas analogs and the change in emissive behavior was observed. All the spectral studies were performed in acetonitrile.

3.13.1 Interaction of Receptor-II with DCP

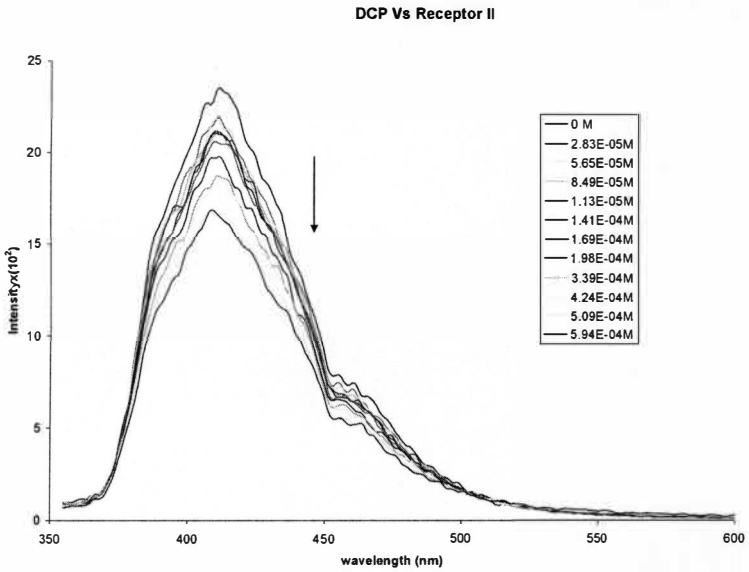

Figure 3.20 Change in emission intensity of Receptor-II [1.01E-05M] after interacting with various concentrations [2.83E-05M to 5.94E-04M] of DCP

3.13.2 Interaction of Receptor-II with DMMP

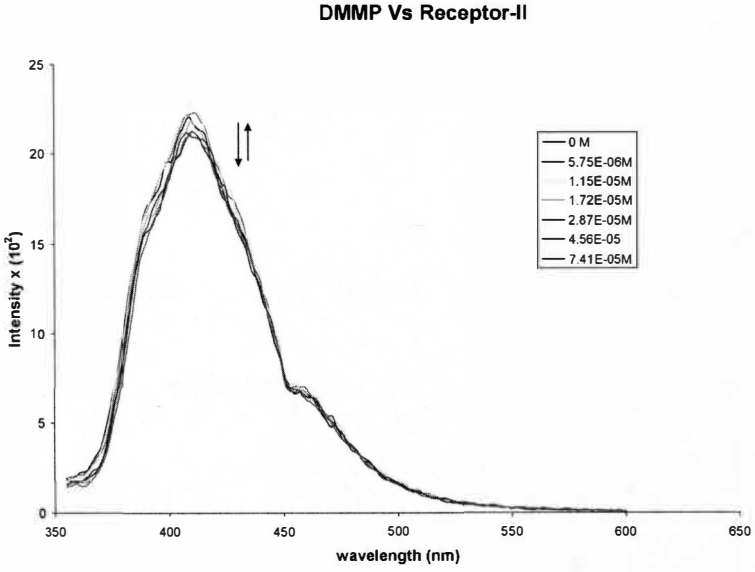

Figure 3.21 Change in emission intensity of Receptor-II[1.01E-05M] after interacting with various concentrations [5.75E-06M to 7.41E-05M] of DMMP

3.13.3 Interaction of Receptor-II with HCl

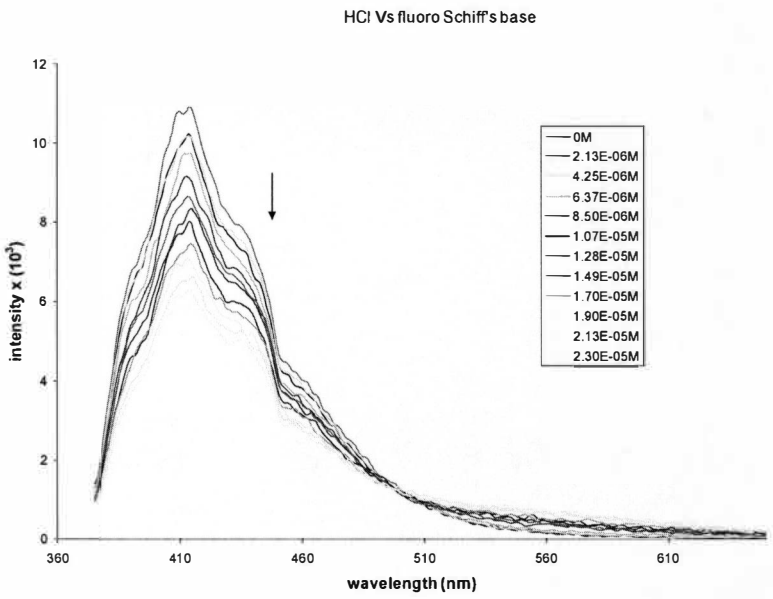

Figure 3.22 Change in emission intensity of Receptor-II [1.01E-05] after interacting with various concentrations [2.13E-06M to 2.30E-05M] of HCl

Figures 3.20, 3.21, and 3.22 show change in emission intensity of Receptor-II after interacting with DCP, DMMP, and HCl respectively. As compared to the interaction of Receptor-II with DMMP; DCP and HCl interactions with Receptor-II were strong and showed consistent quenching in the emission intensity. Receptor-II has a free (OH) group which interacts with DCP, DMMP and HCl. Additionally, highly electronegative fluorine atoms might make the phosphonyl group of the nerve gas analog a strong electrophyle and thus forms a strong leaving group. DMMP lacks this ability to form a strong leaving group. Therefore, the interaction of DCP and HCl with Receptor-II were stronger as compared to DMMP.

3.14 Association Constant Calculation of Receptor-II with Nerve Gas Analogs

As mentioned earlier in section 3.7, a C/I model was used to calculate the equilibrium association constant of Receptor-II. The association constant indicates the strength of interaction between Receptor-II and nerve gas analog. It is directly related to the strength of interaction i.e. the higher the association constant, greater would be the interaction.

3.14.1 Association Constant Calculation of Receptor-II with DCP

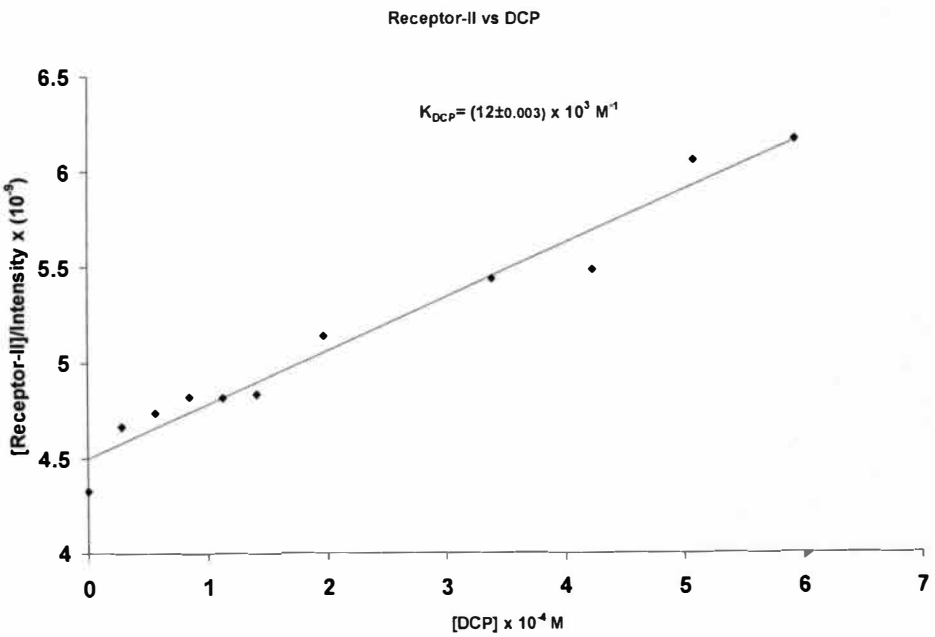

Figure 3.23 Association constant plot of Receptor-II Vs DCP

3.14.2 Association Constant Calculation of Receptor-II with DMMP

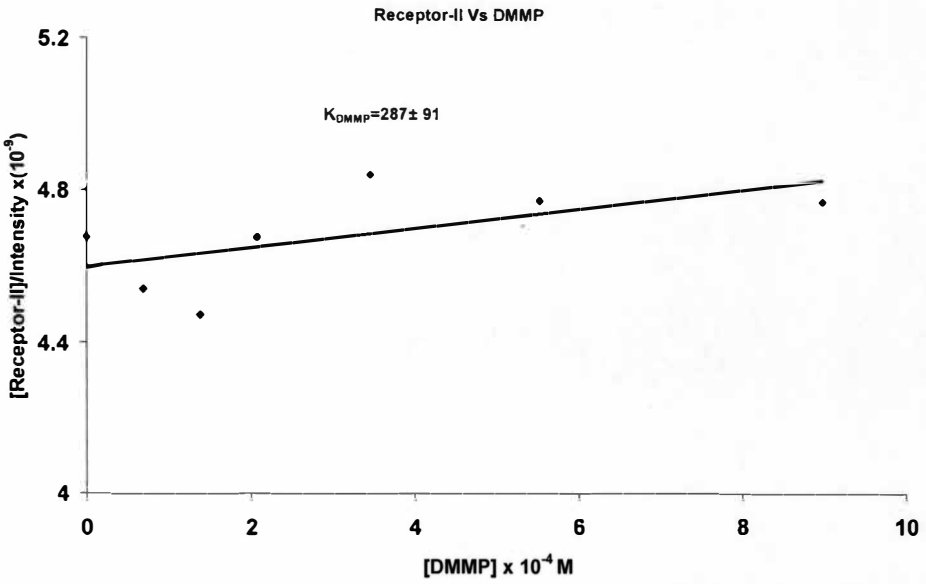

Figure 3.24 Association constant plot of Receptor-II Vs DMMP

3.14.3 Association Constant Calculation of Receptor-II with HCl

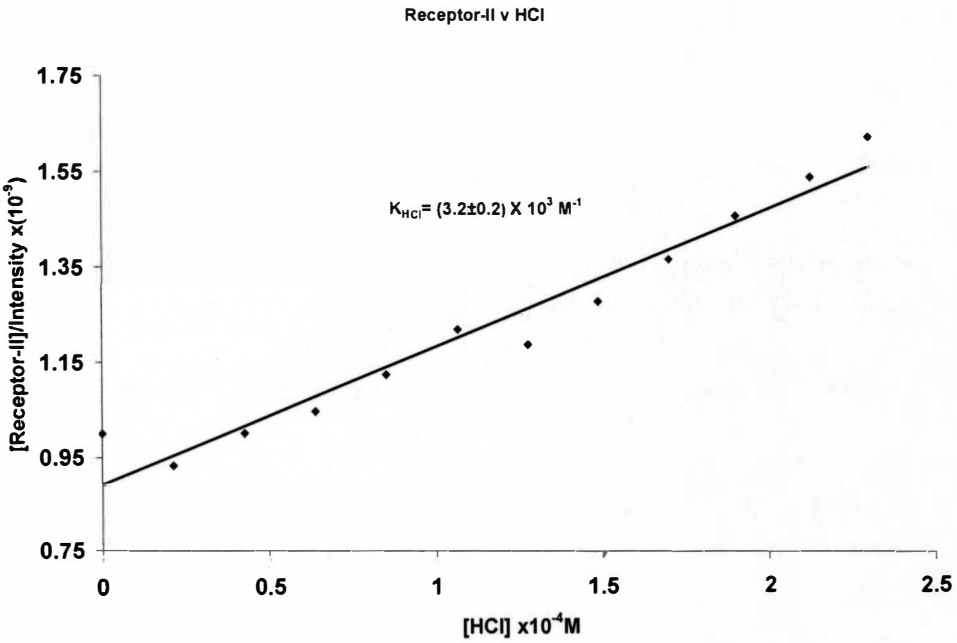

Figure 3.25 Association constant plot of Receptor-II Vs HCl

3.15 Summary of Association Constants of Receptor-II Vs DCP, DMMP, and HCl

Table 3.3 Association constants of Receptor-II Vs DCP, DMMP, and HCl

	K_{DCP} M^{-1}	K_{DMMP} M^{-1}	K_{HCl} M^{-1}
Receptor-II	(12±0.003) x 10^3	287±91	(3.2±0.2) x10^3

The association constants of Receptor-II Vs nerve gas analogs are summarized in the table 1.4. These values suggest that the interaction of DCP with Receptor-II was stronger as compared to DMMP which is also analogues to the change in emission intensity of Receptor-II after interacting with DMMP. (Figure 3.21) HCl showed better interaction with Receptor-II as compared with DCP and DMMP. This might be due to decrease in the pH of Receptor-II solution. The decrease in pH quenches fluorescence and in this case the quenching shown is consistent with additions of HCl. The nature of interaction suggested by association constant values indicating that Receptor-II can also be used as a building block for nanosensor.

3.16 Emission Lifetime Study of Receptor-II

As mentioned earlier, fluorescence lifetime decay of luminescent molecules such as Receptor-II provides detailed information about excimer formation, emission behavior. It also provides preliminary information on response time of the sensor. Therefore it is necessary to analyze chromophoric molecules for their fluorescence decay. A solution of known concentration [1.01E-05M] of Receptor-II in CH_3CN was excited at 354nm having emission maxima at 409nm.

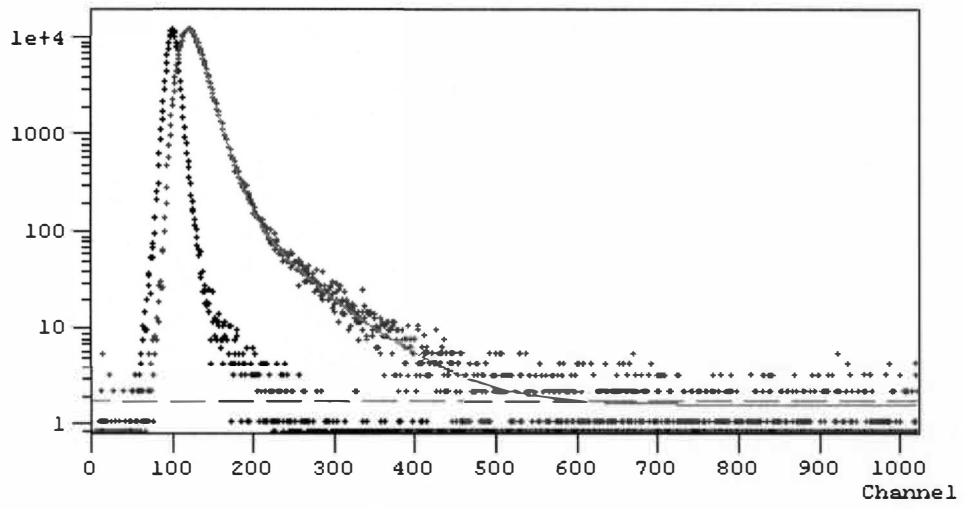

Time (ns)

Figure 3.26 Emission lifetime decay of Receptor-II, excited at 354nm, λmax= 409nm

Lifetime decay of Receptor-II (Figure 3.26) shows two lifetimes however, the shorter lifetime (below 1.3ns) is because of instrument response as well as exponential fitting of curve. This lifetime falls into the time of rise of excimer and thus needs not be considered but for application purposes, should be considered for the mathematical fitting of the curve to obtain the actual lifetime of excimer. The fluorescence lifetime data obtained by the instrument was then exponentially fitted with the help of software (F-900) to obtain the actual values of lifetime. The normalized fluorescence data was obtained by using a Distribution Analysis (Reconvolution) method and results obtained are as follows:

Table 3.4 Normalized fluorescence decay of Receptor-II

χ^2 : 1.066

Peak Num	B	F	τ (ns)	T (ns)	Std τ (ns)
1	0.987	94.17	1.331	1.315	0.069
2	0.013	5.828	6.331	6.474	0.240

The above shown emission lifetime decay of Receptor-II shows emission lifetime of 6.47ns, which is lower when compared to Receptor-I (8.85ns).The lower lifetime of Receptor-II could be due to low crystallinity or trace impurities left during the synthesis.

Another reason could be the different chemical structure of Receptor-II where the π-π^* interaction is less as compared to Receptor-I. However, the highly electronegative fluorine atoms might change the electron density around the molecule. This change in electron density could be one of the reasons behind a shorter lifetime of Receptor-II. The spectral characterization of Receptor-II enabled us to use it as an optical probe in the nanosensor.

3.17 Summary of Spectral Characteristics of Receptor-I and Receptor-II

Table 3.5 Summary of spectral properties of Receptor-I and II

	UV-Vis (nm)	Excitation (nm)	Emission (nm)	Lifetime (ns)
Receptor-I	338	344	434	8.85
Receptor-II	334	354	409	6.33

3.18 Summary of Interaction of Receptor-I and Receptor-II with Nerve Gas Analogs

Table 3.6 Summary of association constants of Receptor-I and II after interacting with nerve gas analogs DCP, DMMP, and HCl

	K_{DCP} M^{-1}	K_{DMMP} M^{-1}	K_{HCl} M^{-1}
Receptor-I	83.3±2.5	35	4.03×10^6
Receptor-II	$(12.0 \pm 0.003) \times 10^3$	287±91	$(3.2 \pm 0.2) \times 10^3$

CHAPTER IV

NANOSENSORS

4.1 Introduction to Nanosensors

As described in Chapter 1 and 2, development of an optical sensor is an area of research interest due to the increasing terrorist activities and stockpiling of CWAs by considerable number of countries.[11] In order to surpass the limitations put up by conventional detection techniques, such as expensive instrumentation, space consuming larger devices, delayed time response of the instrument and most importantly false signaling due to interaction with any other substance chemically similar to CWAs, development of a novel sensor is a necessity. The nanosensors described in this study have potential to be the best candidates for detection purposes.

Among the most studied sensory systems; "Lab-on-chip" system is at the acme of current research. "Lab-on-chip" concept is based on developing a sensor or library of sensors (optical probes) which will respond to the presence of nerve gas analogs or nerve gas agents. In order to achieve these optical sensors, self-assembling components are used so that a particular component of the complete sensor system can be exchanged with a different component which will have different properties. Thus a sensor can be made with high selectivity and high target specificity. Also a library of sensors or optical probes can be used to enhance the signal transduction.

Nanosensors described in this thesis are based on various building blocks. The sensors developed during the research are based on Nanoparticle-Monomer-Receptor (NMR) technology. (Figure 1.6) In the study presented here, nanoparticles used were made up of

silica, nanocrystals were made from ZnS:Mn/ZnS (core/shell) ($1/16^{th}$) QDs, stilbene compound (1S) which acts as a monomer, and Receptor-I and II act as receptors for the nanosensors. Research and development of these building blocks (Si-NPs, QDs, stilbene compound (1S), Receptor-I and II are described in Chapter 2, and 3. A brief discussion of the building blocks of nanosensors is given below:

Si-NPs serve the purpose of providing robust and photostable support as well as being highly monodispersed, Si-NPs can be used as solid support of the sensor. The Si-NPs form self-assembling monolayer which is very useful in achieving monolayers of complete sensors on a glass chip.

Monomers or oligomers are the compounds which improves the signal transduction by offering high conjugation. These monomer or oligomers (OPVs) comprise excellent luminescent properties. Conjugated with a target specific receptor, OPVs can be used as the ideal candidates for optical sensing.

Receptors are highly fluorescent molecules which interact with a specific target molecule to form an adduct. The adduct formation would change the emissive behavior of receptor as well as OPV and in turn the emissive behavior of the complete nanosensor. The change in emissive behavior of nanosensor indicates the presence of target molecule

The nanosensor developed during the research, enabled us to detect nerve gas analogs even at micro-molar level.

4.2. Synthesis of Nanosensors-I

Nanosensor-I was developed by reacting Receptor-I with silanized Si-NPs. In this particular synthesis, the carboxylic acid (COOH) group of Receptor-I was reacted with functional amine (NH_2) group of silanized Si-NPs to form an amide bond.[24] Generally, amide bond formation reactions need to be performed in the presence of coupling reagents. A complete assembly of modified Si-NPs attached to highly conjugated Receptor-I molecule is considered as Nanosensor-I and analyzed for its efficacy for detecting nerve gas molecules.

Synthesis of Nanosensor-I- In a 25 mL round bottom flask, silanized silica nanoparticles (50mg, 0.226moles) were dispersed in 1 mL of dimethyl formamide (DMF) with vigorous stirring. To this dispersion of silanized silica nanoparticles, Receptor-I (85mg, 0.226 moles) was added and the reaction mixture was stirred for another 15-20 minutes. In another glass vial, all the three coupling agents (HATU=206mg, PyBOP=282mg, NMM=75μL) were dissolved in 1-2 mL DMF. This solution of coupling agents was then added to the dispersion of silanized silica nanoparticles and Receptor-I. Reaction was carried out at room temperature for 12 hours. After 12 hours, DMF was removed by rotary evaporation to get dry solid orange colored powder.[61] The solid powder was then dried in vacuum oven for twenty four hours. Schematic representation of synthesis of Nanosensor-I is shown as below:

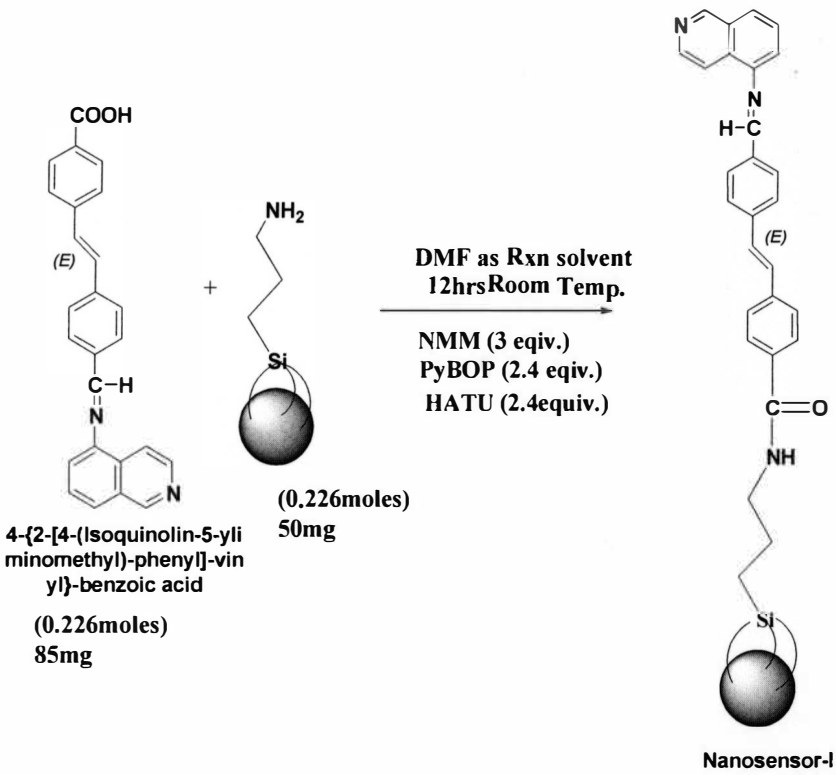

Scheme 4.1 Synthesis of Nanosensor-I based on silanized Si-NPs and Receptor-I

4.3 Results and Discussion

Nanosensor-I developed as shown above was then characterized by FT-IR and formation of amide bond was confirmed by comparing the FT-IR spectra of silanized Si-NPs and Receptor-I.

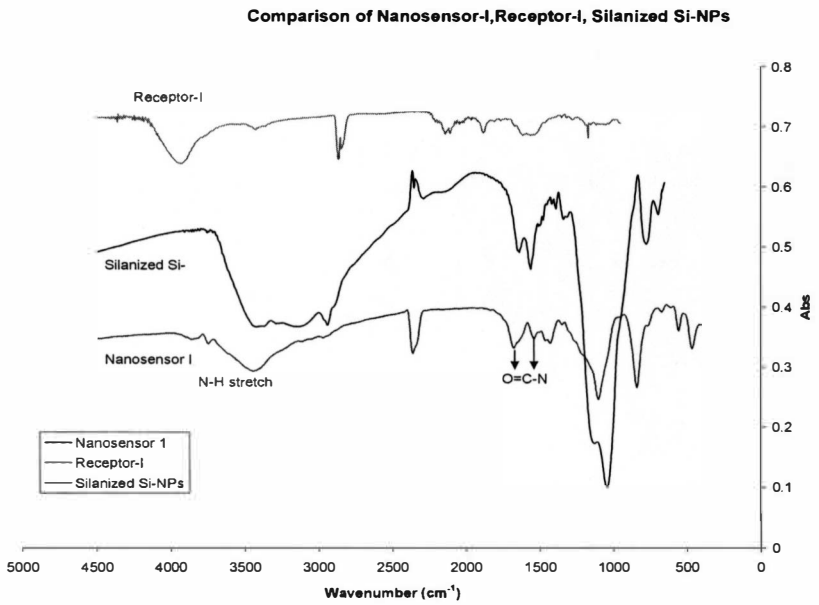

Figure 4.1 Comparison of FT-IR spectra of Nanosensor-I, silanized Si-NPs, Receptor-I

As shown in the above FT-IR spectrum (Figure 4.1), a comparison of FT-IR spectra of Receptor-I, silanized Si-NPs, and Nanosensor-I, where a new peak is noticeable at 1651cm^{-1} which is a typical of amide bond.[62] A broad peak at 3419cm^{-1} can be attributed to N-H stretch of secondary amine. Another broad peak at 3900cm^{-1} can be attributed to O-H stretch. A broad peak between 2850cm^{-1}-2950cm^{-1} can be attributed to C-H stretching vibration.[13, 63] Peak present between 1620cm^{-1}-1500cm^{-1} could be due to C=C stretching or C=O stretching.[25]

The above prepared Nanosesnsor-I was then checked for its performance towards detecting nerve gas analogs.

4.4 Interaction of Nanosensor-I with DCP, DMMP, and HCl

Nanosensor-I prepared as shown in the above scheme 4.1 was then analyzed for its efficacy toward detecting nerve gas analogs by monitoring the change in emission intensity.

4.4.1 Nanosensor-I Interaction with DCP

Nanosensor-I [9.27E-06M] was reacted with varying concentrations [5.65E-05M to 7.35E-04M] of DCP and the change in its emission behavior was observed.

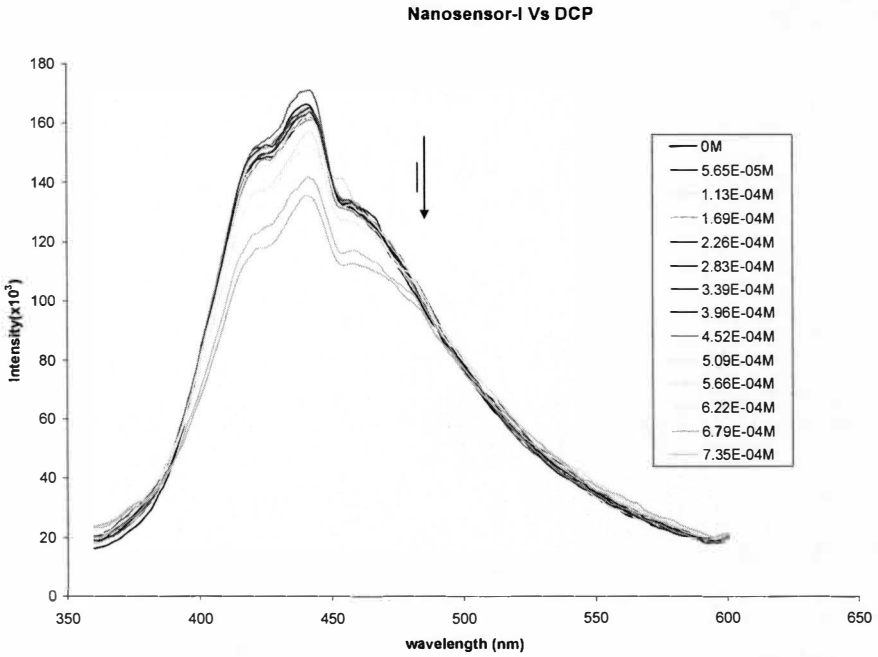

Figure 4.2 Change in emission intensity of Nanosensor-I [9.27E-06M] after interacting with DCP, excited at 354nm, λ_{max} =442nm

4.4.2 Nanosensor-I Interaction with DMMP

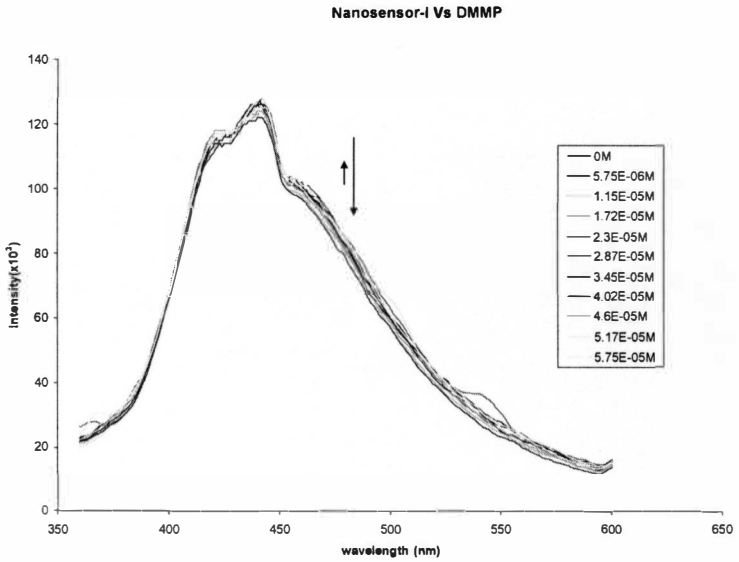

Figure 4.3 Change in emission intensity of Nanosensor-I [9.27E-06M] after interacting with varying concentrations of DMMP, excited at 354nm, λ_{max}= 439nm

4.4.3 Nanosensor-I Interaction with HCl

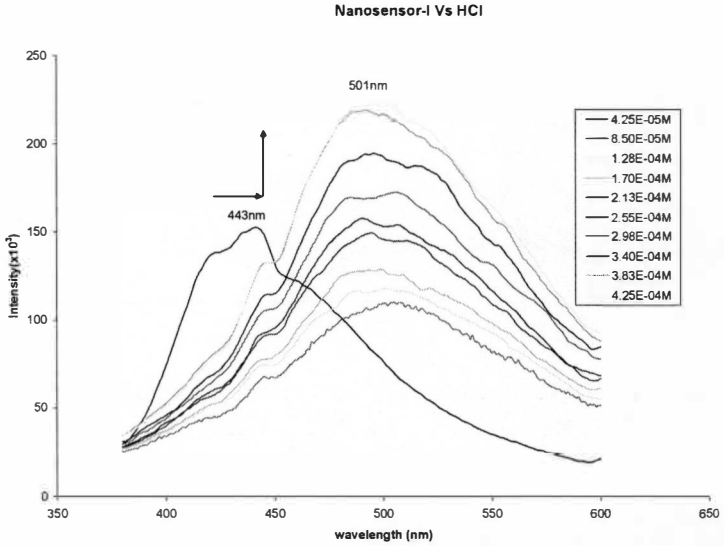

Figure 4.4 Change in emission intensity of Nanosensor-I [9.27E-06M] after reacting with HCl, excited at 354nm, λ_{max} shifted to 501nm

The above shown figures 4.2, 4.3, and 4.4 represent the emissive behavior of Nanosensor-I towards DCP, DMMP, and HCl respectively. In general, the interaction of

Nanosensor-I with DCP showed quenching in the emission intensity with successive additions [5.65E-05M to 7.40E-04M] of DCP. Though the emission intensity increased for few additions overall it was overall quenching of emission intensity. This behavior is very much similar to the emissive behavior of Receptor-I interacting with DCP, (figure 3.6) which proves the use of Receptor-I as an optical probe.

When Nanosensor-I interacted with DMMP [5.75E-06M to 5.75E-05M], it showed very little change in emission intensity compared to the interaction of Nanosensor-I with DCP. The change in emission intensity of Nanosensor-I after interacting with DMMP is smaller than the emission intensity change in Receptor-I after interacting with DMMP.(Figure 3.7) As mentioned earlier DMMP does not form strong leaving group after interacting with Nanosensor-I and not able to form adduct (Nanosensor-I + DMMP). Also as mentioned in the literature, DMMP might get adsorbed on the Si-NPs and might not affect emission behavior of Nanosensor-I.[64]

In the case of HCl interacting with Nanosensor-I, surprisingly there was enhancement in the emission intensity of Nanosensor-I. Also, there was blue shift in emission maxima (from 443nm to 501nm). This blue shift might be attributed to a decrease in pH because of addition of HCl. This decrease in pH might cause alterations in emission maxima. However, the enhancement in the emission intensity was unexpected, because Receptor-I showed quenching in emission intensity after interacting with HCl.[6] A possible reason for the emission enhancement could be the formation of highly luminescent adducts which decays radiatively to show enhancement in the emission.

4.5 Association Constants Calculations for Nanosensor-I

As mentioned in Chapter 2, the equilibrium association constant indicates the ability of Nanosensor-I to detect DCP, DMMP, and HCl. In general, higher association constant values suggest better sensing ability of the sensor. The association constants were calculated based on the C/I model (Chapter 3, 3.7) and are shown below:

4.5.1 Association Constant for Nanosensor-I Vs DCP

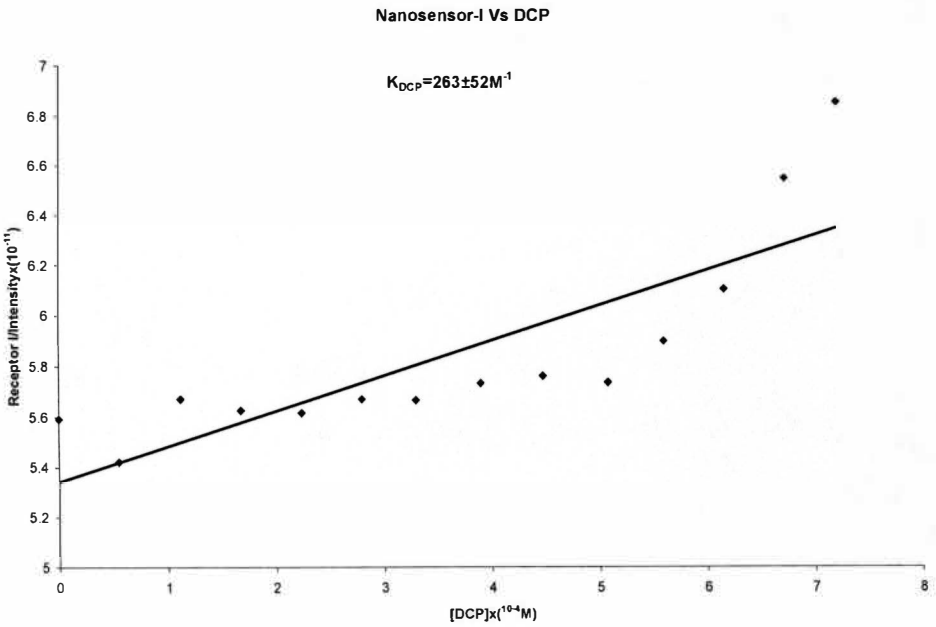

Figure 4.5 Association constant plot of Nanosensor-I Vs DCP

4.5.2 Association Constant of Nanosensor-I with DMMP

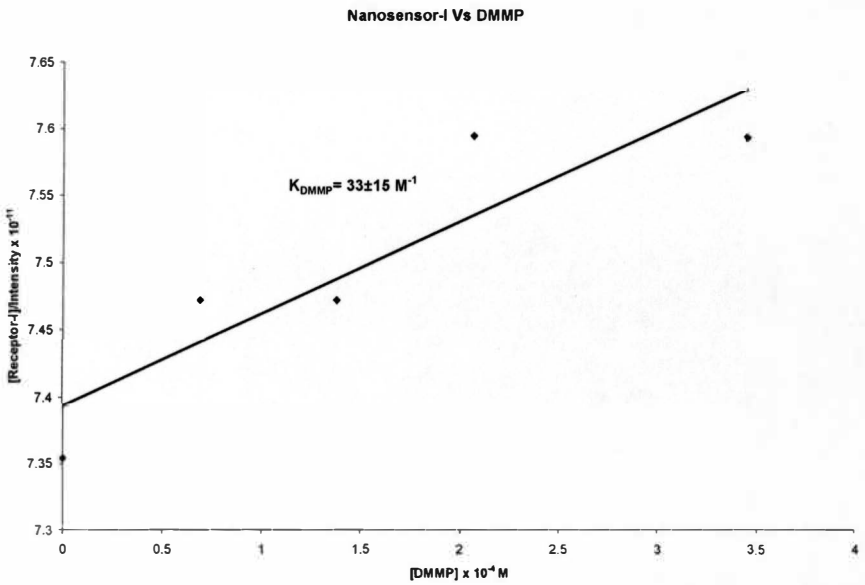

Figure 4.6 Association constant plot of Nanosensor-I Vs DMMP

4.5.3 Association Constant for Nanosensor-I with HCl

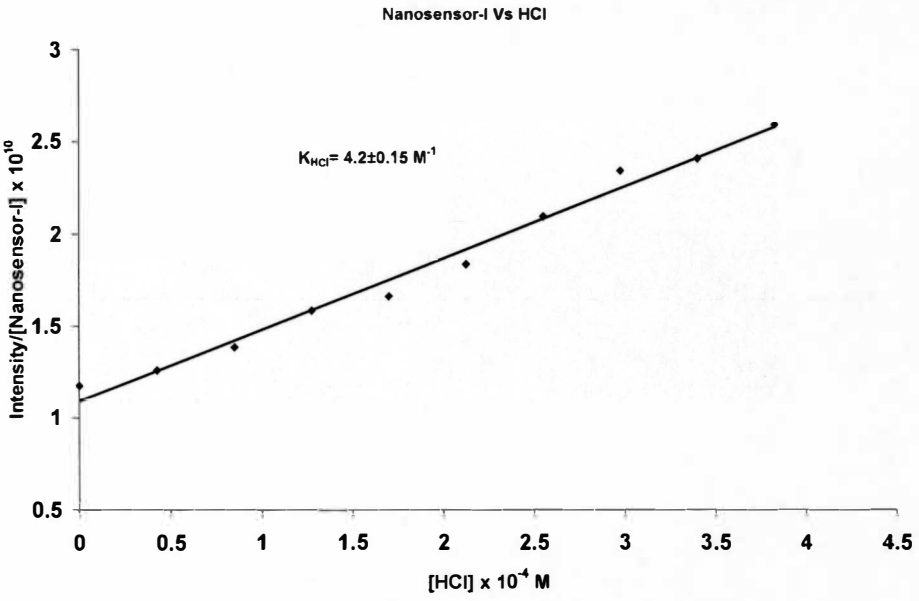

Figure 4.7 Association constant plot of Nanosensor-I Vs HCl

4.6 Summary of Association Constants of Nanosensor-I and Receptor-I

Table 4.1 Association constants of Nanosensor-I and Receptor-I with DCP, DMMP, and HCl

	K_{DCP} M^{-1}	K_{DMMP} M^{-1}	K_{HCl} M^{-1}
Nanosensor- I	263±52	33±15M^{-1}	4170 M^{-1}
Receptor-I	83.3±2.5	190	4.04 $X10^{6}$

The figures shown above (Figure 4.5, 4.6, and 4.7) represents association constant plot of Nanosensor-I with nerve gas analog DCP, DMMP, and HCl respectively. As expected, the ability of Nanosensor-I to detect DCP and DMMP is relatively weaker than the ability to detect HCl. From the change in emission behavior it can be predicted that Nanosensor-I showed better interaction with HCl than with DCP and DMMP, because in the case of HCl interaction with Nanosensor-I, there was a change in emission maxima and as well as there was enhancement in emission intensity. As shown in table-1.8 association constant values for Nanosensor-I with DCP and DMMP are smaller as compared to HCl. However, in the case of DMMP, due to the irregular behavior, the association constant was calculated by considering the change in emission intensity is quenching. The same behavior was shown by Receptor-I. (Figure 3.7) Thus the adduct formation ability of Nanosensor-I with HCl is better than that of DCP and DMMP. Overall, Nanosensor-I has shown better sensing abilities for the hydrolysis product of DCP i.e. HCl as compared to DCP and DMMP.

4.7 Development of Nanosensor-II

Nanosensor-II was based on conjugating ZnS:Mn/ZnS ($1/16^{th}$) QDs to Receptor-I. The ion pairing of Receptor-II with QDs was achieved by addition of the solution of Receptor-I in acetonitrile to the dispersion of QDs in acetonitrile by titration method.

4.8 Synthesis of Nanosensor-II

Synthesis of ZnS:Mn/ZnS ($1/16^{th}$) QDs and Receptor-I was done as described in Chapter 2 (section 2.9).and 3 (section 3.3) respectively. In order to build Nanosensor-II, 4mL solution of ZnS:Mn/ZnS (core/shell) ($1/16^{th}$) QDs in CH_3CN was mixed by using titration method to Receptor-I solution having 3.51E-05M final concentration The solution of QDs was sonicated for 30minutes before addition of Receptor-I to avoid the aggregation effects. The schematic representation of synthesis of Nanosensor-II based on Receptor-I and ZnS: Mn/ZnS (core/shell) ($1/16^{th}$) is shown as below:

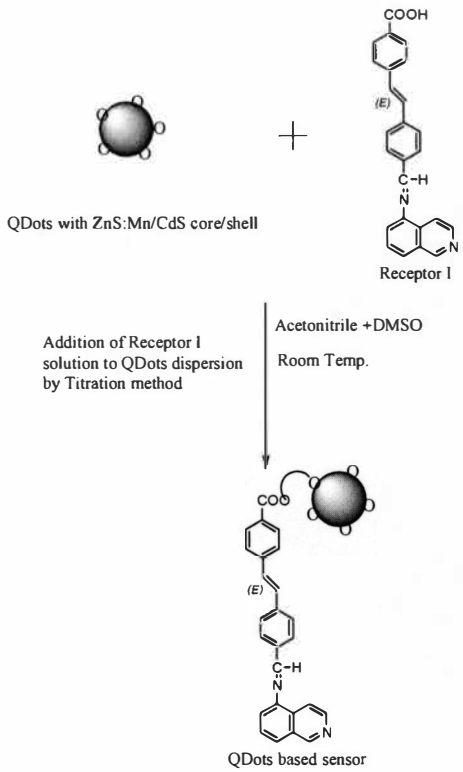

Scheme 4.2 Synthesis of Nanosensor-II

The above prepared Nanosensor-II was then analyzed for its spectral properties as well as its efficiency to detect DCP, DMMP and HCl. The spectral properties of Nanosensor-II were analyzed by UV-Vis, excitation and emission spectroscopy.

4.9 Results and Discussion

Nanosensor-II was checked for its spectral properties. The results are discussed below:

4.9.1 UV-Vis Absorption Study of Nanosensor-II

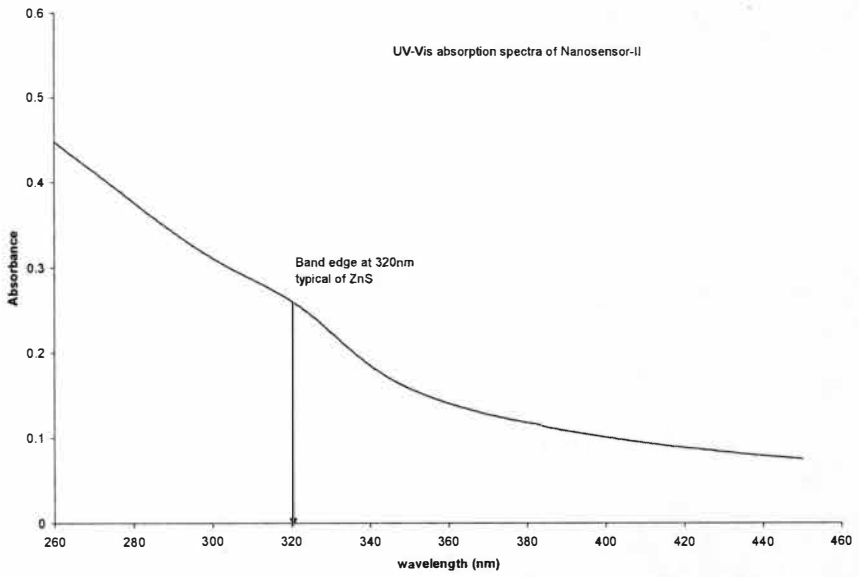

Figure 4.8 UV-Vis absorption spectrum of Nanosensor-II in CH_3CN

4.9.2 Excitation Spectrum of Nanosensor-II

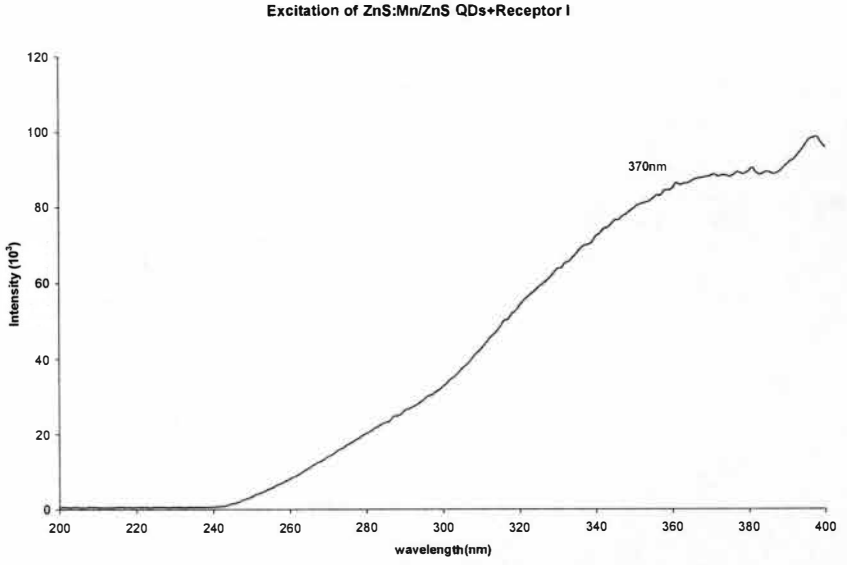

Figure 4.9 Excitation spectrum of Nanosensor-II in CH_3CN

4.9.3 Emission Spectrum of Nanosensor-II

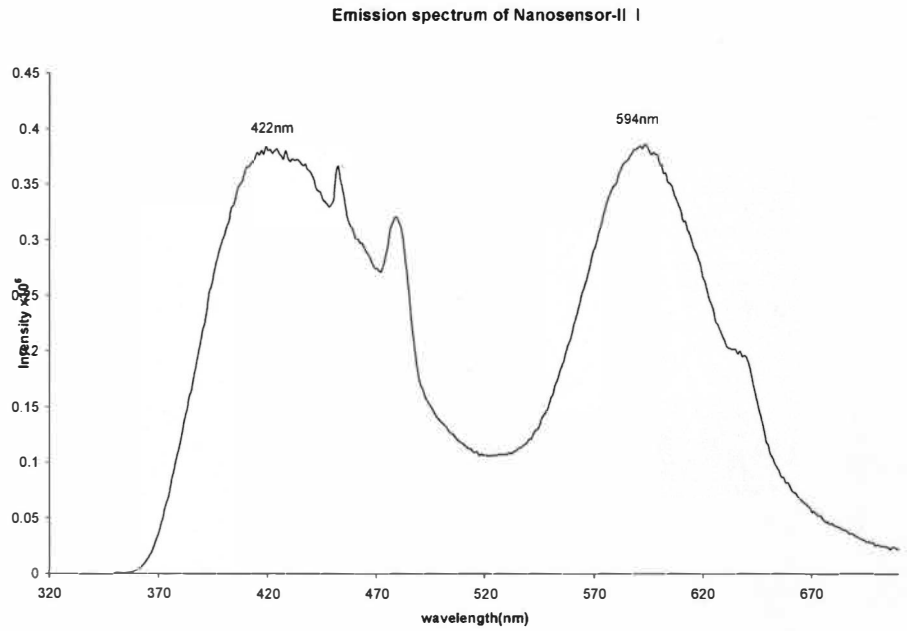

Figure 4.10 Emission spectrum of Nanosensor-II in CH_3CN excited at 320nm

The spectral properties of Nanosensor-II were analyzed and compared with spectral properties of ZnS:Mn/ZnS QDs. Figures 4.8, 4.9, and 4.10 represents UV-Vis, excitation, and emission spectrum of Nanosensor-II. In UV-Vis spectrum, the band edge at 320nm is clearly visible which is very similar to UV-Vis spectrum of QDs alone. (Figure 2.6) The excitation spectrum of Nanosensor-II was very much different than the excitation spectrum of ZnS:Mn/ZnS (core/shell) ($1/16^{th}$) QDs. The excitation peak at around 370nm incase of Nanosesnor-II has undergone blue shift as compared to the excitation peak 330nm of ZnS:Mn/ZnS QDs. The blue shift could be due to the attachment of highly conjugated Receptor-I to QDs. The emission spectrum of Nanosensor-II clearly shows two different peaks. The peak having emission maxima at 422nm is attributed to luminescent Receptor-I and a peak having emission maxima at 594nm is attributed to ZnS:Mn/ZnS (core/shell) ($1/16^{th}$)QDs. The emission maxima at 422nm is due to π-π^* interactions in Receptor-I and emission maxima at 594nm is an orange luminescence

generating from Mn^{2+} ions. The presence of two emission peaks could be due to the free molecules of Receptor-I (not conjugated to QDs), as well as due to the QDs attached to Receptor-I. Thus the spectral analysis of Nanosensor-II suggests the formation of ion-pair between ZnS:Mn/ZnS (core/shell) ($1/16^{th}$) and Receptor-I. Further confirmation of development of Nanosensor-II was done by performing emission lifetime studies on Nanosensor-II.

4.10 Emission Lifetime Study of Nanosensor-II

The emission lifetime study on Nanosensor-II was performed by using a hydrogen lamp as a source of excitation for Nanosensor-II at 320nm which is the UV-Vis absorption band edge of ZnS:Mn/ZnS (core/shell) ($1/16^{th}$) QDs. The UV-Vis absorption of Nanosensor-II in CH_3CN was maintained below 0.25Abs in order to avoid the saturation effects. The emission lifetime data obtained was plotted by using a F-900 software and an exponential fitting was performed in order to get the accurate result.

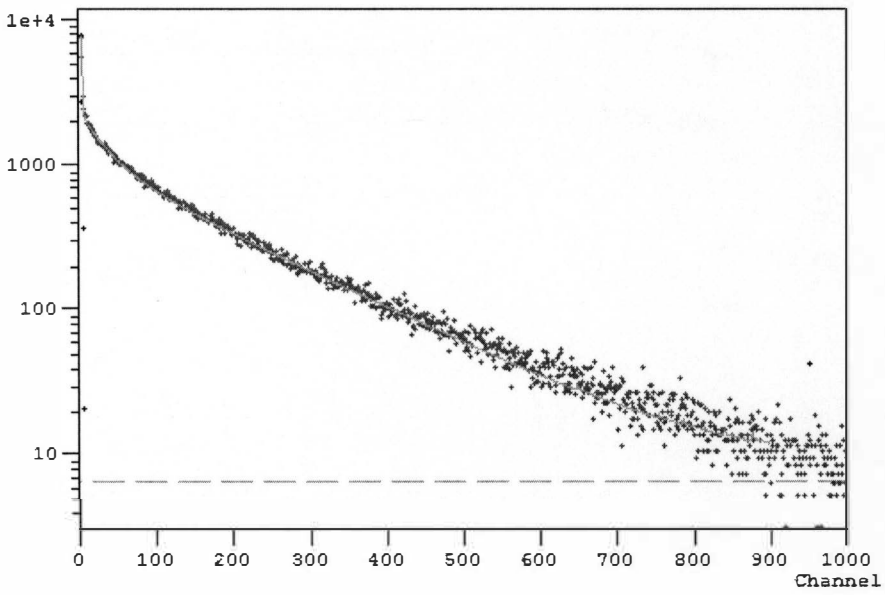

Figure 4.11 Emission lifetime decay of Nanosensor-II, excited at 320nm

The emission lifetime data shown here (Figure 4.11) is normalized and instrument response is subtracted from this spectrum. Nanosensor-II has multiple lifetimes as shown in the table 1.9, the multiple lifetimes of Nanosensor-II could be because of mixed system of mobile Receptor-I and Receptor-I immobilized on ZnS:Mn/ZnS QDs. However, the longer lifetimes of Nanosensor-II are much different from the emission lifetime of Receptor-I. (Table 1.3) The longer emission lifetimes of Nanosensor-II could be attributed to highly luminescent QDs giving rise to high quantum efficiency. The high quantum efficiency of QDs could be enhanced due to the highly conjugated Receptor-I which has higher electron density. The complete system of Nanosensor-II is surrounded by high electronic density. The higher electron density makes an electron to stay in the excited state for longer time and makes the radiative decay of excited electron a slower process thus giving rise to longer lifetime.

Table 4.2 Emission lifetime of Nanosensor-II

χ^2 : 1.101

Exp Num	B	F	τ (ns)
1	4.019	10.27	1.3e+4
2	0.125	15.39	6.3e+5
3	0.116	74.34	3.3e+6

The fluorescence decay of Nanosensor-II showing multiple lifetimes (τ=6.3E+5ns, 3.3E+6ns) as compared to single emission lifetime of Receptor-I (τ= 8.85ns) is an indication of forming Nanosensor-II by ion pairing between ZnS:Mn/ZnS (core/shell) ($1/16^{th}$) QDs and Receptor-I and not just a mixture of Receptor-I and ZnS:Mn/ZnS (core/shell) ($1/16^{th}$) QDs. The shorter lifetime of Receptor-I is no longer evident which supports our conclusion that there is an interaction between ZnS:Mn/ZnS (core/shell)

(1/16th) QDs and Receptor-I. The lifetime of QDs is correlated to the emission intensity. It is known that single exponential decay exists at higher intensities and multiexponential decay exists at lower intensities.[30] As mentioned in Chapter 2, ZnS:Mn/ZnS (core/shell) (1/16th) QDs show size dependent lifetimes, which indicates two different recombination centers may be involved in the decay process. Another possibility of multiple lifetimes is aggregation of Receptor-I molecules as it is a member of extended conjugation systems which behave similar to stilbene like compounds and which are known to form aggregates. Thus the combination of Receptor-I and ZnS:Mn/ZnS (core/shell) (1/16th) QDs (Nanosensor-I) posses different emission lifetime than the Receptor-I itself, which is a clear indication of successful development of Nanosensor-II.

4.11 Interaction of Nanosensor-II with DCP, DMMP, and HCl

Nanosensor-II prepared by combining ZnS:Mn/ZnS (core/shell) (1/16th) QDs and Receptor-I was then analyzed for its efficacy to detect DCP, DMMP, and HCl. A typical Nanosensor-II solution containing dispersed QDs in CH_3CN and Receptor-I of 0.351E-04M.concentration. Various concentrations of DCP, DMMP, and HCl were added to the solution of Nanosensor-II and its emissive behavior was observed.

4.11.1 Interaction of Nanosensor-II with DCP

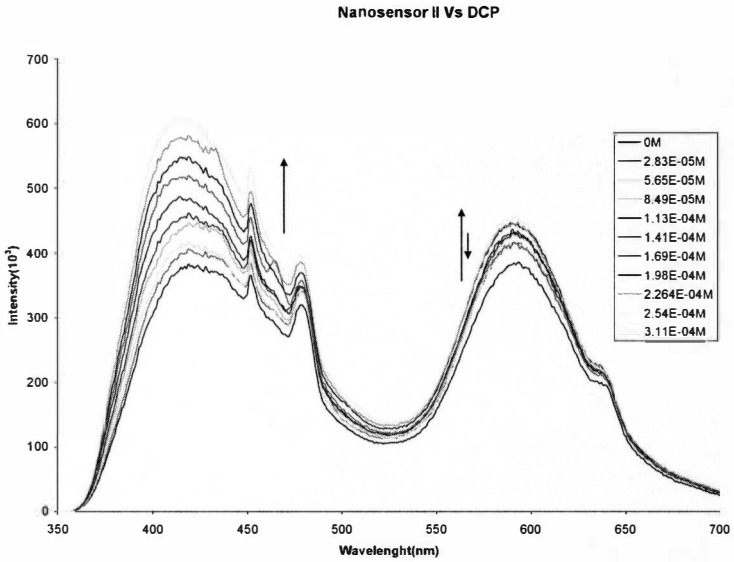

Figure 4.12 Change in emission intensity of Nanosensor-II after reacting with different concentration [2.83E-05M to 3.11E-04M] of DCP

4.11.2 Interaction of Nanosensor-II with DMMP

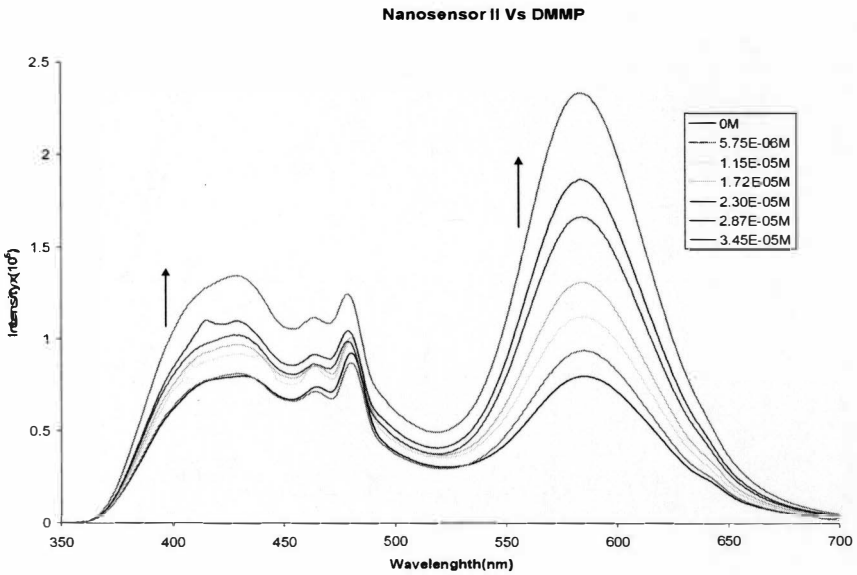

Figure 4.13 Change in emission intensity of Nanosensor-II Vs varying concentrations [5.75E-06M to 3.45E-05] of DMMP

4.11.3 Interaction of Nanosensor-II with HCl

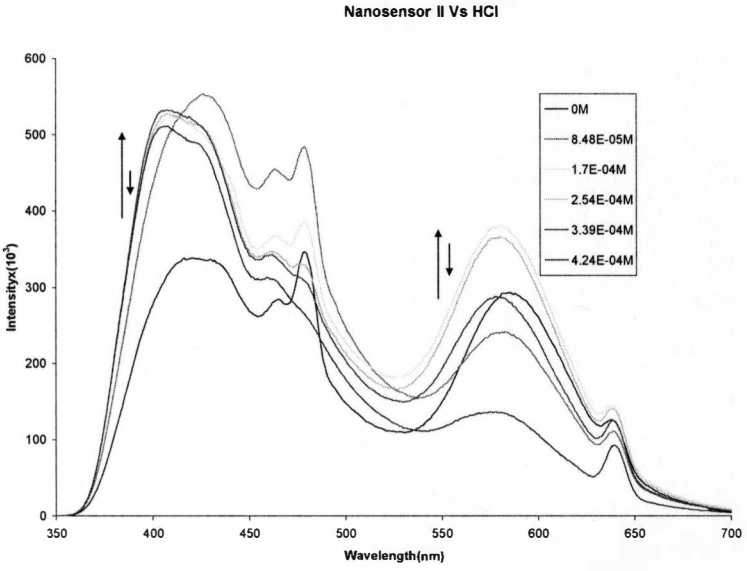

Figure 4.14 Change in emission intensity of Nanosensor-II after reacting with various concentrations [8.48E-05 to 4.24E-04M] of HCl

Interaction of Nanosensor-II with DCP, DMMP, and HCl is represented above in figures 4.12, 4.13, and 4.14 respectively. QDs show continuous absorption and their excitation wavelength is not dependent of their bandshape, a combined system such as Nanosensor-II can be excited by using a single excitation source or wavelength.[28] As it can be seen from figure 4.14, QDs surface modified with Receptor- I showed enhancement in the emission behavior after interacting with DCP. This change in emission can be attributed to the selective interaction of DCP with freely hanging groups of Receptor-I. As Receptor-I and QDs are coupled through electronic interaction, change in electron density of Receptor-I can be observed at Mn^{2+} luminescent centers. This behavior is similar to the behavior of ZnS:Mn/ZnS (core/shell) ($1/16^{th}$) QDs. (Figure 2.8) Though DCP interacts with Receptor-I, the electron distribution throughout the system is altered. This could be the reason behind signal amplification of QDs at λ_{max}=590nm. The interaction of nerve gas analog, DCP with Receptor-I is manifested to the exciton energy transfer of the

Mn^{2+} and change the emission intensity of Mn^{2+}. The possibility of charge transfer could also be one of the reasons behind signal transduction.

In the case of interaction of Nanosensor-II with DMMP, the change in emission intensity of QDs is greater than the change in emission intensity of Receptor-I. This could be due the direct interaction of DMMP with uncovered QDs. The other possible explanation could be interaction of DMMP with the Receptor-I attached to QDs. This interaction modulates the electron density around Receptor-I showing change in emission intensity of Receptor-I and in turn it also alters electron density distribution into the center (Mn^{2+}) of QDs. The irregular behavior of HCl could not be interpreted except for the fact that the decreased pH could alter the emissive behavior of Nanosensor-II.

4.12 Association Constant Calculation for Nanosensor-II

As mentioned in Chapter 2, association constants for Nanosensor-II are calculated based on the C/I model. The C/I model does not account for colloison quenching or dynamic quenching. During interaction of Nanosensor-II with nerve gas analogs, the surface occupied by Receptor-I molecules is unknown, hence the association constant is based on the concentration (1.01E-05M) of solution of Receptor-I used to match the intensity of Receptor-I and QDs. The exact concentration of Receptor-I can not be determined since the emission of ZnS:Mn/ZnS (core/shell)($1/16^{th}$) QDs is based on their size which varied from synthesis to synthesis due to the several factors such as solvent media, exposure to oxygen etc. One assumption made during this study was, matching the intensity of ZnS:Mn/ZnS (core/shell)($1/16^{th}$) QDs with emission intensity of Receptor-I as shown in the figure 4.10 will cover maximum surface of QDs. The surface coverage determination,

and finding the exact concentration of Receptor-I required matching the emission intensity of QDs with the Receptor-I would be the future scope of this study.

4.12.1 Association Constant of Nanosensor-II with DCP

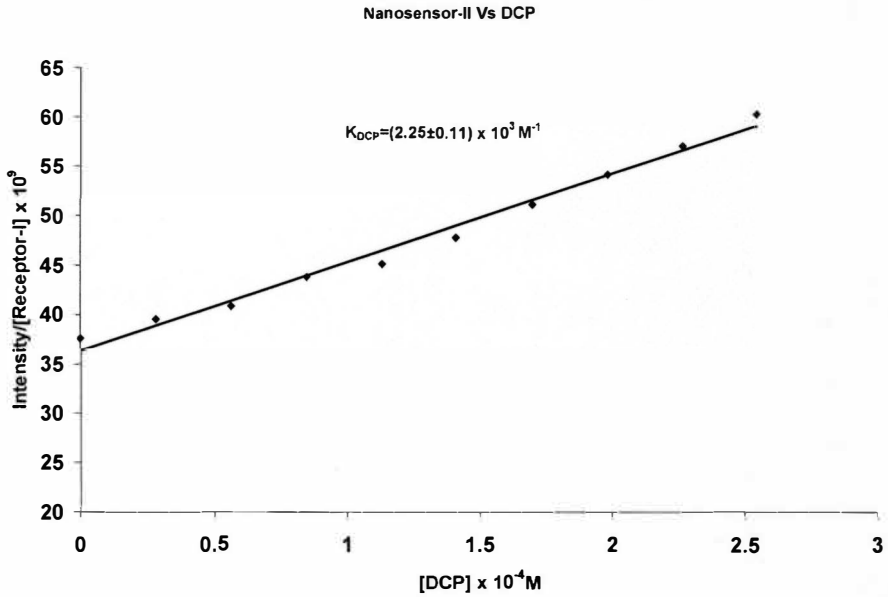

Figure 4.15 Association constant plot of Nanosensor-II Vs DCP

4.12.2 Association Constant of Nanosensor-II with DMMP

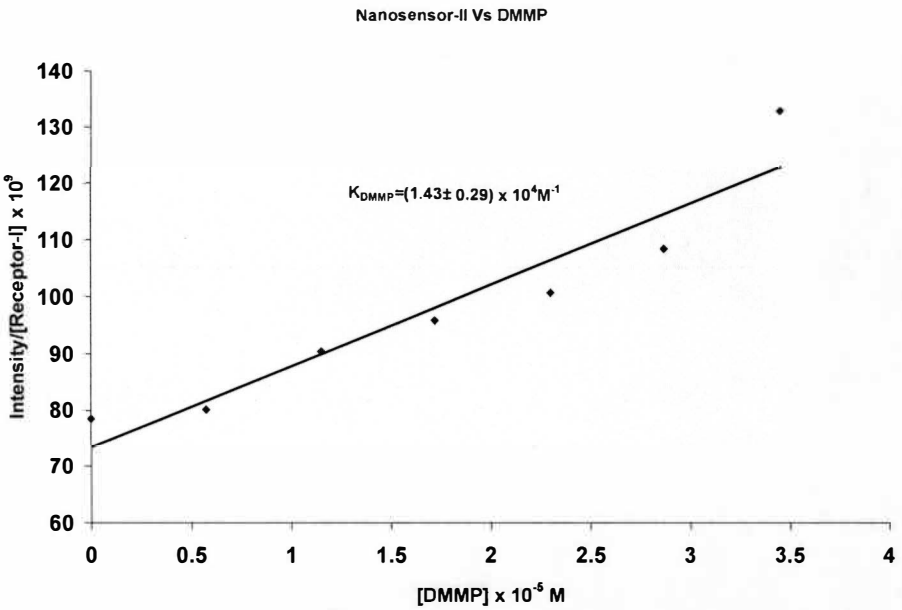

Figure 4.16 Association constant plot of Nanosensor-II Vs DMMP

4.12.3 Association Constant of Nanosensor-II Vs HCl

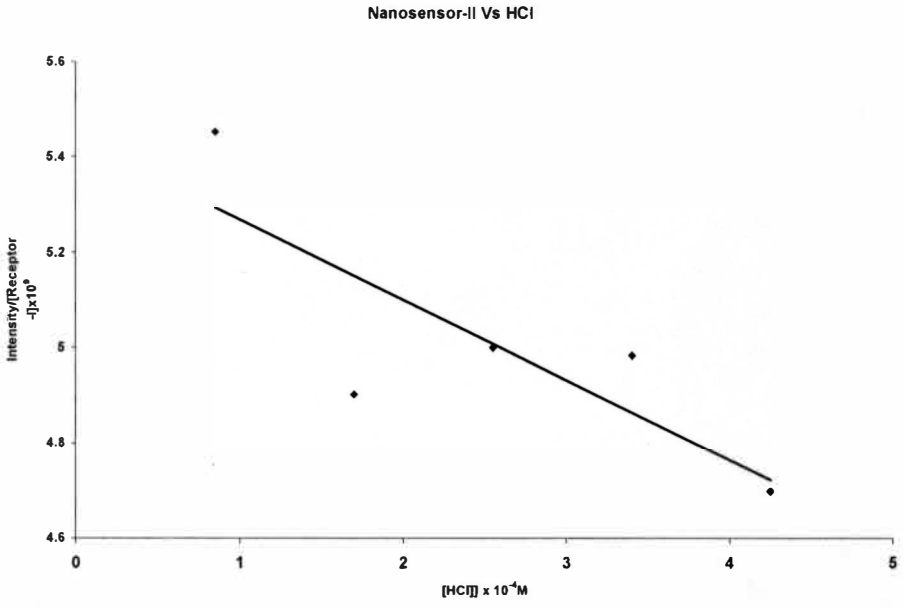

Figure 4.17 Association constant plot of Nanosensor-II Vs HCl

4.13 Summary of Association Constants of Nanosensor-II and Receptor-I

Table 4.3 Association constants of Nanosensor-II and Receptor-I

	K_{DCP} M^{-1}	K_{DMMP} M^{-1}	K_{HCl} M^{-1}
Nanosensor-II	$(2.25\pm0.11) \times 10^3$	$(1.43\pm0.29) \times 10^4$	$(5.0\pm4.8) \times 10^2$
Receptor-I	83.3 ±2.5	190	4.0390×10^6

As it can be seen from the Figures 4.15, 4.16, and 4.17 the association constant plots for Nanosensor-II Vs DCP, DMMP, HCl respectively, the association constants for DCP and DMMP are relatively higher than HCl. By carefully observing the change in emission intensity of Nanosensor-II after interacting with DCP (Figure 4.12) it would be expected to show a better association constant value, since the interaction between DCP and Nanosensor-II is considerable. However, in the case of DMMP the change in emission intensity of ZnS:Mn/ZnS (core/shell) ($1/16^{th}$)QDs was higher than the change in emission

intensity of Receptor-II.(Figure 4.13) This could be due to direct interaction between QDs and DMMP. This interaction gave much higher association constant value which can be attributed to conjugation of QDs with DMMP. This is a very rare possibility, since the control experiment showed in Chapter 2 (Figures 2.8, 2.9, and 2.10) indicates that ZnS:Mn/ZnS (core/shell)($1/16^{th}$)QDs alone does not interact with nerve gas analogs. Another possibility could be maximum surface coverage would have been achieved by the addition of Receptor-II, which means more Receptor-II molecules on the QDs surface are interacting with target moiety (DMMP) to amplify the signal. Surprisingly, HCl did not yield higher value of association constant as compared to DCP and DMMP. The irregular behavior shown by HCl after interacting with Nanosensor-II could be due to the pH effects caused by HCl. Though certain factors need to be addressed in detail, in general, Nanosensor-II proved to be a better sensor than Nanosensor-I.

4.14 Synthesis of Nanosensor-III

Synthesis of ZnS:Mn/ZnS ($1/16^{th}$) QDs and Receptor-II was done as described in Chapter 2 (section 2.9) and in Chapter 3 (section 3.10) respectively. In order to build Nanosensor-III, 4mL solution of ZnS:Mn/ZnS (core/shell) ($1/16^{th}$) QDs in CH_3CN was mixed by using titration method to Receptor-II solution having 1.143E-06M final concentration The solution of QDs was sonicated for 30 minutes before addition of Receptor-II as to avoid the aggregation effects. The schematic representation of synthesis of Nanosensor-III based on Receptor-II and ZnS: Mn/ZnS (core/shell) ($1/16^{th}$) is shown as below:

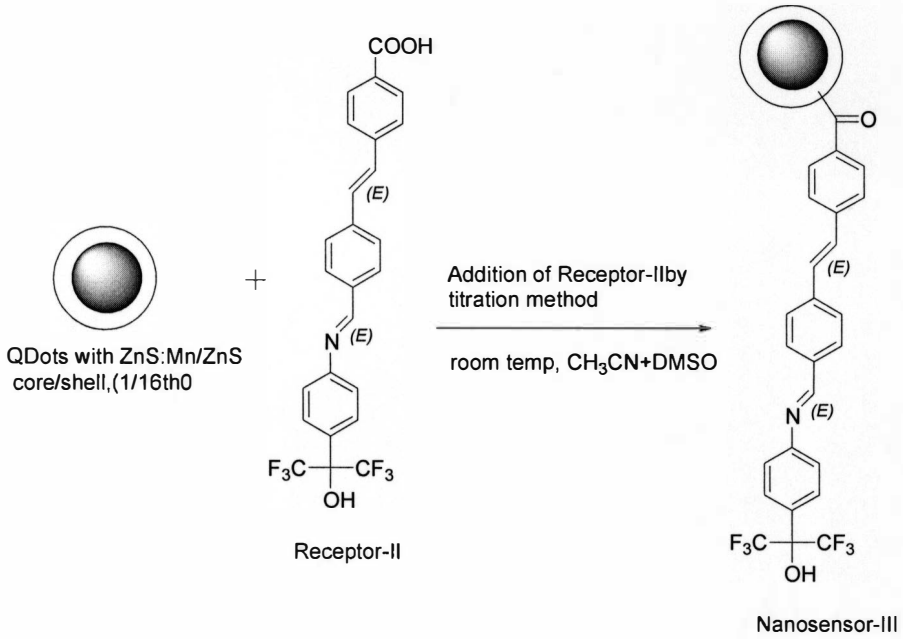

Scheme 4.3 Synthesis of Nanosensor-III

4.15 Results and Discussion

The above prepared Nanosensor-III was characterized for its spectral properties such as UV-Vis, excitation, and emission. The spectra obtained are shown below:

4.16 Spectral Characteristics of Nanosensor-III

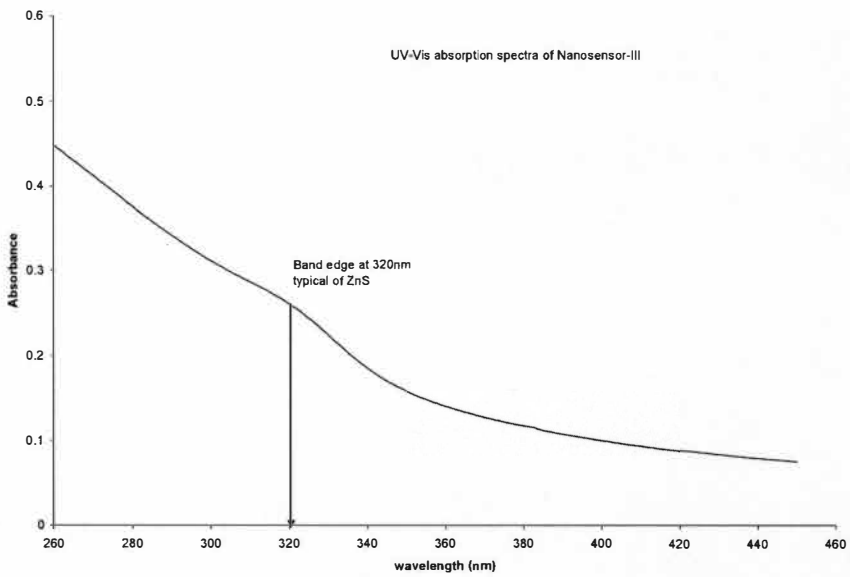

Figure 4.18 UV-Vis absorption spectrum of Nanosensor-III taken in CH_3CN

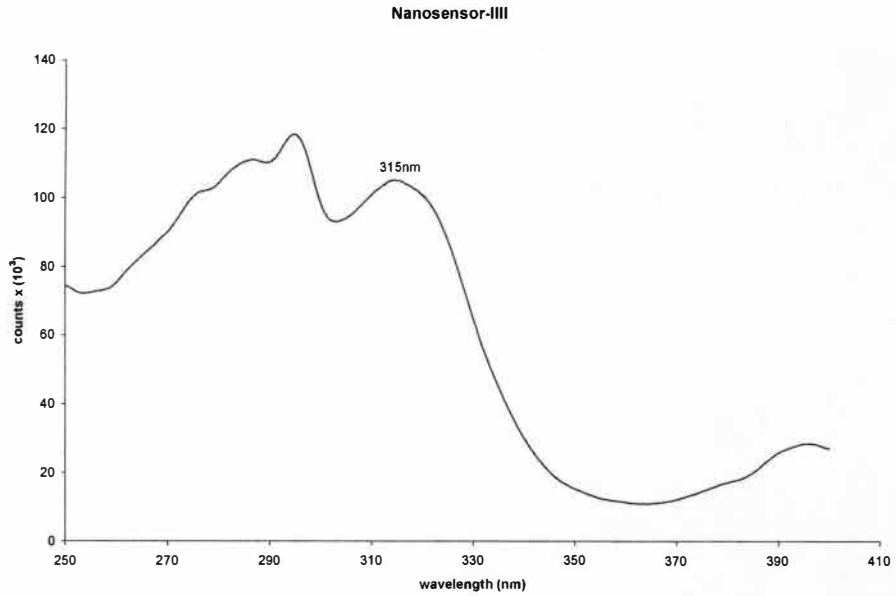

Figure 4.19 Excitation spectrum of Nanosensor-III, emission maximas at 415nm and 586nm

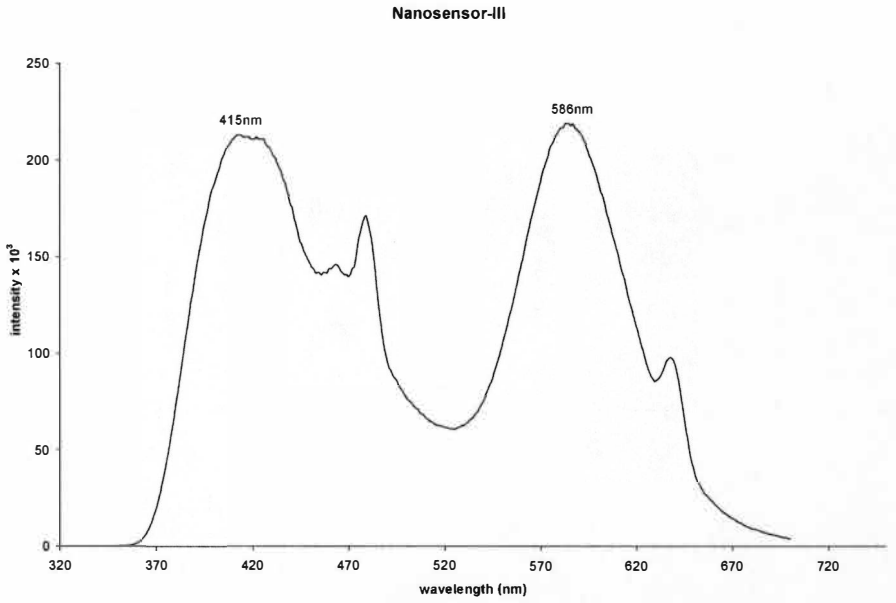

Figure 4.20 Emission spectrum of Nanosensor-III, excited at 320nm

4.17 Emission Lifetime Study of Nanosensor-III

Nanosensor-III was analyzed for its fluorescence decay after exciting at 320nm wavelength which is a band edge of ZnS:Mn/ZnS (core/shell) ($1/16^{th}$) QDs. The solution

of Nanosensor-III in CH_3CN was maintained below 0.300Abs for its UV-Vis absorption. The emission lifetime decay of Nanosensor-III is as shown below:

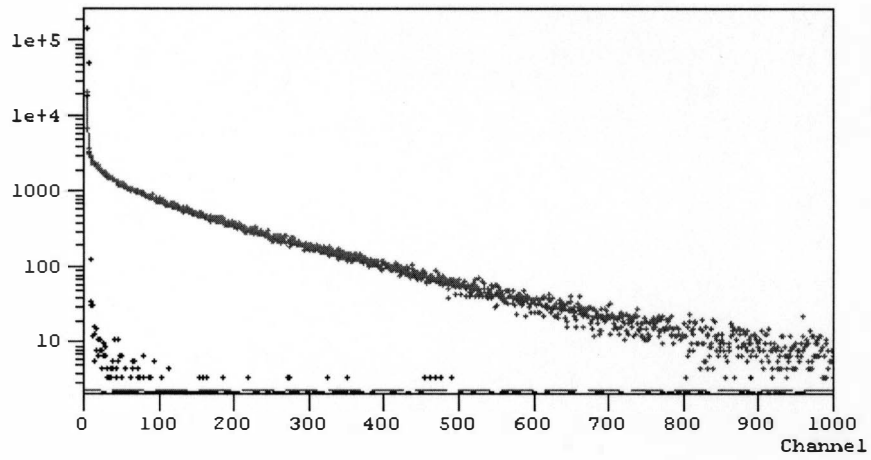

Time (ns)

Figure 4.21 Emission lifetime decay of Nanosensor-III

The fluorescence decay of Nanosensor-III shown above represents radiative decay of excited electron. The multiple lifetimes observed in the above figure 4.21 might be due to aggregation of freely moving Receptor-II molecules (mobile Receptor-II). It is well know that QDs of different size show different lifetimes due to the presence of multiple recombination centers. Also, as QDs posses' continuous absorption spectrum, only one excitation source is needed to excite an assembly like Nanosensor-III.

The data obtained from instrument was fitted by using F-900 software by using multiexponential fit. A distribution analysis (Tail fitting mode) method was used to fit the data. The data from the software is as follows:

Table 4.4 Normalized fluorescence decay of Nanosensor-III

χ^2 : 1.813

Peak Num	B	F	τ (ns)	Std τ (ns)
1	0.850	6.001	2.1e+4	413.0
2	0.074	17.55	7.0e+5	1.4e+5
3	0.076	76.45	3.0e+6	1.1e+6

Nanosensor-III showed multiple lifetimes as shown in the table 2.1, it has 3 different lifetimes 2.1E+4ns, 7.0E+5ns, and 3.0E+6ns. As mentioned earlier in this Chapter, multiple lifetime could be due to aggregation of freely moving Receptor-II molecules or due to size dependent properties of ZnS:Mn/ZnS (core/shell) ($1/16^{th}$) QDs. However, the shorter lifetime of (6.33ns) Receptor-II is completely absent, which is a clear indication of formation of an ion-paired assembly of Nanosensor-III. Though multiple lifetimes arises due to several factors verifying the exact reason would be the future scope of this project.

4.18 Interaction of Nanosensor-III with Nerve Gas Analogs

4.18.1 Interaction of Nanosensor-III with DCP

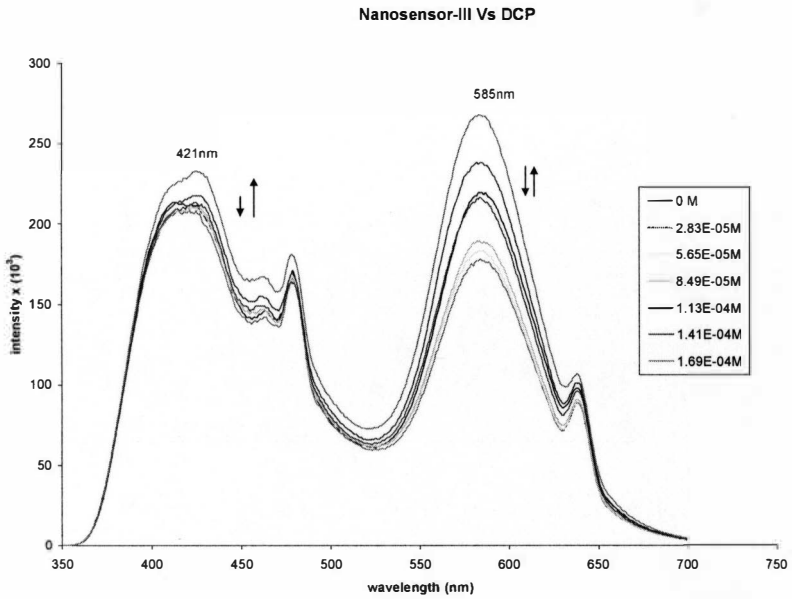

Figure 4.22 Change in emission intensity of Nanosensor-III after interacting with various concentrations [2.83E-05M to1.69E-04M] of DCP

4.18.2 Interaction of Nanosensor-III with DMMP

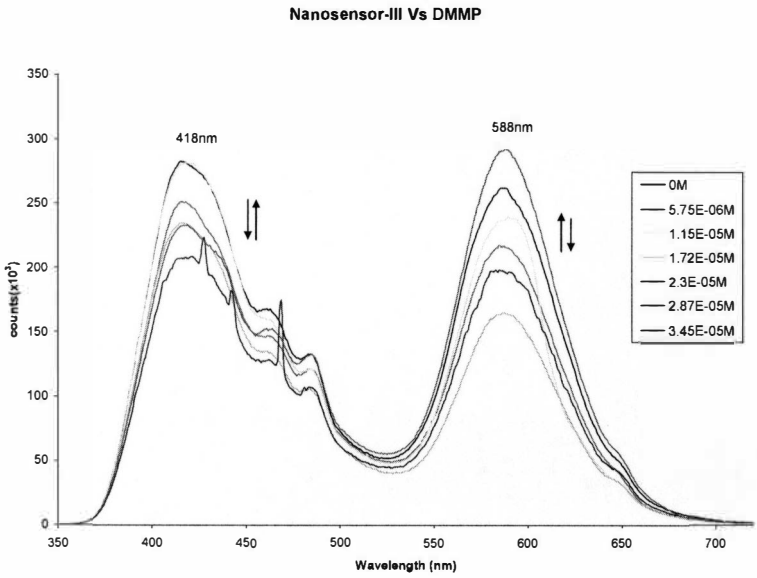

Figure 4.23 Change in emission intensity of Nanosensor-III after interacting with various concentrations [5.75E-06M to 3.45E-05M] of DMMP

4.18.3 Interaction of Nanosensor-III Vs HCl

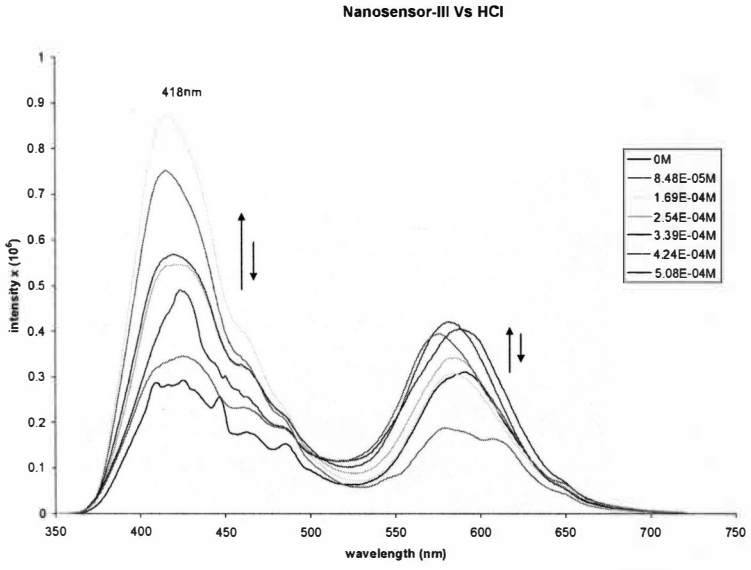

Figure 4.24 Change in emission intensities of Nanosensor-III after interacting with various concentrations [8.45E-05M to 5.08E-04M] of HCl

Figures 4.22, 4.23, and 4.24 represent change in emissive behavior of Nanosensor-III after interacting with DCP, DMMP, and HCl. In the case of DCP, change in emissive

behavior is irregular, but the change in emission intensity at 590nm (QDs emission) is larger as compared to change in emission of Receptor-II emission (421nm). (Figure 4.22) This behavior is different than the emission behavior of Receptor-II alone (Figure 3.21) where Receptor-II showed quenching. This behavior confirms that fact that Receptor-II behaves in a different way when conjugated to another fluorophore. In case of DMMP, the emissive behavior is irregular with smaller change in emission intensity of Receptor-II emission (421nm) and greater change in emissive behavior at QDs emission (588nm). Interestingly, Nanosensor-III showed mixed behavior though it was dominated by *"Switch-On"* type behavior. Also unlike DCP, and DMMP Nanosensor-III showed considerable change in emissive behavior of Receptor-II (418nm) and smaller change in emission intensity of Mn^{2+} in ZnS:Mn/ZnS (core/shell) ($1/16^{th}$) quantum dots. In general, Nanosensor-III showed irregular behavior with DCP, DMMP, and HCl though it showed mostly *"Switch-On"* type sensing with HCl.

4.19 Association Constants Calculations for Nanosensor-III

Association constants of Nanosensor-III after interacting with DCP, DMMP, and HCl were calculated by using C/I model as mentioned in Chapter 3 (section 3.7). Similar to the case of Nanosensor-II, the exact concentration of Receptor-II present on the ZnS:Mn/ZnS (core/shell)($1/16^{th}$) QDs is unknown. So the association constant values are calculated based on the concentration [1.14E-06M] of Receptor-II solution used for titration method. The association constants calculated are shown as below:

4.19.1 Association Constant of Nanosensor-III with DCP

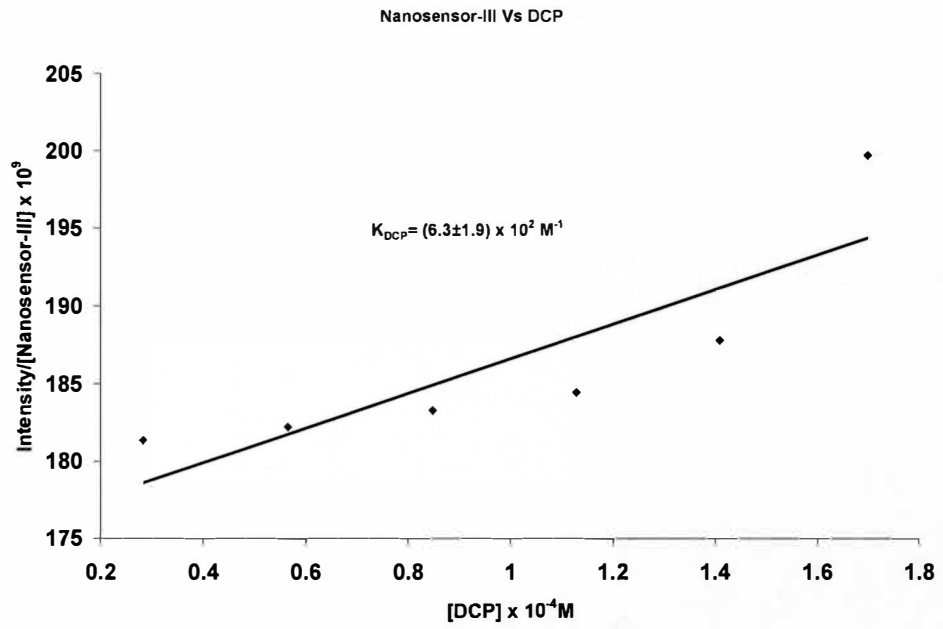

Figure 4.25 Association constant plot of Nanosensor-III Vs DCP

4.19.2 Association Constant of Nanosensor-III with DMMP

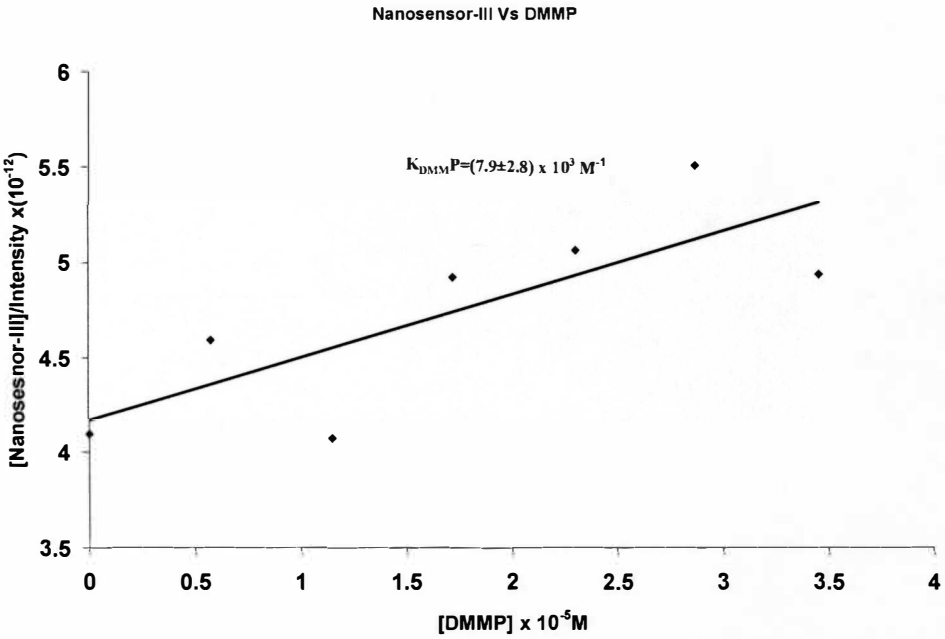

Figure 4.26 Association constant plot of Nanosensor-III Vs DMMP

4.19.3 Association Constant for Nanosensor-III with HCl

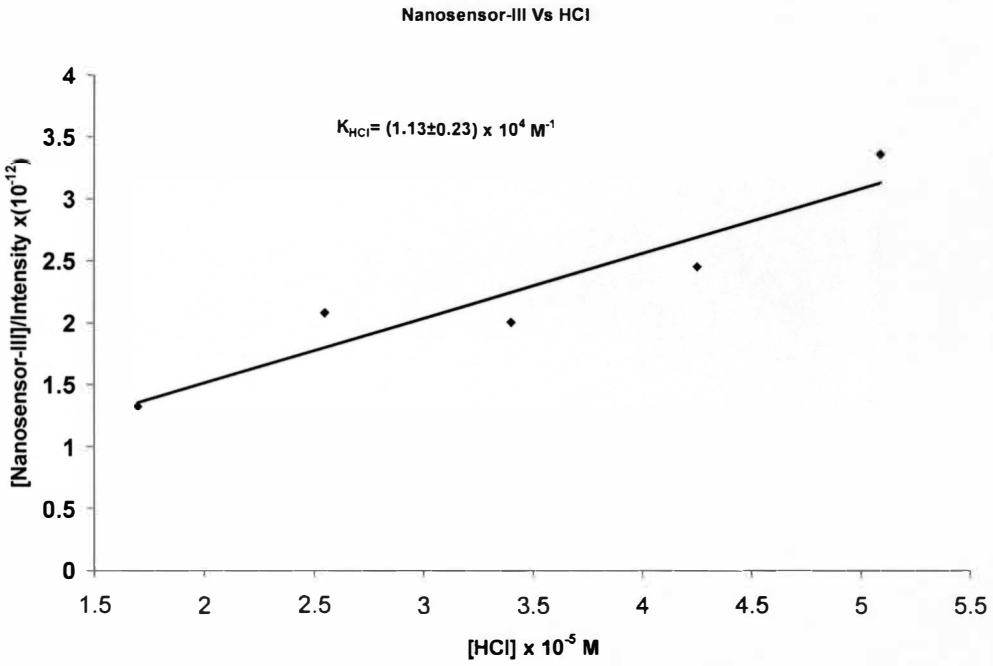

Figure 4.27 Association constant plot of Nanosensor-III Vs HCl

4.20 Summary of Association Constants of Receptor-II and Nanosensor-III

Table 4.5 Association constants of Receptor-II and Nanosensor-III

	K_{DCP} M^{-1}	K_{DMMP} M^{-1}	K_{HCl} M^{-1}
Nanosensor-III	(6.3±1.9) x 10^2	(7.9±2.8) x 10^3	(1.1±0.2) x 10^4
Receptor-II	(12.0±0.03) x 10^3	287±91	(3.22±0.23) x10^3

From the above shown table 2.2, it can be seen that Nanosensor-III (ZnS:Mn/ZnS QDs covered with Receptor-II) showed different association constants as compared to Receptor-II alone. These results clearly indicates that ion pairing of Receptor-II with ZnS:Mn/ZnS (core/shell)(1/16th) QDs resulted into a new assembly named Nanosensor-III. From the table 2.2 it is clear that Nanosensor-III showed weaker interaction with DCP as compared to Receptor-II. However, in case of DMMP and HCl the interaction of Nanosesnsor-III was stronger than the Receptor-II itself. These results can be explained

by the type of interaction of nerve gas analog with Nanosensor-III. In case of DCP interaction, the ability of Receptor-II to form an adduct with DCP might have been altered due to ion pairing with ZnS:Mn/ZnS (core/shell) ($1/16^{th}$) QDs. This must have been resulted in weaker interaction of Nanosensor-III with DCP. However, in case of DMMP, the interaction should have been even weaker as compared to DCP, but this is not the case. The interaction of DMMP with Nanosensor-III is stronger than that of DCP. This phenomenon can not be interpreted very well with available set of studies. Also, the irregular behavior shown by HCl resulted in stronger interaction with Nanosensor-III, as can be seen from the association constant values. The irregular emissive behavior showed by Nanosensor-III was very different as compared to Receptor-II. (Figures 3.20, 3.21, 3.22) Overall, Nanosensor-III showed better interaction with DMMP and HCl as compared to DCP.

4.21 Summary of Spectral Properties of Building Blocks of Nanosensors and Nanosensors

Spectral characterization of building blocks ZnS:Mn/ZnS (core/shell) ($1/16^{th}$) QDs, Receptor-I, II and Nanosensors-II, III was done in CH_3CN in solution form. The UV-Vis absorption of these solutions was maintained below 0.3Abs, so as to avoid the saturation effects.

Table 4.6 Summary of spectral characterization of components of nanosensors and nanosensors

	UV-Vis (nm)	Excitation (nm)	Emission (nm)	Lifetime (ns)
Receptor-I	338	344	434	8.85
Receptor-II	334	354	409	6.33
ZnS:Mn/ZnS QDs	320	315	590	
Nanosensor-II	320	370	422,594	6.3E5, 3.3E6
Nanosensor-III	320	330	415, 586	2.1E4, 7.0E5, 3.0E6

4.22 Summary of Association Constants of Nanosensors-I, II, and III

Table 4.7 Association constants of Nanosensor-I, II, and III

	K_{DCP} M^{-1}	K_{DMMP} M^{-1}	K_{HCl} M^{-1}
Nanosensor-I	263	33	4170
Nanosensor-II	$(2.2\pm0.1) \times 10^3$	$(1.43\pm0.29) \times 10^4$	$(5.0\pm4.8) \times 10^2$
Nanosensor-III	$(6.3\pm1.9) \times 10^2$	$(7.9\pm2.8) \times 10^3$	$(1.1\pm0.2) \times 10^4$

CHAPTER V

CONCLUSION

5.1 Conclusion

A nanoparticle-monomer-receptor (NMR) concept was successfully implemented to build nanosensors for the detection of nerve gas analogs DCP, DMMP, and HCl. Three sensors were developed by using different building blocks towards selective detection of model nerve gas analogs. The following outlines the building blocks and nanosensors.

1. Nanosensor-I is based on:

   Silica nanoparticles

   Receptor-I

2. Nanosensor-II is based on:

   ZnS:Mn/ZnS (core/shell)($1/16^{th}$) quantum dots

   Receptor-I

3. Nanosensor-III is based on:

   ZnS:Mn/ZnS (core/shell)($1/16^{th}$) quantum dots

   Receptor-II

5.2 Nanosensor-I

Nanosensor-I was synthesized by conjugating a stilbene like monomer compound (1S) with a receptor molecule (5-aminoisoquinoline) to form an imine bond through Schiff's base reaction to form Receptor-I. The Receptor-I was then attached to silanized Si-NPs through the formation of an amide bond to make a complete Nanosensor-I. The Nanosensor-I was then characterized by FT-IR spectroscopy and checked for its efficacy in detecting DCP, DMMP, and HCl.

Receptor-I was analyzed for its performance in detection of DCP, DMMP, and HCl. Receptor-I showed *"Switch-Off"* type behavior with DCP, DMMP, and HCl. However, Nanosensor-I showed irregular emissive behavior after interacting with DCP, and DMMP. Nanosensor-I showed enhancement in the signal *"Switch-On"* type behavior after interacting with HCl and more interestingly, it showed a shift in emission maxima. Nanosensor-I showed a better interaction with HCl when compared to DCP and DMMP. These changes in emissive behavior of Nanosensor-I confirm the chemical linkage between the components of Nanosensor-I.

5.3 Nanosensor-II

Nanosensor-II was constructed by ion-pairing Receptor-I with semimagnetic Mn^{2+} doped ZnS:Mn/ZnS (core/shell) ($1/16^{th}$) QDs. Nanosensor-II was characterized by its spectral properties such as UV-Vis spectroscopy, excitation spectroscopy, emission spectroscopy, and emission lifetime. Nanosensor-II was reacted with DCP, DMMP, and HCl and the change in emission intensity was observed. Unlike Nanosensor-I, Nanosensor-II showed a *"Switch-On"* type behavior in general. Though the interaction of Nanosensor-II was weaker with DCP and DMMP, it showed a stronger interaction with HCl. The weak interaction of Nanosensor-II could be due to the slow reaction between the receptor moiety (5-aminoisoquinoline) and DCP.

5.4 Nanosensor-III

Nanosensor-III was constructed by anchoring Receptor-II on ZnS:Mn/ZnS (core/shell)($1/16^{th}$) QDs through an ion-pair formation. The ion-pair formation of Receptor-II with ZnS:Mn/ZnS (core/shell) ($1/16^{th}$) quantum dots was characterized by UV-Vis, excitation spectroscopy, and emission spectroscopy. Fluorescence lifetime

decay was performed on Nanosensor-III to further confirm the ion-pairing. In the case of DMMP, Nanosensor-III showed irregular emissive behavior similar to the emissive behavior of Receptor-II. However, in the case of DCP and HCl, Nanosensor-III showed irregular behavior which is different from *"Switch-Off"* type behavior shown by Receptor-II alone. It is evident from the association constant values that the interaction of Nanosensor-III with DMMP and HCl is stronger when compared to that of DCP.

In general, these nanosensors exhibited *"Switch-On"* and *"Switch-Off"* type behaviors based on the type of analyte. Conclusively, the use of NMR sensors built on *"bottom-up"* technology toward the detection of nerve gas analogs proved to be a target selective and efficient approach.

5.5 Future Scope

1. Fundamental characterization of *"Switch-On"* type sensor based on the lifetime decay of nanosensor after interacting with DCP, DMMP, and HCl.
2. Employing receptor molecules of varying conjugations and changing the conjugation lengths of stilbene like monomers to improve signal transduction.
3. Use of ZnS:Mn/ZnS (core/shell) ($1/16^{th}$) QDs with various doping concentrations.
4. Exact estimation of receptor concentrations required to completely cover the surface of nanoparticles in order to quantify the association constants precisely.

REFERENCES

1. Eubanks, L., Dickerson, T.; Janda, K., "Technological advancement for the detection of and protection against biological and chemical warfare agents". *Chemical Society Reviews* **2007,** *36*, 458-470.

2. Seto, Y., Kanamori-Kataoka, M.; Tsuge, K.; Ohsawa, I.; Matsushita, K.; Sekiguchi, H.; itoi, T.; Iura, K.; Sano, Y.; Yamashiro, S., "Sensing technology for chemical-warfare agents and its evaluation usng authentic agents" *Sensors and Actuators B* **2005,** *108*, 193-197.

3. Royo, S., Manez-Martinez, R.; Sancenon, F.; Costero, A.; Margarita, P.; Gil, S., "Chromogenic and fluorogenic reagents for chemical warfare nerve gas agents detection" *Chemical Communications* **2007,** DOI 10.1039/b707063b.

4. Tomchenko, A., Harmer, G., Marquis, B., "Detection of chemical warfare agents using nanostructured metal oxide sensors". *Sensors and Actuators B* **2005,** *108*, 41-55.

5. Jenkins, A., Uy, O.M., O.; Murray, G.,"Polymer-based lanthanide luminescent sensor for detection of the hydrolysis product of the nerve agent Soman in water" *Analytical Chemistry* **1999,** *71*, 373-378.

6. Bencic-Nagale, S., Sternfeld, T.; Walt, D., "Microbead chemical switches: An approach to detection of reactive organophosphate chemical warfare agent vapors" *Journal of American Chemical Society* **2005,** *128*, 5041-5048.

7. Burdon, J., Nerve Gases. 139-162.

8. Simoniana, A.L., Good, T.A., Wang, S.S, Wild, J.J.,"Nanoparticle-based optical biosensors for the direct detection of organophosphate chemical warfare agents and pesticides" *Analytica Chimica Acta* **2005,** *534*, 69–77.

9. Knapton, D., Burnworth, M., Rowan, S., Weder, C., "Fluorescent Organometallic Sensors for the Detection of Chemical-Warfare-Agent Mimics". *Angew. Chem. Int. Ed.* **2006,** *45*, 5825-5829.

10. Mohr, G., "New Chromogenic and fluorogenic reagents and sensors for neutral and ionic analytes based on covalent bond formation - a review of recent developments" *Analytical Bioanalytical Chemistry* **2006,** *386*, 1201-1214.

11. Rampazzo, E., Brasola, E.; Marcuz, S.; Mancin, F.; Tecilla, P.; Tonellato, U., "Surface modification of silica nanoparticles: a new strategy for the realization of self-organized fluorescence chemosensors" *Journal of Materials Chemistry* **2005,** *15*, 2687-2696.

12. Wolfbeis, O., "Materials for fluorescence based optical chemical sensors" *Journal of Materials Chemistry* **2005**, *15*, 2657-2669.

13. Mori, H., Lanzendorfer, M.; Muller, H., "Organic-Inorganic Nanoassembly based on complexation of cationic silica nanoparticles and weak anionc polyelectrolytes in aqueous and alcohol media" *Langmuir* **2004,** *20*, 1934-1944.

14. Gao, F., Wang, L., Tang, L., Zhu, C., "A Novel Nano-Sensor Based on Rhodamine-b-Isothiocyanate –Doped Silica Nanoparticle for pH Measurement" *Microchim Acta* **2005,** *152*, 131–135.

15. Bagwe, R., Hilliard, L.; Weihong, T., "Surface modification of silica nanoparticles to reduce aggregation and nonspecific binding" *Langmuir* **2006,** *22*, 4357-4362.

16. Tolnai, G., Csempesz., F.; Faix-Kabai, M.; Kalman, E.; Keresztes, Z.; Kovacs, A.; Ramsden,j.; Horvolgyi,Z., "Preparation and characterization of surface- modified silica- nanoparticles" *Langmuir* **2001,** *17*, 2683-2687.

17. Rao K, El-Hami, K., Kodaki, T., Matsushige, K., Makino, K., "A novel method for synthesis of silica nanoparticles" *Journal of Colloids and Interface Science* **2005,** *289*, 125-131.

18. Wang, L., Yang, C., Tan, W., "Dual-luminophore- doped silica nanoparticles for multiplexed signaling"*Nano letters* **2005,** *5*, *1*, 37-43.

19. Bailey, J. K., Mecartney, M.,L., "Formation of colloidal silica particles from alkoxides" *Colloids and Surfaces* **1992,** *63*, 151-161.

20. Nozawa, K., Gailhanou, H., Raison, L., Panizza, P., Ushiki, H., Sellier, E, Delville, J.P., Delville, M.H. "Smart Control of Monodisperse Stober Silica Particles: Effect of Reactant Addition Rate on Growth Process". *Langmuir* **2005**, *21*, 1516-1523.

21. Song Liu, H., Tian-Cai Liu, Bo Liu, Cao, Y., Zhen-Li Huang, Yuan-Di Zhao; Luo, Q.-M., "Optimization of the methods for introduction of amine groups onto the silica nanoparticle surface" *Journal of Biomedical Materials Research Part A DOI 10.1002/* **2006**, 752-758.

22. Santra, S., Yang, H., Dutta, D., Stanley, J., Walter, W., Tan, W., Moudgil, B., Mericle, R., " Synthesis and characterization of fluorescent, radio-opaque and paramagnetic silica nanoparticle for multimodel bioimaging applications" *Advanced Materials* **2005,** *17*, 2165-2169.

23. A.Vrij, Blaaderen, V.,"Synthesis and characterization of monodisperse colloidal organo-silica spheres" *Journal of Colloid and Interface Science* **1993,** *156*, 1-18.

24. Li, H., Perkas, N., Li, Q., Gofer, Y., Koltypin, Y., Gedanken, A., "Improved Silanization Modification of a Silica Surface and Its Application to the Preparation of a Silica-Supported Polyoxometalate Catalyst" *Langmuir* **2003,** *19*, 10409-10413.

25. Rogozhina, E., Eckhoff, D.; Gratton, E.; Braun, P., "Carboxyl functionalization of ultrasmall luminescent silicon nanoparticles through thermal hydrosilyation" *Journal of Materials Chemistry* **2006,** *16*, 1421-1430.

26. Miller, J., Ishida, H., "Quantitative Monomolecular Coverage of Inorganic Particulates by Methacryl-functional silanes" *Surface science* **1984,** *148*, 601-622.

27. Sen, T., Bruce I., "Surface Modification of Magnetic Nanoparticles with Alkoxysilanes and Their Application in Magnetic Bioseparations" *Langmuir* **2005,** *21*, 7029-7035.

28. Somers, R. Bawendi, M.; Nocera, D., "CdSe nanocrystal based chemi-/bio-sensors" *Chemical Society Reviews* **2007,** *36*, 579-591.

29. Larson, D., Zipfel, L.; Williams, R.; Clark, S.; Bruchez, M.; Wise, F.; Webb, W., "Water-soluble quantum dots for multiphoton fluorescence imaging in vivo" *Science* **2003,** *300*, 1434-1436.

30. Gomez, D. Califano, M., Mulvaney, P., "Optical properties of single semiconductor nanocrystals". *Physical Chemistry Chemical Physics* **2006,** *8*, 4989-5011.

31. Raymo, F. Yildiz, I., "Luminescent chemosensors based on semiconductor quantum dots" *Physical Chemistry Chemical Physics* **2007,** *9*, 2036-2043.

32. Murphy, C. J., Optical Sensing with Quantum Dots. *Analytical Chemistry* **2002**, 520-527.

33. Ji, X. Zheng, J.; Xu, J.; Rastogi, V.; Cheng, T.; Defrank, J.; Leblanc,R, "(CdSe)ZnS quantum dots and organophosphorus hydrolase bioconjugate as biosensors for detection of paraoxon" *Journal of Physical Chemistry B* **2005,** *109*, 3793-3799.

34. Goldman, E., Medintz, I.; Whitley, J.; Hayhurst, A.; Clapp, A.; Tetsuo, H.; Deschamps, E.; Lassman, M.; Mattoussi, H, "A hybrid quantum dot-antibody fragment fluorescence resonance energy transfer based TNT sensor" *Journal of Aamerican Chemical Society* **2005,** *127*, 6744-6751.

35. Bol, A., Meijerink, A., "Luminescence quantum efficiency of nanocrystals ZnS:Mn^{2+}.1. Surface passivation and Mn^{2+} concentration" *Journal of physical chemistry B* **2001,** *105*, 10197-10202.

36. Costa-Fernandez, J. M., "Optical sensors based on luminescent quantum dots" *Anal Bioanal Chem* **2006,** *384*, 37--40.

37. Dabbousi, B., Rodriguez-Veijo, J., Mikulee, F.; Heine, J.; Mattoussi, H.; Ober,R.; Jensen, K.; Bawendi, M., "(CdSe)ZnS core-shell quantum dots: synthesized and characterization of a size series of highly luminescent nanocrystallites" *Journal of physical chemistry B* **1997,** *101*, 9463-9475.

38. Sookial, K., Cullum, B.; Angel, S.; Murphy, C.,"Photophysical properties of ZnS nanoclusters with spatially localized Mn^{2+}" *Journal of Physical chemistry* **1996,** *100*, 4551-4555.

39. Lin, C., Liedl, T., Sperling, R.; Arguelles, F.; Fernandez,J.; Pereiro, R.; Medel, A.; Chang, W.; Parak, W.,"Bioanalytics and biolabeling with semiconductor nanoparticles (quantum dots)" *Journal of Materials Chemistry* **2007,** *17*, 1343-1346.

40. Suyver, J. , Kelly, J.; Wuister,S.; Meijerin, A., "Synthesis and photoluminesence of nanocrystalline ZnS:Mn^{2+}" *Nano letters* **2001,** *1*, *8*, 429-433.

41. Liu, W.T., "Nanoparticle and Their Biological and Environmental Applications". *Journal of Bioscience and Bioengineering* **2006,** *102*, *1*, 1-7.

42. Beerman, P., McGarvey, B.; Muralidharan, S.; Sung, R., "EPR spectra of Mn2+ doped ZnS Quantum dots". *Chemistry of materials* **2004,** *16*, (915-918).

43. Bhargava, R., Gallagher., D., Hong, X., Nurmikko, A.,"Optical properties of Manganese-doped nanocrystals of ZnS" *Physical review letters* **1994,** *72*, (3), 416-419.

44. Borse, P., Srinivas, D.; Shinde, R.; Date,S.; Vogel, W.; Kulkarni, S., "Effect of Mn^{2+} concentration in ZnS nanoparticles on photoluminescence and electron-spin-resonance spectra" *Physical Review* **1999,** *60*, *12*, 8659-8662.

45. Wageh, S., Shu-Man, L.; You, F.; Rong, X., "Optical properties of strongly luminescing mercaptoacetic acid-capped ZnS nanoparticles" *Journal of Luminescence* **2003,** *102-103*, 768-773.

46. Surin, M., Sonar, P.; Grimsdale, A.; Mullen, k.; Feyter, S.;Habuchi, S.; Sarzi, S.; Bracken, E.; Heyen, A.; Auweraer, M.; Schryver, F.; Cavallini, m.; moulin, J.; Biscarini, F.; Femoni, C.; Lazzaroni, R.; Leclere, P., "Solid state assemblies and

optical propertie sof conjugated oligomers combining fluorene and thiophene units" *Journal of Materials Chemistry* **2007,** *17*, 728-735.

47. Hulvat, J., Sofos, M.; Tajima, K., Stupp, S.,"Self-assembly and luminescence of oligo(p-phenylenevinylene) amphiphiles" *Journal of American Chemical Society* **2005,** *127*, 366-372.

48. Kim, Y., Kwon, S., "Novel blue-light emitting polymers based on a diphenylanthracene moeity" *Journal of Applied Polymer Science* **2006,** *100*, 2151-2157.

49. LIN, H., Tsai, C., Tao, Y., "Synthesis and Characterization of Light-Emitting Oligo(p-phenylene-vinylene)s and Polymeric Derivatives Containing Three- and Five-Conjugated Phenylene Rings. II. Electro-Optical Properties and Optimization of PLED Performance" *Journal of Polymer Science: Part A: Polymer Chemistry,* **2006,** *44*, 2922–2936.

50. Gaylord, B., Wang, S.; Heeger, A.; Bazan, G., "Water-soluble conjugated oligomers: effect of chain length and aggregation on photoluminescnce-quenching efficiencies". *Journal of American Chemical Society* **2001,** *123*, 6417-6418.

51. Ye, M., Lei, X.; Liu, L.; Wang, W., "Synthesis of novel cross-linked polyurethane containing modified stilbene and schiff base chromophores for second-order nonlinear optics" *Journal of Nonlinear Optical Physics and Materials* **2006,** *15*, 2, 275-285.

52. Aerts, G. Wuyts, C.; Dermaut, W.; Goovaerts, E.; Geise,H.; Blockhuys, F., "Synthesis and optical properties of polystyrene bearing stilbenoid side chains" *Macromolecules* **2004,** *37*, 5406-5414.

53. Jorgensen, M., Krebs, F., "Stepwise and directional synthesis of end-functionalized single oligomer OPVs and their applicaiton in organic solar cells" *Journal of organic chemistry* **2004,** *69*, 6688-6696.

54. Krebs, F., Jorgenson, M., "High carrier mobility in a series of new semiconducting PPV-type polymers" *Macromolecules* **2003,** *36*, 4374-4384.

55. Pucci, A., Cuia, F.; Signori, F.; Ruggeri, G., "Bis(benzoxazolyl) stilbene excimers as temperature and deformation sensors for biodegradable poly(1,4-butylene succinate) films". *Journal of Materials Chemistry* **2007,** *17*, 783-790.

56. Bergmann, F., Weinberg, Z., "Remarks on the synthesis of substituted stilbenes and diphenylbutadienes" **1940**, 134-139.

57. Berlicki, L., Rudiziska, E., MLynarz, P., Kafarski, P.,Organophosphorus Supramolecular Chemistry Part-1 Receptors for organophosphorus compounds. *Current Organic Chemistry* **2006**, *10*, 2285-2305.

58. Shemirani, F. M., A.; Nissari, M.; Kozani, R., "Silica gel coated with schiff's base: synthesis and application as an adsorbent for cadmium, copper,Zinc and nickel. Determination after preconcentration by flame atomic absorption spectroscopy" *Journal of analytical chemistry* **2004,** *59*, (3), 228-233.

59. Maton, L., Taziaux, D.; Soumillion, J.; Louis, J.; Jiwan, H, *Journal of Materials Chemistry* **2005,** *15*, 2928-2937.

60. Frey-Mason, G., Leuschen, M.; Wald, L.; Paul, K.; Hancock, L., "Reactive chromophores for sensitive and selective detection of chemical warfare agents and toxic industrial chemicals" *Proc. of SPIE* **2005,** *5778*, 337-346.

61. Perrin, S. R., Pirkle, W. H.," Commercially available brush-type chiral selectors for the direct enantiomers" *Chiral separations by liquid chromatography* **1991**, 43-66.

62. Coates, J.,"Interpretation of Infrared Spectra, A practical approach" *Encyclopedia of analytical chemistry* **2000**, 10815-10837.

63. El Harrak, A., Carrot, G., Oberdisse; J., Eychenne-Baron, C., Boue, F., "Surface-Atom Transfer Radical Polymerization from Silica Nanoparticles with Controlled Colloidal Stability" *Macromolecules* **2004,** 37, 6376-6384.

64. Kanan, S., Tripp, C., "An Infrared Study of Adsorbed Organophosphonates on Silica: A Prefiltering Strategy for the Detection of Nerve Agents on Metal Oxide Sensors" Langmuir 2001, 17, 2213-2218.